Simultaneous Waste Heat and Water Recovery from Power Plant Flue Gases for Advanced Energy Systems

DE-FE0024092

Final Report

October 1, 2014 to September 30, 2016

Prepared For: DOE NETL, Barbara Carney

by

Dexin Wang

Report Issued December 2016

Gas Technology Institute

1700 S Mount Prospect Rd

Des Plaines, IL 60018

Acknowledgment:

This material is based upon work supported by the Department of Energy under Award Number DE-FE0024092.

Disclaimer:

List of Acronyms and Abbreviations

LSFO	Limestone with forced oxidation
FGD	flue gas desulfurization
TMC	transport membrane condenser
DOE	Department of Energy
GTI	Gas Technology Institute
ICCI	Illinois Clean Coal Institute
MPI	Media and Process Technology, Inc.
FIU	Florida International University
SOPO	Statement of Project Objectives
CFD	Computational Fluid Dynamics
C	constants
B_t , ΔZ	tube transversal pitch (*m*)
B_l ,ΔY	tube longitudinal pitch (*m*)
D	diameter (*m*)
D_h	hydraulic diameter of flue gas channel (*m*)
E	total energy (*J*)
F	external body force term (N/m^3)
g	gravity (m/s^2)
G_b	generation of turbulence kinetic energy due to buoyancy ($kg/m.s^3$)
G_k	generation of turbulence kinetic energy due to mean velocity gradients ($kg/m.s^3$)
h	enthalpy (*J/kg*)
ID	inner diameter
J_i	diffusion flux of species j (kg/m3s)
k	turbulence kinetic energy (m^2/s^2)
M_v	inlet vapor mass fraction
OD	outer diameter
p	static pressure (*Pa*)
R_i	net rate of production by chemical reaction of species($kg/s.m^3$)
S	source term in equations
S_i	rate of creation by addition from the dispersed phase($kg/s.m^3$)
STM	species transport model
t	time (*s*)
T	temperature (*K*)
TMC	transport membrane condenser
u	velocity (*m/s*)
x	distance (*m*)
Y_i	local mass fraction of chemical species
α	inverse effective Prandtl numbers for k or ε
ε	turbulence kinetic energy dissipation rate (m^2/s^3)
λ	thermal conductivity (*W/m K*)
μ	molecular viscosity (*kg/m s*)
ρ	density (kg/m^3)
τ	stress tensor (*Pa*)
τ_w	shear stress on tube wall (*Pa*)
eff	effective
i, j, k	special direction
fg	flue gas
l	Liquid

Executive Summary

This final report presents the results of a two-year technology development project carried out by a team of participants sponsored by the Department of Energy (DOE). The objective of this project is to develop a membrane-based technology to recover both water and low grade heat from power plant flue gases. Part of the recovered high-purity water and energy can be used directly to replace plant boiler makeup water as well as improving its efficiency, and the remaining part of the recovered water can be used for Flue Gas Desulfurization (FGD), cooling tower water makeup or other plant uses. This advanced version Transport Membrane Condenser (TMC) with lower capital and operating costs can be applied to existing plants economically and can maximize waste heat and water recovery from future Advanced Energy System flue gases with CO_2 capture in consideration, which will have higher moisture content that favors the TMC to achieve higher efficiency.

As fresh water is becoming a less abundant natural resource, retrieving water from different waste water sources, such as industrial waste water, brackish water, produced water, as well as sea water, becomes a promising choice to produce fresh water. These processes are typically energy intensive, regardless of the process whether a thermal process or a membrane separation process. Consequently, they are still not cost competitive for wide commercial uses. However, there is another waste water source not being considered, the water vapor contained in many waste gas streams, which is present in many industrial and power generation processes. Minimal external energy sources are needed to recover this water because the water is already at a high energy state. Also, the water vapor latent heat from these waste gas streams, is substantial compared with the sensible heat associated with the temperatures of these streams. This vapor can release significant amounts of heat when turned to liquid phase. As a result, recovery of these waste water vapors can also greatly improve the overall industrial process thermal efficiency.

For instance, a large portion of energy consumed today comes from hydrocarbon fuel combustion, and one of the major combustion by-products is water vapor. For a coal-fired power plant boiler equipped with a FGD unit, flue gas exits at 130 to 160°F with nearly 100% relative humidity which contains up to 30% water vapor by volume. If 40 to 60% of this water vapor and its latent heat could be recovered and reused, the plant thermal efficiency can be greatly improved in addition to the water recovery benefit.

Until now, there has been no practical commercial technology available for recovering waste heat and water vapor from power plant flue gases. Condensing flue gas moisture by simply removing heat in a heat exchanger presents the problem of a large surface area requirement for the low-temperature flue gas, and also raises the issue of equipment corrosion by the acidic condensate. The recovered water needs further treatment before it can be used for any other processes, due to the high acidity and other contaminates present in the water.

Gas Technology Institute (GTI) has developed a new technology based on a nanoporous ceramic separation membrane to extract a portion of the water vapor and its latent heat from flue gases and return the recovered water and heat to the steam cycle. This is achieved through the use of its patented Transport Membrane Condenser (TMC). Water vapor condenses and passes through the membrane, which has the permeate side in direct contact with a low-temperature water stream. Contaminants such as CO2, O2, NOx, and SO2 are inhibited from passing through the membrane by its high selectivity. The recovered water is of high quality and mineral free, therefore it can be used as supplemental makeup water for other processes. The TMC has been developed and commercialized at the industrial demonstration scale for gas-fired package boilers and commercial laundry applications.

This project is a continuation of previous development efforts, to further develop the TMC system for water and waste heat recovery from power plant flue gases. Based on GTI's successful experience on developing the TMC for industrial boiler flue gas water and heat recovery and coal power plant flue gas slip stream tests, this project aims at increasing the TMC technology water and energy recovery efficiency and lowering

its capital and operating costs. This advanced version of TMC can achieve lower capital and operating costs, higher efficiency, and can be applied for broader flue gas applications thanks to the membrane developments advanced during this project. Through this project, we were able to improve the TMC efficiency by around 30% through new designs, developed higher stability membrane for low pH conditions, also as important we have explored methods to reduce TMC module fabrication cost. By using compression molding method for major parts fabrication plus low cost TMC membrane tubes, as much as 60% cost reduction for the TMC module is possible.

The project also evaluated the integration of the TMC system in a coal-fired power plant, the cost-benefit analysis and the design of TMC arrangement with detailed module layout. Based on the operating data of typical coal-fired power plants, the performance of a coal-fired power plant with a basic configuration and the addition of integrated TMC technology was analyzed and assessed by calculating changes in both the water recovery rate and the heat rate. The results showed that the TMC heat and water recovery efficiency is related to both its inlet water flow rate and its inlet flue gas moisture content. The higher the TMC inlet cooling water flow rate and the higher the moisture content in the flue gas, the larger amount of water and heat that can be recovered by the TMC system. Besides strategies for integrating the TMC system in coal-fired power plants along with economic analysis including capital cost, O&M cost and annual cost for retrofit units and new units with a FGD system, other effects introduced by the TMC systems including pressure drop and auxiliary power needs were also analyzed. The payback for a typical PC 550 MW power plant for installing a TMC system may vary from 1.2 to 5.7 years depending on different plant and operating factors.

The TMC can recover 5% or more of the boiler feed water flow rate equivalent amount of water with heat, but only a small fraction of it is typically needed for a power plant boiler makeup which is a waste of the high quality water and the associated heat. We will continue the evaluation on using the recovered hot water to preheat air or dry coal, to further improve the boiler efficiency.

Table of Contents

List of Figures

List of Tables

1. Introduction – Project Participants and Roles

This final report presents the results of a two-year technology development project carried out by a team of participants sponsored by the Department of Energy (DOE). This project is in the program announcement Area of Interest 1-A: Utilization of Low Grade Heat within Existing Power Generation Systems.

The objective of this project is to develop a membrane-based technology to recover both water and low grade heat from power plant flue gases. Part of the recovered high-purity water and energy can be used directly to replace plant boiler makeup water as well as improving its efficiency, and the remaining part of the recovered water can be used for Flue Gas Desulfurization (FGD), cooling tower water makeup or other plant uses. This advanced version Transport Membrane Condenser (TMC) with lower capital and operating costs can be applied to existing plants economically and can maximize waste heat and water recovery from future Advanced Energy System flue gases with CO_2 capture in consideration, which will have higher moisture content that favors the TMC to achieve higher efficiency.

Figure 1-1 shows the team members, the principal investigators for each team, and their roles and responsibilities as they relate to the tasks in the Statement of Project Objectives (SOPO). Illinois Clean Coal Institute (ICCI) has provided cost share support for this project.

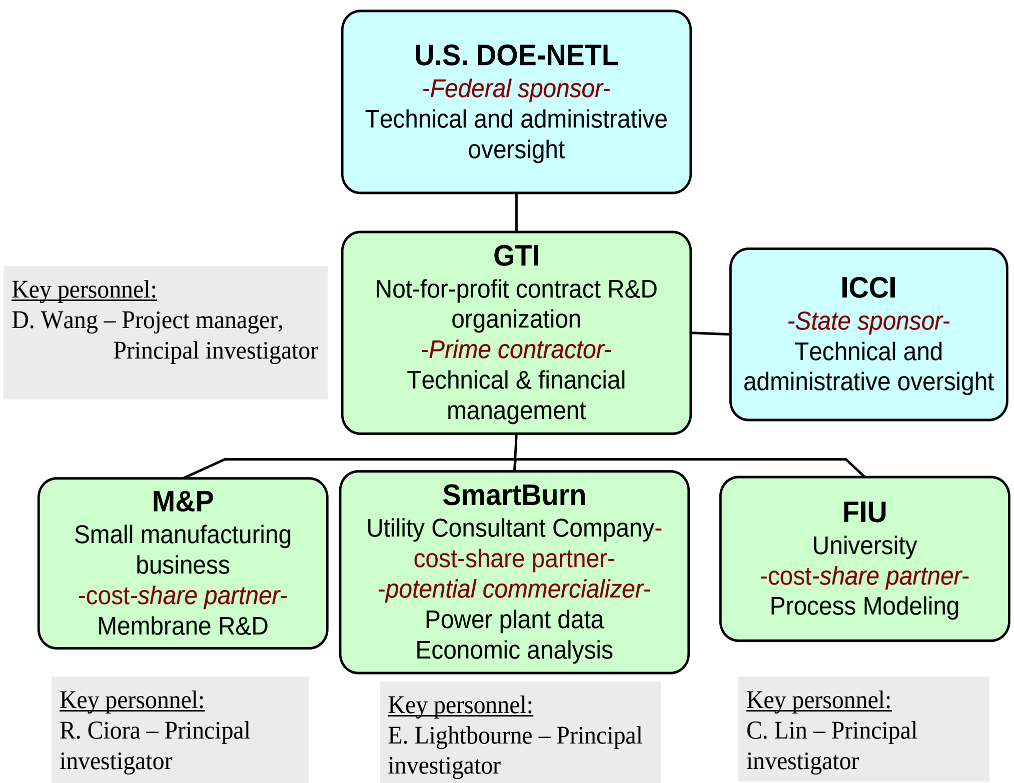

Figure 1-1. Project Organization Chart and Participant roles

Table 1-1 summarizes the capabilities and roles of the member organizations for this project, including Gas Technology Institute (GTI), Media and Process Technology, Inc. (MPT or M&P), SmartBurn LLC (SmartBurn), and Florida International University (FIU).

Table 1-1. Project Participants and their Roles in the Project

Organization	Credentials, Capability, Experience and Roles
Gas Technology Institute (GTI)	• Independent, not-for-profit institute that: – Performs contract laboratory and field R&D – Manages R&D projects for the natural gas industry and other clients – Commercializes new energy technology through business arrangements • In business serving the energy industries and the public for 70 years • Campus-like setting on 18 acres – 280,000 square feet of laboratory and office facilities – Approximately 100 ongoing R&D projects annually – 23 energy technology laboratories including combustion, coal gasification, biomass gasification, air treatment, gas processing, etc. • Highly qualified staff – 250 employees, 175 R&D staff, 45% with advanced degrees – Power Generation Group consisting of 12 engineers and scientists • Project roles – Prime contractor of the project, responsible for technical and financial management – Major technology development, including redesign of the TMC for lower cost, higher efficiency, and testing at GTI's industrial combustion lab at pilot scale.
Media & Process Technology Inc. (MPT)	Independent small business for over 20 years: – Spun off from Alcoa Separations business in 1991 – Maintains high-technology advantage through sponsored R&D • Commercially oriented technology innovator specializing in the development and application of inorganic membranes • *Only* US-based commercial ceramic membrane manufacturer • Worked closely with GTI on DOE Super Boiler project and other NETL projects including membrane separator for water recovery from flue gas • Project roles – TMC new membrane development for higher performance, lower cost, and low pH resistance for high SO_2 flue gases. – Provide full scale, large quantity new membrane tubes for GTI pilot scale TMC fabrication and testing
SmartBurn LLC (SmartBurn)	• Utility consulting company headquartered in Wisconsin – Coal-fired and gas-fired power plants – Environmental services • Worked closely with GTI on previous NETL projects • Providing cost-share for this project, potential commercialization partner • Project roles – Utility partner to provide existing power plant information, TMC plant integration technical analysis, and economic analysis for TMC application in commercial scale
Florida International University (FIU)	• Extensive research activities on numerical modeling for various engineering problems, advanced computational fluids and energy lab available. • Worked closely with GTI on previous DOE projects for numerical simulation works, including the TMC. Provides cost share. • Project roles – CFD simulation to assist new TMC design and data analysis

2. Project Background and Previous Development Work

2.1 Background

As fresh water is becoming a less abundant natural resource, retrieving water from different waste water sources, such as industrial waste water, brackish water, produced water, as well as sea water, becomes a promising choice to produce fresh water. These processes are typically energy intensive, regardless of the process whether a thermal process or a membrane separation process. Consequently, they are still not cost competitive for wide commercial uses. However, there is another waste water source not being considered, the water vapor contained in many waste gas streams, which is present in many industrial and power generation processes. Minimal external energy sources are needed to recover this water because the water is already at a high energy state. Also, the water vapor latent heat from these waste gas streams, is substantial compared with the sensible heat associated with the temperatures of these streams. This vapor can release significant amounts of heat when turned to liquid phase. As a result, recovery of these waste water vapors can also greatly improve the overall industrial process thermal efficiency.

For instance, a large portion of energy consumed today comes from hydrocarbon fuel combustion, and one of the major combustion by-products is water vapor [1]. For a coal-fired power plant boiler equipped with a FGD unit, flue gas exits at 130 to 160°F with nearly 100% relative humidity which contains up to 30% water vapor by volume. If 40 to 60% of this water vapor and its latent heat could be recovered and reused, the plant thermal efficiency can be greatly improved in addition to the water recovery benefit.

Until now, there has been no practical commercial technology available for recovering waste heat and water vapor from power plant flue gases. Condensing flue gas moisture by simply removing heat in a heat exchanger presents the problem of a large surface area requirement for the low-temperature flue gas, and also raises the issue of equipment corrosion by the acidic condensate. The recovered water needs further treatment before it can be used for any other processes, due to the high acidity and other contaminates present in the water.

Gas Technology Institute (GTI) has developed a new technology based on a nanoporous ceramic separation membrane to extract a portion of the water vapor and its latent heat from flue gases and return the recovered water and heat to the steam cycle. This is achieved through the use of its patented Transport Membrane Condenser (TMC). Water vapor condenses and passes through the membrane, which has the permeate side in direct contact with a low-temperature water stream. Contaminants such as CO2, O2, NOx, and SO2 are inhibited from passing through the membrane by its high selectivity. The recovered water is of high quality and mineral free, therefore it can be used as supplemental makeup water for other processes. The TMC has been developed and commercialized at the industrial demonstration scale for gas-fired package boilers and commercial laundry applications. The TMC technology was developed by GTI as a key component for the high-efficiency Super Boiler program, which was sponsored by the United States Department of Energy (DOE) and other industrial sponsors and started in 2000.

This project intended to further develop a new two-stage TMC design for recovering water vapor and its latent heat from power plant flue gases, lowering its cost for commercial applications. The new two-stage TMC seeks to achieve maximum heat and water recovery. The recovered high-purity water and heat can be used directly to replace power plant boiler makeup water to improve its efficiency, and any remaining recovered water can be used for FGD water makeup or other plant uses. The TMC technology will be particularly beneficial to coal-fired power plants that use high-moisture coals and/or FGD for flue gas cleanup. The TMC can be used to process high-moisture flue gas from the FGD to recover its water vapor and latent heat to increase boiler efficiency and decrease its water consumption.

The economic benefits of water vapor removal from flue gas are substantial. GTI calculates a reduction in the flue gas dew point from 140°F down to 100°F, which corresponds to recovering 84 lb/h water per 1 million Btu/h firing rate. For the year 2000, the net U.S. electric power generation was 3,802 billion kWh, of which coal-fired generation was 1,966 billion kWh, and natural gas-fired generation was another 613 billion kWh[2]. This water recovery technology can be used for both coal and gas-fired power plants so up to 2,579 billion kWh of capacity could be impacted. Assuming 35% baseline fuel-to-electricity efficiency, the total firing rate is estimated at 25 trillion Btu/h. The corresponding total water savings, if this technology were applied to all U.S. power generation, would be 8.3 billion tons per year. At a typical treated water price of $0.52/ton [3], the total annual U.S. cost saving in water alone would be $4.3 billion/year. Additionally, the use of TMC can increase boiler thermal efficiency by 0.1-0.2% as described above by recovering the water vapor latent heat. This efficiency increase would increase power output by 3.0 billion kWh nationwide per year.

2.2 TMC Technology Concept and Previous Development

Membrane separation technology has been used commercially for many years for gas separation and liquid filtration, and features low energy cost and high separation ratio compared with competing separation methods. There are two kinds of membranes, porous and non-porous. For porous membranes, the pore size is normally in the sub-micron (nanoporous) range, and varies for different applications. To achieve a good separation ratio with a porous membrane for gaseous species, including the separation of water vapor from flue gas, the typical pore size must be less than 50 nm. Water vapor transport through a porous ceramic membrane must follow some combination of the following four modes: Knudsen diffusion, surface diffusion, capillary condensation, and molecular sieving.

For water vapor, the molecular sieving mode can only occur when the pore size of the membrane is smaller than 1 nm. The pore size used in the TMC is 4 nm and larger, so this mode does not apply. This operating mode can achieve high separation ratio, but the permeate flux is too low for bulk separation applications. For the Knudsen and surface diffusion modes, water vapor passes through the membrane pores in the gas phase, as can many other gas components, but the water vapor molecules transport faster because of their lower molecular weight. The water vapor separation ratio in these modes is not high. The permeate flux is also too low at the water vapor partial pressure difference presented in the flue gas.

When one of the gas components is a condensable vapor and the pores are small, capillary condensation can occur. In this case, the condensate can block gas phase diffusion through the pores, allowing only the condensed phase to pass through. The Kelvin equation predicts that condensation can occur in small pores even though the partial pressure of that component is below its vapor pressure. In most cases, capillary condensation begins to occur at 50-80% of the saturation vapor pressure, which in the case of water is equal to relative humidity because of the surface tension in the pores. As a result, the pores can be completely filled with condensed water. The flux of other components in the flue gas through the membrane will be very small, limited by their solubility in water and by the limited mobility of solvated molecules. Therefore, a very high separation ratio can be achieved for water vapor. Also, under the same pressure difference across the membrane, H_2O mass transport rate in liquid phase can be as high as 40 times the rate in the gas phase. This is mainly due to the more than a thousand-fold difference of their densities, although viscosity change adversely affects liquid transport, but much less than the favorable effect of the density difference. The above evidence proves that membrane water vapor separation in a capillary condensation mode can promote both a high transport rate and a high separation ratio.

GTI investigated water vapor transport from flue gas using both non-porous and porous membranes. GTI concluded that a nanoporous ceramic membrane can achieve both a high water vapor transport rate and a high separation ratio when it works at favorable capillary condensation conditions. For flue gas from natural gas firing, the flue gas moisture content is typically at 18% in volume for the high hydrogen element content in the fuel. With coal firing, the moisture produced from combustion itself is usually lower for the lower hydrogen content of coal. But for high moisture content coals and plants equipped with FGDs, the flue gas humidity is comparable, or much higher than the natural gas firing flue gas. This provides a favorable condition for extracting water vapor from their flue gases. In the TMC, water vapor from flue gas passes through a permselective membrane (Figure 2-1), and is condensed by direct contact with low-temperature water. In this way, the transported water is recovered along with virtually all of its latent heat. The conditioned flue gas leaves the TMC at a reduced temperature and relative humidity below saturation.

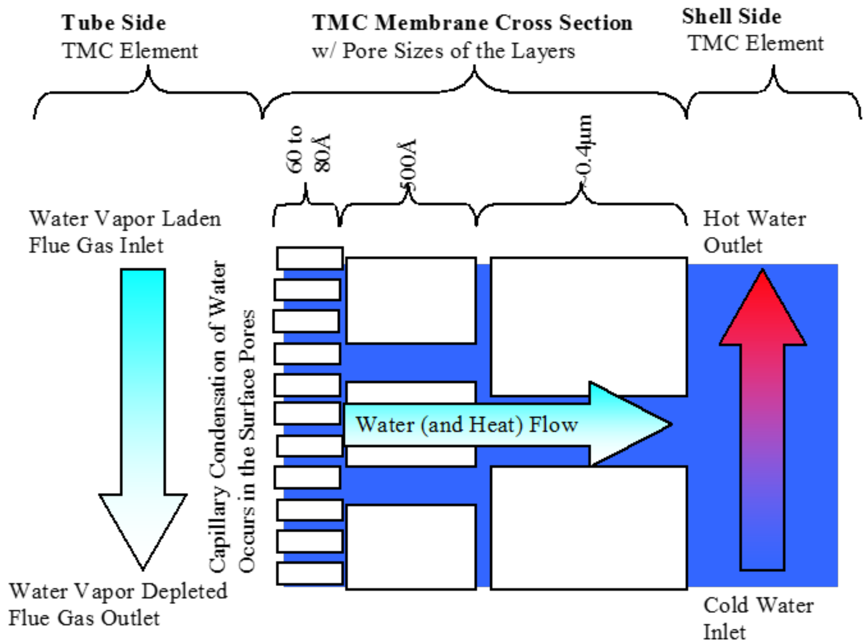

Figure 2-1. TMC Concept Schematic

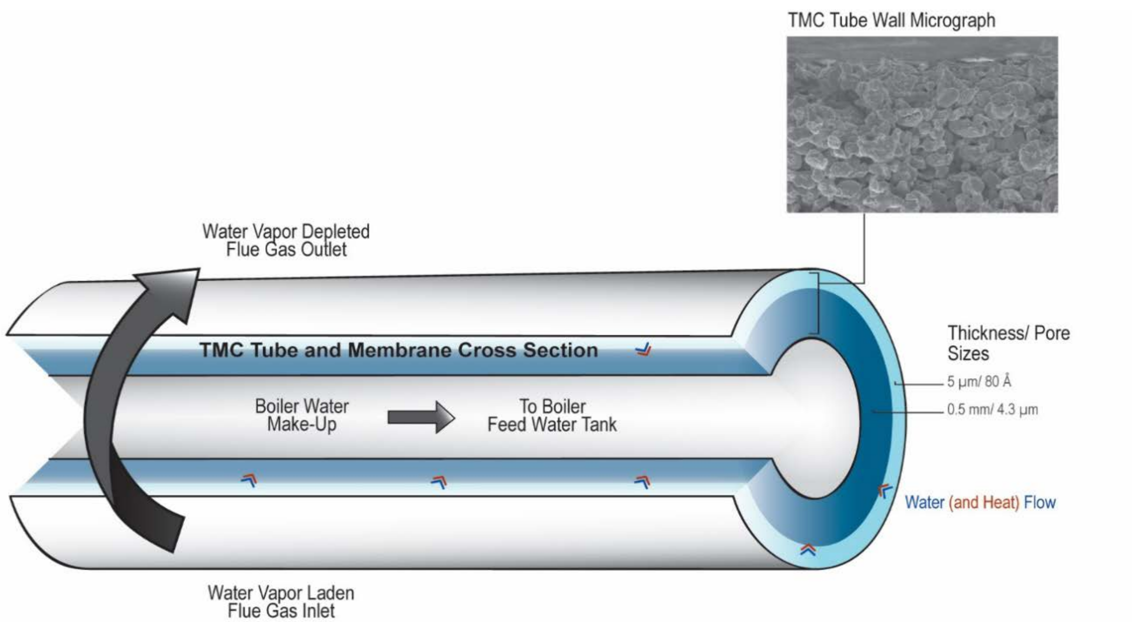

Figure 2-2. TMC concept shown with a single membrane tube

Figure 2-2 shows the TMC working concept in a practical single membrane tube with each layer thickness/pore sizes shown. Many of these membrane tubes bundled together form a TMC module. Boiler feed water flows inside the tube and flue gas flows from the outside of the tube. GTI experimental data in Figure 2-3, shows that the water vapor transport rate in capillary condensation mode is more than five-fold higher than in its gas phase Knudsen diffusion mode. GTI has also done extensive studies on other factors that affect the ceramic membrane transport performance, including membrane pore size, permeate side vacuum, water inlet temperature, flow rate, flue gas inlet temperature, and flue gas humidity. These fundamental test data provide a solid foundation for the development of the TMC unit. Figure 2-4 shows the typical ceramic membrane structure and pore size distribution used for the TMC (refer back to Figure 2-1 and Figure 2-2). It consists of a top layer with a pore size of 60 to 80 Å (~ 2 to 4 µm thick), a 500 Å pore size intermediate layer (typically 20 to 50 µm thick), and a ~0.4 µm pore size substrate (~1 mm thick). This is called an "asymmetric" structure and is used for both polymeric and ceramic nanoporous separation membranes to achieve high separation ratio with minimal resistance to flux of the permeating species.

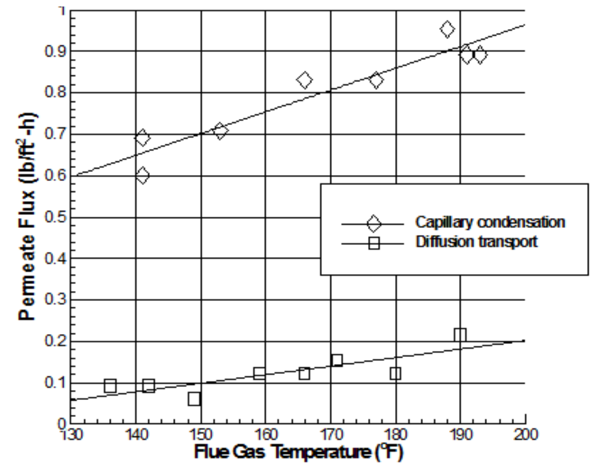

Figure 2-3. Water Vapor Transport Mode Effect

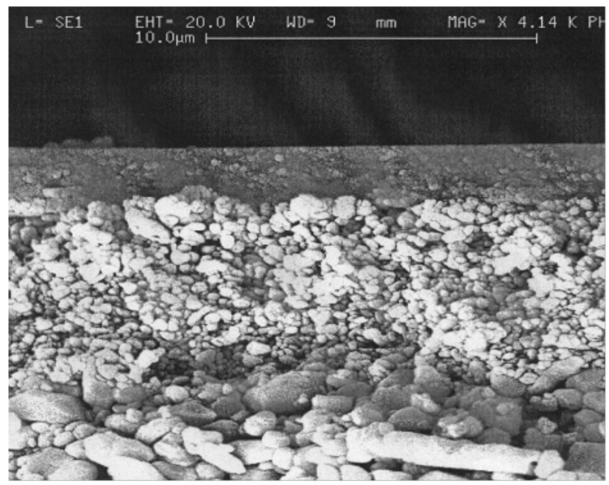

Figure 2-4. Photomicrograph of TMC Membrane Cross-Section

GTI has already demonstrated the use of the TMC in four industrial gas-fired boilers for long-term operations, with the first unit being in continuous operation for nearly three years with no detectable performance degradation. The customer has confirmed 12% fuel saving and 20% makeup water saving. However, economic analysis showed that the earlier version of the TMC (version 1.0) was too expensive to manufacture, assemble, and maintain. As a result, GTI has developed a version 2.0 design of the TMC for industrial and commercial boilers with more cost-effective characteristics. With water flowing inside the tubes, the water side management allows for a more flexible design, with the TMC designed with several passes (Figure 2-5 shows a three-pass design in the middle picture). Hot water can be pumped out from the lower section of the TMC instead of the upper section, which results in simplified water level controls. Another important advantage of the new design (2.0 design?) is that flue gas now flows upwards instead of downwards as in the previous TMC, allowing the unit to be mounted directly on top of a boiler stack without the lengthy ductwork needed to direct the flue gas downwards and then reverse direction to go upwards to the atmosphere. This greatly reduces the installation cost. Also shown in Figure 2-5 (left picture) is the larger tube count of the new membrane module – a four-fold increase – which reduces manufacturing and assembly cost. An optimum spacing between tubes allows flue gas to flow through with a favorable tradeoff between turbulence and pressure drop. The tubes are protected from both sides by metal plates, which also reinforce the overall module structure strength. For a typical 300 HP industrial boiler, only 9 of these modules are needed instead of 94 modules in the original TMC design, which facilitates assembly and service. Figure 2-5 also shows the first Version 2.0 TMC unit installed on a 200HP natural gas fired boiler (left picture). The redesigned TMC is more efficient and cost-effective, and the modular design is more user friendly for assembly and maintenance.

Under previous DOE NETL support, GTI has developed a TMC system specifically for coal power plant flue gas water and waste heat recovery. It has been tested in a pilot scale coal power plant using a slip stream of its flue gas, and the results are very encouraging. Figure 2-6 and 2-7 show the pilot test TMC system in the power plant. This preliminary development was proved successful and achieved stable performance during the continuous five (5)-week test. More work needs to be done to further improve both the water recovery efficiency and reduce the system capital cost, to economically use the technology in a commercial plant.

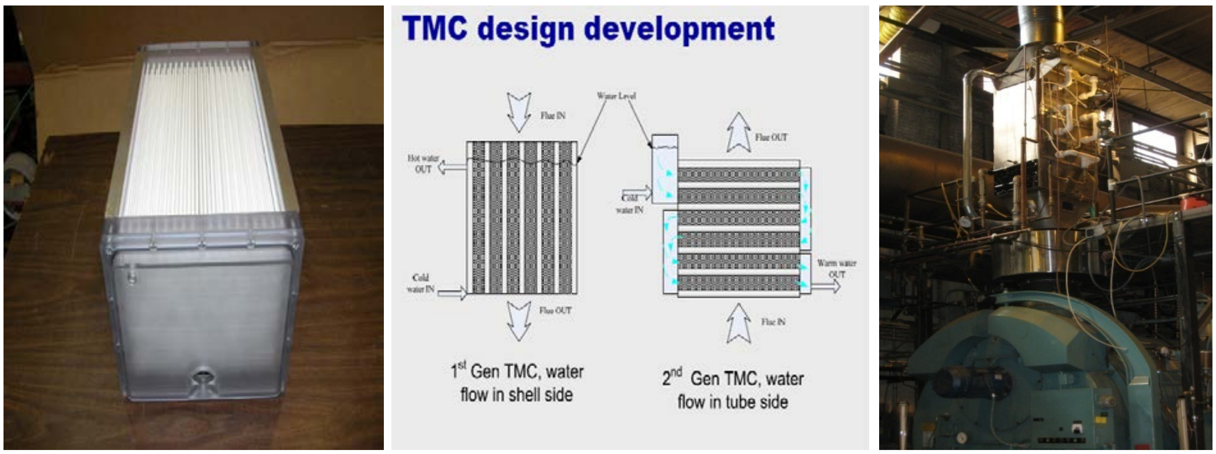

Figure 2-5. TMC development history and an installed unit for a 200HP boiler (right)

Figure 2-6. Installation of the pilot unit in the field

Figure 2-7. Pilot unit inside the tent during field testing

2.3 Project Description

This project is a continuation of previous development efforts, to further develop the TMC system for water and waste heat recovery from power plant flue gases. Based on GTI's successful experience on developing the TMC for industrial boiler flue gas water and heat recovery and coal power plant flue gas slip stream tests, this project aims at increasing the TMC technology water and energy recovery efficiency and lowering its capital and operating costs.

References:

1. J. Boyen, Thermal Energy recovery, JOHN WILEY&SONS, (1980)
2. Bend Research, Research on an Energy-Efficient Drying Process, DOE Final Report, DOE/ID/12293-1 (DE 86013369, Feb.25, (1986).
3. I. Rabovister, R. Knight, R. Remick, "Method and Apparatus for Selective Removal of a Condensable Component from a Process Stream with Latent Heat Recovery", U.S. Patent No. 6,517, 607 B2, Feb.11, 2003.
4. A. Bao, D. Wang, and C.X. Lin, "Nanoporous Membrane Tube Condensing Heat Transfer Enhancement Study", IMECE 2011-63530, Denver, CO, Nov. 11-17, 2011
5. K. Keizer, R. Uhlhorn, V. Zaspalis and A. Burggraaf, "Transport and Related (Gas and Vapor) Separation in Ceramic Membranes", Key Engineering materials, v.61&62, p. 143-154, 1991
6. R. Knight, "Compact Package Boiler Combining Ultra-High-Efficient and Ultra-Low Emissions: Development and Demonstration", Natural Gas Technology Conference II, Buena Vista, FL, 2005
7. D. Wang, W. Liss, and A. Bao, "Water Reclamation from High Moisture Content Waste Heat Streams", IMECE 2011-63513, Denver, CO, Nov. 11-17, 2011
8. R. Knight, I. Rabovister, D. Wang, "Method and Apparatus for Enhanced Heat Recovery from Stream Generators and Water Heaters", U.S. Patent No. 7,066.396 B2, Jun.27, 2006
9. D. Wang, R. Knight, D. Chojnacki, P. Molvie, B. Tynkov, and D. Willems, "Reduce Energy Cost with the Super Boiler", WEEC 2007, Atlanta, GA, August 15-16, 2007
10. D. Wang, R. Knight, D. Chojnacki, P. Molvie, B. Tynkov, and D. Willems, "Saving Energy with the High Efficiency Super Boiler", Journal of Energy Engineering, Vol. 105, No.3, pp.38-48, 2008.

3. TMC Power Plant System Integration Evaluation and Modeling

3.1 TMC Plant Integration Concept and Modeling

The objective of this task is to develop, model, and evaluate the novel two-stage TMC flue gas waste heat and water recovery concept by using analytical and numerical methods, resulting in a design basis for power plant application. The TMC simulation model the team developed in previous projects and the commercial software ANSYS Fluent and ASPEN, have been used for this purpose. The team has analyzed and identified potential design features and parameters to improve the TMC system performance for greater heat and water recovery, as well as determined effects of operating parameters, and membrane transport flux improvement directions. For the two-stage TMC concept, two separate cooling water streams have been used for the TMC. TMC/Stage 1 uses the turbine steam condensate as the cooling stream to recover both water and heat from the inlet hot flue gas stream, and send the hot water to the deaerator. TMC/Stage 2 uses part of the condenser cooling water stream to recover water and part of latent heat from the flue gas stream coming out of TMC/Stage 1. This task requires details on power plant cycles and operating information from our utility team member SmartBurn. This analysis has been performed for a specific existing plant, and for a conceptual plant of typical capacity and flow characteristics. The team has optimized the two stage design so that the TMC/Stage 1 can recover maximum heat and just enough water for the boiler makeup and other pure water usage, and the TMC/Stage 2 can recover maximum water with heat recovery. A plan on how to use the recovered water, including the proper injection points has been developed.

Figure 3-1 illustrates how GTI envisions the two-stage TMC can be integrated into a power plant system. GTI has performed TMC and plant modeling and simulation work to further improve the waste heat and water recovery concept, which includes Aspen modeling to determine the best way to integrate the TMC into a power plant steam cycle, cooling tower cycle and their impacts.

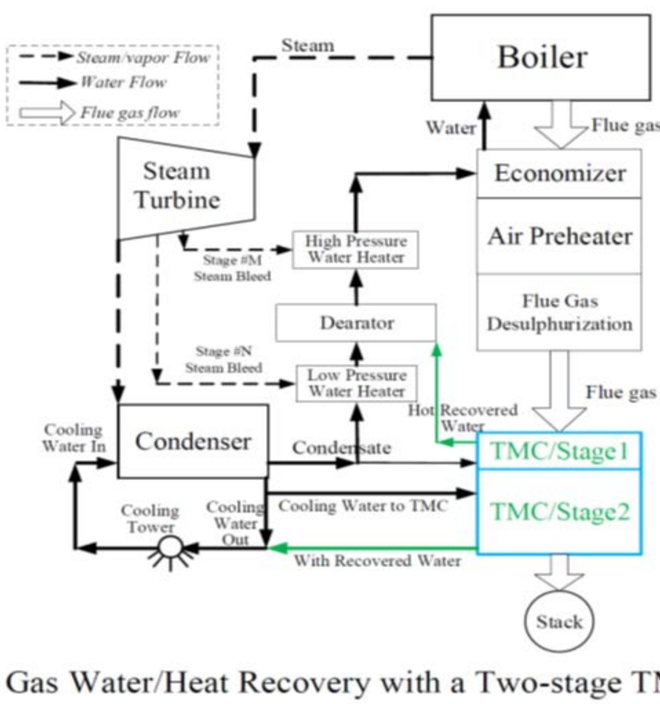

Figure 3-1. Concept Arrangement for TMC Integration into a power plant

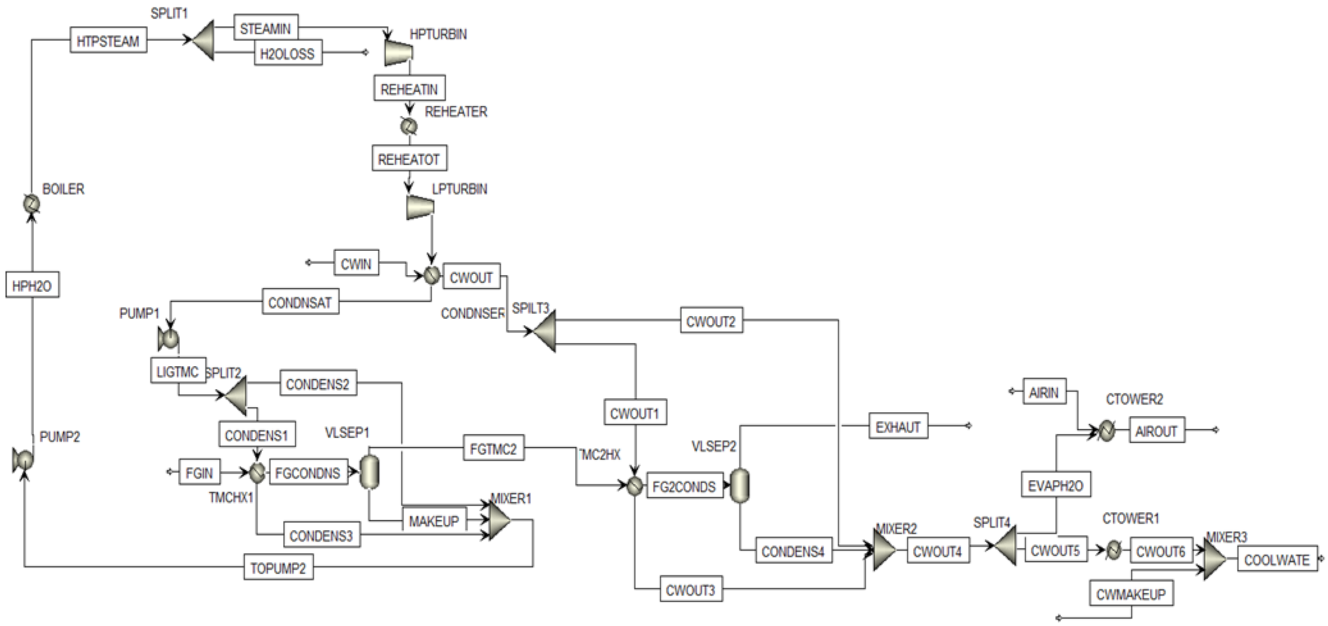

Figure 3-2. Aspen modeling result for integrating TMC into both steam and cooling tower cycles

In this Aspen study (Figure 3-2), the new two-stage TMC concept has been used. TMC/stage 1 receives flue gas from the FGD, transfers part of its water vapor and latent heat to increase the steam boiler efficiency and supply all the makeup water for the boiler (2% of its feed water); then TMC/stage 2 receives the lower temperature flue gas coming out from the TMC/stage 1, transfers a significant part of its remaining water vapor to supplement the cooling tower water flow. The Aspen study shows, if the TMC/stage1 is integrated into the steam cycle, it can increase the cycle efficiency by 0.72% from a baseline 36.3%, save 2% makeup water which is 500kg/min for a 550MW unit. TMC/stage 2 can recover about 3,506 kg/min water for cooling water makeup.

3.2 Integration Study of TMC in Coal-Fired Power Plants

Detailed coal-fired power plant operation data including coal analysis data, flue gas temperature and compositions were collected. Based on this data, integration of TMC in a coal-fired power plant was analyzed and assessed by calculating water recovery and heat rate changes. The analysis and evaluation revealed feasible and optimal approaches of TMC's contribution in CO_2 emissions reduction and economic benefits in power plant operation. First, an efficiency analysis tool was developed to calculate coal-fired power plant heat rate and to evaluate water and heat recovered by TMC. The analysis tool contains three Modules: Module I, a basic coal-fired power plant heat rate calculator; Module II, a TMC integration water and heat analyzer; Module III, a wet FGD calculator. Second, typical coal-fired power plant data were collected and the tool was applied to evaluate the possibility of TMC system integration. The feasibility of potential approaches and the benefits of integrating TMC system into coal-fired power plants are discussed and summarized below.

3.2.1 Flue Gas of Coal-Fired Power Plants

Data from two coal-fired power plants were used to analyze and evaluate the impact of integrating the TMC system into the plants. Descriptions of the power plants, flue gas parameters and coal data are listed in Table 3-1 and Table 3-2 below. Plant A has a 535 MW cyclone-fired supercritical boiler with flue gas of

332°F with 11.4% moisture volume content. Plant B has a 197 MW T-fired subcritical boiler with flue gas of 324°F with 11% moisture volume content.

Table 3-1. Profiles of Coal-Fired Power Plants

	Plant A	**Plant B**
Firing System	Cyclone-fired	T-fired
Technology Detail	Supercritical	Subcritical
Gross Generation(MW)	535	197
Net Generation (MW)	488	179
Coal Feeder Rate (kpph)	535	228
Flue Gas Parameters		
Flue Gas Temperature (°F)	331.9	323.8
Flue gas Oxygen Content (vol%)	2.62	2.97
Flue Gas Flow Rate (kpph)	4,547.4	2,114.0
Dew Point (°F)	119.6	118.4
Relative Humidity (%)	1.56	1.69
Moisture Content (vol%)	11.4	11.0
Moisture Content (wt%)	7.1	6.8

Table 3-2. Coal Analysis Data for the Coal-Fired Power Plants

	Plant A	**Plant B**
Fuel	Sub-bituminous Coal	Sub-bituminous Coal
Higher Heating Value (Btu/lb)	8,792	8,600
Proximate Analysis		
Moisture	27.03	21.45
Ash	5.76	5.97
Volatile Matter	32.44	42.11
Fixed Carbon	34.77	30.47
Ultimate Analysis		
Ash	5.76	5.97
H_2O	27.03	21.45
C	50.12	54.09
H	3.68	3.86
S	0.40	0.23
N	0.68	0.81
O	12.35	13.59

3.2.2 Water Recovery

By using the efficiency analysis tool in Module I, the heat rate of the original power plants can be obtained. Then, by combining Module I and Module II, a modeled TMC integration can be built. The designed TMC outlet flue gas has a relative humidity of 90%. Outlet water temperature is assumed to be 10°F lower than outlet flue gas temperature. The TMC outlet flue gas temperature was calculated by mass and heat balance. Results are listed in Table 3-3.

TMC water inlet flow rate ratio is the ratio of the TMC inlet water flow rate to moisture flow rate in the flue gas inlet. The inlet water flow ratio is 40 in Case A1 and Case B1 with inlet water flow rates of 12,890 kpph (kilo pounds per hour) and 5,780 kpph respectively. In Case A2 and Case B2, the inlet water flow ratio is 20 and the flow rate is half of that in Case A1 and Case B1. Results show that under conditions where the inlet water flow ratio is high (Case A1 and Case B1), more than 30% of the total moisture in the flue gas can be recovered. However, when decreasing the water flow ratio to 20 as shown in Cases A2 and B2, the total ratio of recoverable moisture in the flue gas drops to 5%. This is because the moisture volume content in the flue gas is only about 11% in a power plant that has a typical basic configuration. The recovery rate will be higher in a power plant with a wet FGD. Such a system will be studied in the following sections.

Table 3-3. Heat and Water Recovery from TMC System on Coal-Fired Power Plant

Parameters			**Plant A**		**Plant B**	
			Case A1	**Case A2**	**Case B1**	**Case B2**
TMC Flue Gas Inlet	Flow Rate	kpph	4,547.4	4,547.4	2,114.0	2,114.0
	Temperature	°F	331.8	331.8	323.8	323.8
	Dew Point	°F	119.6	119.6	118.4	118.4
	Relative Humidity	%	1.6	1.6	1.7	1.7
	Moisture Content	vol%	11.4	11.4	11.0	11.0
	Moisture Content	wt%	7.1	7.1	6.8	6.8
TMC Flue Gas Outlet	Flow Rate	kpph	4,439.3	4,534.2	2,067.9	2,110.1
	Temperature	°F	108.8	120.3	108.4	119.5
	Dew point	°F	106.2	118.2	105.7	117.4
	Relative Humidity	%	90	90	90	90
	Moisture Content	vol%	7.8	11.0	7.7	10.7
	Moisture Content	wt%	4.8	6.8	4.8	6.7
TMC Water Inlet	Flow Rate Ratio		40	20	40	20
	Flow Rate	kpph	12,890	6,445	5,780	2,890
	Temperature	°F	70	70	70	70
TMC Water Outlet	Flow Rate	kpph	12,997.8	6,458.1	5,826.5	2,894.2
	Temperature	°F	98.8	110.3	98.4	109.5
Moisture Recovered Flow Rate		kpph	108.1	13.2	46	4.0
Transfer Rate		%	33.5	4.1	31.9	2.7

3.2.3 Heat Rate Improvement

Potential benefits of installing a TMC system in a coal-fired power plant are not only to recover the water but also to recover heat and increase the power plant efficiency. Using the efficiency analysis tool GTI developed, GTI can estimate the heat rate improvement when applying the TMC system. Table 3-4 shows the heat rate of the four cases listed in Table 3-3, as well as the baseline cases of the two plants (Case A0 and Case B0). The turbine heat rate was assumed to be the same as in the original operating condition. Typically, the two largest heat losses by firing PRB coal include dry gas losses and moisture losses. Other losses include unburned carbon, radiation, and manufacturer's margin unaccounted and sensible heat in fuel. Losses which are caused by radiation and manufacturer's margin unaccounted are empirical values. These other losses are assumed to be the same as the original operation data in this research.

As shown in Table 3-4, the heat rate will improve dramatically if all of the recovered water and heat can be reused. The original efficiency of Plant A's boiler was 85.7%, but with the application of a TMC system, the efficiency increases to 93.5% and 91.1% in Case A1 and Case A2 respectively. Similarly, for Plant B, boiler efficiency increases to 93.4% and 91.1% in Case B1 and Case B2 respectively from the original efficiency of 86.6%. The estimated unit heat rate would increase by 5% to 8% in these two plants. This is a significant contribution to CO_2 reduction and holds great potential in helping coal-fired power plants to meet or exceed ever more stringent emissions regulations.

Table 3-4. Heat Rate Improvement by Installing a TMC System

Parameters		**Plant A**			**Plant B**		
		Case A0	**Case A1**	**Case A2**	**Case B0**	**Case B1**	**Case B2**
Moisture Loss	%	7.9	5.0	7.1	7.0	5.0	7.1
Dry Gas Loss	%	5.6	0.7	1.0	5.5	0.8	1.0
Other Loss	%	0.8	0.8	0.8	0.8	0.8	0.8
Boiler Efficiency	%	85.7	93.5	91.1	86.6	93.4	91. 1
Unit Net Heat Rate	Btu/kWh	9,813	8,997	9,230	9,710	9,002	9,234
Heat Rate Improvement	%		8.3	6.0		7.3	4.9

3.3 Integration Study of TMC in Coal-Fired Power Plants with FGD

The analysis and results shown above indicate that integrating a TMC system directly into a coal-fired boiler with a basic configuration can increase the efficiency. However, such an approach may require a larger amount of TMC make-up water and a large heat exchange surface, which appears to cause some inefficiency. On the other hand, if there is a wet FGD system in the configuration of the coal-fired power plant, integrating the TMC system downstream from the FGD will be more efficient in terms of recovering water and improving heat rate. In this section, TMC integration in a coal-fired power plant with a FGD unit is investigated.

3.3.1 FGD System and Application Status

FGD is a set of technologies used to remove sulfur dioxide from exhaust flue gases of coal-fired utility boilers. These systems can be categorized as wet, semi-dry or dry scrubbers. There were 678 FGD systems operating on a total capacity of roughly 229 GW worldwide in 2000. Approximately 85% of FGD systems installed in the US are wet systems, 12% are spray dry (semi-dry) and 3% are dry systems. Wet FGD technology is a wet scrubbing process which is based on using limestone or lime as a reagent. The wet

FGD system is typically installed after the removal of particulate matter from the flue gas either by a baghouse or by an electrostatic precipitator. In typical absorber designs, the gas flows upward through the absorber countercurrent to the spray liquor flowing downward through the absorber. Figure 3-3 shows the process of FGD technology using limestone with forced oxidation (LSFO). Limestone slurry is pumped through banks of spray nozzles to atomize it in order to produce fine droplets and contact the gas uniformly. The droplets absorb SO_2 from the gas, facilitating the reaction of the SO_2 with reagent in the slurry. Some of the water in the spray droplets evaporates, cooling the gas at the inlet from approximately 300°F to 125-130°F. The evaporation also saturates the flue gas with water. The desulfurized flue gas passes through mist eliminators to remove entrained droplets before the flue gas is sent to the stack.

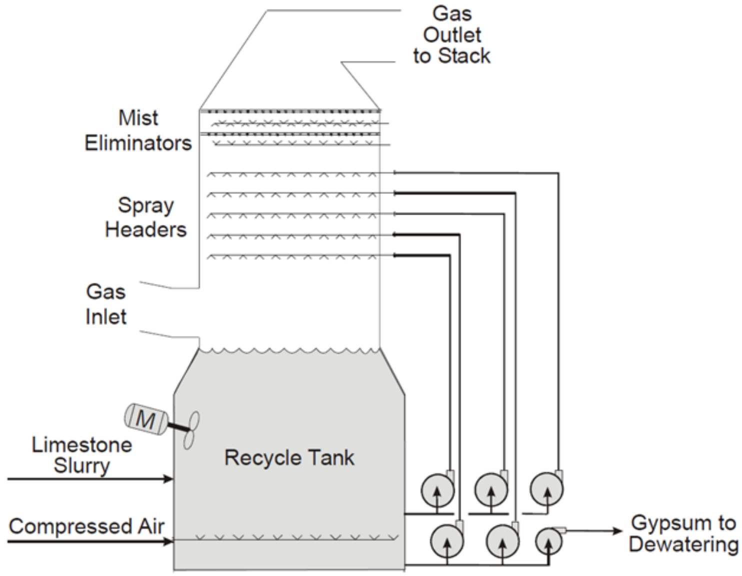

Figure 3-3. Typical Limestone with Forced Oxidation (LSFO) SO_2 Absorber

3.3.2 Integration Study of TMC in a Coal-Fired Boiler with Wet FGD

Using Modules I, II and III of the efficiency analysis tool, we were able to build models where performance of integrating TMC system downstream from the wet FGD in coal-fired power plants can be evaluated. As presented in Table 3-5 and Table 3-6, Case A0 and Case B0 show the original conditions of Plant A and Plant B respectively, which are used as baselines for comparison. Cases A3-A7 and Cases B3-B7 show the incorporation of the wet FGD and TMC systems. It assumed that the heat transfer process in the FGD system in Case A3-A5 is adiabatic and flue gas at FGD outlet saturated. Thus, FGD will add 209.7 kpph 70°F water into the flue gas of Plant A. Also the flue gas entering the TMC system will saturate at 136.6°F with 18% moisture content. This makes the TMC system more efficient in recovering flue gas moisture.

Comparing Case A3 with Case A1, recovering about the same amount (110 kpph and 108 kpph) of water, the TMC system needs 6,362 kpph of make-up inlet water, which is much less than the 12,890 kpph required in Case A1. In Case A4, the temperature of flue gas and recovered water from the TMC is 10°F higher than those in Case A3. This means the recovered water has higher enthalpy and better usability. Even though the transfer rate in Case A4 is lower than in Case A3, the TMC make-up water is about 1/3 of that required in Case A3. This means less heat exchanging surface would be required meaning less TMC modules would be needed saving costs. Case A5 was designed to evaluate the impact of TMC make-up/inlet water temperature. The temperature of the TMC inlet water in Case A5 is 10°F higher than it is in Case A3. It can be seen that the inlet water flow rate will increase but the transfer rate won't increase as much when the TMC inlet water temperature increases 10°F. This indicates that the lower the inlet water temperature, the better the TMC performance to be expected.

Table 3-5. Integration of FGD and TMC System in Plant A

			Case A0	Case A3	Case A4	Case A5	Case A6	Case A7
FGD Flue Gas Inlet	Flow Rate	kpph		4,547.4	4,547.4	4,547.4	4,547.4	4,547.4
	Temperature	°F		331.8	331.8	331.8	331.8	331.8
	Dew Point	°F		119.6	119.6	119.6	119.6	119.6
	Relative Humidity	%		1.6	1.6	1.6	1.6	1.6
	Moisture Content	vol%		11.4	11.4	11.4	11.4	11.4
	Moisture Content	wt%		7.1	7.1	7.1	7.1	7.1
FGD Water Inlet	Water Added	kpph		209.7	209.7	209.7	55.8	55.8
	Temperature	°F		70	70	70	70	70
FGD Flue Gas Outlet (TMC Flue Gas Inlet)	Flow Rate	kpph		4,757.1	4,757.1	4,757.1	4,603.3	4,603.3
	Temperature	°F		136.6	136.6	136.6	125	135
	Dew Point	°F		136.6	136.6	136.6	125	125
	Relative Humidity	%		100.0	100.0	100.0	100.0	76.6
	Moisture Content	vol%		18.0	18.0	18.0	13.2	13.2
	Moisture Content	wt%		11.2	11.2	11.2	8.2	8.2
TMC Flue Gas Outlet	Flow Rate	kpph		4,531.4	4,645.3	4,531.4	4,531.3	4,531.3
	Temperature	°F		120	130	120	120	120
	Dew point	°F		117.9	128.6	117.9	117.9	117.9
	Relative Humidity	%		90.0	90.0	90.0	90.0	90.0
	Moisture Content	vol%		10.9	14.6	10.9	10.9	10.9
	Moisture Content	wt%		6.8	9.0	6.8	6.8	6.8
TMC Water Inlet	Flow Rate Ratio			12.0	4.6	15.9	5.3	6.1
	Flow Rate	kpph		6,362	2,468	8,483	2,010	2,304
	Temperature	°F		70	70	80	70	70
TMC Water Outlet	Flow Rate	kpph		6,587.4	2,579.6	8,708.6	2,082.1	2,375.9
	Temperature	°F		110	120	110	110	110
Moisture Recovered Flow Rate		kpph		225.8	111.9	225.8	72.0	72.0
Transfer Rate		%		42.4	21.0	42.5	19.0	19.0
Efficiency								
Moisture Loss		%	7.9	7.1	9.6	7.0	7.0	7.0
Dry Gas Loss		%	5.6	1.0	1.2	1.0	1.0	1.0
Loss in FGD		%	0.0	0.0	0.0	0.0	3.8	3.6
Other Loss		%	0.8	0.8	0.8	0.8	0.8	0.8
Boiler Efficiency		%	85.7	91.1	88.4	91.2	87.4	87.6
Unit Net Heat Rate		Btu/kWh	9,813	9,226	9,509	9,217	9,625	9,598
Heat Rate Improved		%		6.0	3.1	6.1	1.9	2.2

Table 3-6. Integration of FGD and TMC System in Plant B

			Case B0	Case B3	Case B4	Case B5	Case B6	Case B7
FGD Flue Gas Inlet	Flow Rate	kpph		2,114	2,114	2,114	2,114	2,114
	Temperature	°F		323.8	323.8	323.8	323.8	323.8
	Dew Point	°F		118.4	118.4	118.4	118.4	118.4
	Relative Humidity	%		1.7	1.7	1.7	1.7	1.7
	Moisture Content	vol%		11.0	11.0	11.0	11.0	11.0
	Moisture Content	wt%		6.8	6.8	6.8	6.8	6.8
FGD water Inlet	Water Added	kpph		93.9	93.9	93.9	31.7	31.7
	Temperature	°F		70	70	70	70	70
FGD Flue Gas Outlet (TMC Flue Gas Inlet)	Flow Rate	kpph		2,208	2,208	2,208	2,146	2,146
	Temperature	°F		135.3	135.3	135.3	125	135
	Dew Point	°F		135.3	135.3	135.3	125	125
	Relative Humidity	%		100.0	100.0	100.0	100.0	76.6
	Moisture Content	vol%		17.4	17.4	17.4	13.2	13.2
	Moisture Content	wt%		10.8	10.8	10.8	8.2	8.2
TMC Flue Gas Outlet	Flow Rate	kpph		2,112	2,165	2,112	2,112	2,112
	Temperature	°F		120	130	120	120	120
	Dew point	°F		117.9	128.6	117.9	117.9	117.9
	Relative Humidity	%		90.0	90.0	90.0	90.0	90.0
	Moisture Content	vol%		10.9	14.6	10.9	10.9	10.9
	Moisture Content	wt%		6.8	9.0	6.8	6.8	6.8
TMC Water Inlet	Flow Rate Ratio			11.3	3.9	15.1	5.3	2.9
	Flow Rate	kpph		2,598	938	3,597	937	509
	Temperature	°F		70	70	80	70	70
TMC Water Outlet	Flow Rate	kpph		2,793	981	3,692	971	542
	Temperature	°F		110	120	110	110	110
Moisture Recovered Flow Rate		kpph		95.7	42.6	96	33.5	33.5
Transfer Rate		%		40.1	17.9	40.1	19.0	19.0
Efficiency								
Moisture Loss		%	7.0	7.2	9.8	7.2	7.2	7.2
Dry Gas Loss		%	5.5	1.0	1.2	1.0	1.0	1.0
Loss in FGD		%	0.0	0.0	0.0	0.0	3.4	3.2
Other Loss		%	0.8	0.8	0.8	0.8	0.8	0.8
Boiler Efficiency		%	86.6	91.0	88.1	91.0	87.6	87.8
Unit Net Heat Rate		Btu/kWh	9,710	9,239	9,543	9,241	9,606	9,578
Heat Rate Improved		%		4.9	1.7	4.8	1.1	1.4

The results shown in Cases A3-A5 and Cases B3-B5 are based on the assumption that no heat was lost in the FGD. Cases A6-A7 and Cases B6-B7 are designed to analyze the situation where heat loss has occurred in the FGD. It is typical for a wet FGD to have a flue gas outlet temperature of 125°F to 130°F. In Case A6, it was assumed that the wet FGD flue gas outlet saturated at a temperature of 125°F. There was an extra 3.8% heat loss in the FGD of Case A6 compared to Case A3. Also, the transfer rate and saved heat rate is much lower. In Case A7, it is assumed that the flue gas from the FGD outlet does not saturate, and the dew point is 10°F lower than the gas temperature. Again, the moisture transfer rate and saved heat rate of the power plant decreased. In conclusion, keeping the FGD in good working condition is very important to achieving the best performance of the TMC system. Plant B shows similar results as presented in Table 3-6.

4. CFD Simulation for TMC Design

Numerical simulation of pilot-scale TMC units based on an accurate model is performed in this project to define TMC design parameters, optimize the designs, and determine a TMC design that can achieve the best performance for this power plant flue gas waste heat and water recovery technology. The model needs to be able to simulate heat and mass transfer inside the TMC unit and predict important parameters such as total heat transfer, condensation rate and pressure drop along the TMC unit. In the second step of this project, a parametric study has been done to investigate the effect of various parameters such as transversal and longitudinal pitches of TMC tubes, inlet velocity of the flue gas and inlet mass fraction of the water vapor on the TMC overall performance.

4.1 Modeling for a TMC Unit

In this section, the governing equations and physical parameters influencing the condensation and heat transfer over the TMC membrane walls are presented. The thermodynamic relation and properties of materials are also presented.

4.1.1 Thermodynamic properties of mixtures and species

In terms of water vapor, air and mixture properties, different authors have made various assumptions for their numerical simulations in the literature. As an example, Benelmir et. al. [8] considered the mixture of air/vapor as an ideal incompressible Newtonian flow. They also neglected the effects of radiation and viscous dissipation. They used the following physical properties for the air: $D_v = 2.065\times10^{-5}\ m^2\ s^{-1}$; $k = 0.0242\ W\ m^{-1}\ K^{-1}$; $c_p = 1{,}013.484\ J\ kg^{-1}\ K^{-1}$; $\rho = 1.219\ kg\ m^{-3}$; $\mu = 1.785\times10^{-5}\ kg\ m^{-1}\ s^{-1}$ and $Pr = 0.747$.

In this work, all of the thermodynamic properties of the water vapor and other non-condensable species are considered to be a function of temperature. During the numerical simulation different properties of the mixture need to be calculated in the solution domain. The thermodynamic properties of the mixture can be calculated using corresponding equations.

4.1.2 Governing Equations

The basic governing equations include mass, momentum, turbulence, and energy conservation equations for fluid flow. They are listed as below:

Continuity:

$$\frac{\partial\rho}{\partial t}+\nabla.\left(\rho\vec{\mathbf{u}}\right)=0 \tag{1}$$

Momentum:

$$\frac{\partial}{\partial t}\left(\rho\vec{\mathbf{u}}\right)+\nabla.\left(\rho\vec{\mathbf{u}}\vec{\mathbf{u}}\right)=-\nabla p+\nabla.(\bar{\tau})+\rho\vec{g}+\vec{F} \tag{2}$$

Where

$$\bar{\tau}=\mu\left[\left(\nabla\vec{\mathbf{u}}+\nabla\vec{\mathbf{u}}^{T}\right)-\frac{2}{3}\vec{\mathbf{u}}I\right] \tag{3}$$

Energy:

$$\frac{\partial}{\partial t}\left(\rho E\right)+\nabla.\left(\vec{\mathbf{u}}\left(\rho E+p\right)\right)=\nabla.\left(\lambda_{eff}\nabla T-\sum_{j}h_j\vec{J}_j+\left(\bar{\tau}_{eff}.\vec{\mathbf{u}}\right)\right)+S_h \tag{4}$$

Where $\rho\vec{g}$ and $\vec{F}$ are the gravitational body forces and external body forces, respectively. λ_{eff} is the effective thermal conductivity ($\lambda+\lambda_t$, where λ_t is the turbulent thermal conductivity). μ_t is the turbulent viscosity. Both λ_t and μ_t are defined according to the turbulence model. $\overline{\tau}_{eff}$ is the effective stress tensor. $\vec{J}_j$ is the diffusion flux of species *j*. *E* is the total energy including enthalpy *h*, flow work $-p/\rho$, and kinetic energy $|\mathbf{u}|^2/2$. And, S_h is a source term.

The multi-species transport which occurs in the flue gas mixture is governed by the following equation:

$$\frac{\partial}{\partial t}(\rho Y_i)+\nabla.\left(\rho\vec{\mathbf{u}}Y_i\right)=-\nabla.\vec{J}_i+R_i+S_i \tag{5}$$

where, Y_i is the mass fraction of the species being calculated, S_i is the rate of creation source term and R_i is the net rate of production by chemical reaction of the species being calculated.

4.1.3 Turbulence Models

The $k-\omega-SST$ model [9] has been employed to simulate heat and mass transfer in turbulent flow regime. The shear-stress transport (SST) $k-\omega$ model gradually changes from the standard $k-\omega$ model in the inner region of the boundary layer to a high-Reynolds-number version of the $k-\varepsilon$ model in the outer part of the boundary layer. The SST $k-\omega$ model was developed to effectively blend the robust and accurate formulation of the $k-\omega$ model in the near-wall region with the free-stream independence of the $k-\varepsilon$ model in the far field. To achieve this, the $k-\varepsilon$ model is converted into a $k-\omega$ formulation. These features make the SST $k-\omega$ model more accurate and reliable for a wider class of flows (e.g., adverse pressure gradient flows, airfoils, transonic shock waves) than the standard $k-\omega$ model.

The SST $k-\omega$ model has a similar form as the standard $k-\omega$ model:

$$\frac{\partial}{\partial t}(\rho k)+\frac{\partial}{\partial x_i}(\rho k u_i)=\frac{\partial}{\partial x_j}\left(\Gamma_k\frac{\partial k}{\partial x_j}\right)+\widetilde{G_k}-Y_k+S_k \tag{6}$$

$$\frac{\partial}{\partial t}(\rho\omega)+\frac{\partial}{\partial x_i}(\rho\omega u_i)=\frac{\partial}{\partial x_j}\left(\Gamma_\omega\frac{\partial \omega}{\partial x_j}\right)+G_\omega-Y_\omega+D_\omega+S_\omega \tag{7}$$

In these equations, $\widetilde{G_k}$ resents the generation of turbulence kinetic energy due to mean velocity gradients and G_ω represents the generation of ω. Γ_k and Γ_ω represent the effective diffusivity of k and ω, respectively. D_ω represents the cross-diffusion term, and S_k and S_ω are user-defined source terms.

The effective diffusivities for the SST $k-\omega$ model are given by

$$\Gamma_k=\mu+\frac{\mu_t}{\sigma_k} \tag{8}$$

$$\Gamma_\omega=\mu+\frac{\mu_t}{\sigma_\omega} \tag{9}$$

Where σ_k and σ_ω are the turbulent Prandtl numbers for k and ω, respectively. The turbulent viscosity, μ_t is computed as follows

$$\mu_t=\frac{\mu_t}{\omega}\frac{1}{\max\left[\frac{1}{\alpha^*},\frac{SF_2}{\alpha_1\omega}\right]} \tag{10}$$

Where S is the strain rate magnitude and

$$\sigma_k = \frac{1}{F_1/\sigma_{k,1} + (1-F_1)/\sigma_{k,2}} \tag{11}$$

$$\sigma_\omega = \frac{1}{F_1/\sigma_{\omega,1} + (1-F_1)/\sigma_{\omega,2}} \tag{12}$$

The blending functions, F_1 and F_2, are given by

$$F_1 = \tanh(\phi_1^4) \tag{13}$$

$$\phi_1 = \min\left[\max\left(\frac{\sqrt{k}}{0.09\omega y}, \frac{500\mu}{\rho y^2 \omega}\right), \frac{4pk}{\sigma_{\omega,2} D_\omega^+ y^2}\right] \tag{14}$$

$$D_\omega^+ = \max\left(2\rho \frac{1}{\sigma_{\omega,2}} \frac{1}{\omega} \frac{\partial k}{\partial x_j} \frac{\partial \omega}{\partial x_j}, 10^{-10}\right) \tag{15}$$

$$F_2 = \tanh(\phi_2^4) \tag{16}$$

$$\phi_2 = \max\left[2\frac{\sqrt{k}}{0.09\omega y}, \frac{500\mu}{\rho y^2 \omega}\right] \tag{17}$$

Where, y is the distance to the next surface and D_ω^+ is the positive portion of the cross-diffusion term.

The term $\tilde{G}_k$: represents the production of turbulence kinetic energy, and is defined as:

$$\tilde{G}_k = \min(G_k, 10\rho\beta^* k\,\omega) \tag{18}$$

Where G_k is defined in the same manner as in the standard $k-\omega$ model. The term G_ω represents the production of ω and is given by:

$$G_\omega = \frac{\alpha}{v_t} G_k \tag{19}$$

Note that this formulation differs from the standard $k-\omega$ model. The difference between the two models also exists in the way the term α_∞ is evaluated. In the standard $k-\omega$ model, α_∞ is defined as a constant (0.52). For the SST $k-\omega$ model, α_∞ is given by

$$\alpha_\infty = F_1 \alpha_{\infty,1} + (1-F_1)\alpha_{\infty,2} \tag{20}$$

Where

$$\alpha_{\infty,1} = \frac{\beta_{i,1}}{\beta_\infty^*} + \frac{\kappa^2}{\sigma_{\omega,1}\sqrt{\beta_\infty^*}} \tag{21}$$

$$\alpha_{\infty,2} = \frac{\beta_{i,2}}{\beta_\infty^*} + \frac{\kappa^2}{\sigma_{\omega,2}\sqrt{\beta_\infty^*}} \quad , \quad \kappa = 0.41 \tag{22}$$

The term Y_k represents the dissipation of turbulence kinetic energy, and is defined in a similar manner as in the standard $k-\omega$ model. The difference is in the way the term $f_\beta{}^*$ is evaluated. In the standard $k-\omega$ model, $f_\beta{}^*$ is defined as a piecewise function. For the SST $k-\omega$ model, $f_\beta{}^*$ is a constant equal to 1. Thus,

$$Y_k = \rho\beta^* k\,\omega \tag{23}$$

The term Y_ω represents the dissipation of ω, and is defined in a similar manner as in the standard $k-\omega$ model. The SST $k-\omega$ model is based on both the standard $k-\omega$ model and the standard $k-\varepsilon$ model. To blend these two models together, the standard $k-\varepsilon$ model has been transformed into equations based on k and ω, which leads to the introduction of a cross-diffusion term (D_ω). D_ω is defined as

$$D_\omega = 2(1-F_1)\rho\sigma_{\omega,2}\frac{1}{\omega}\frac{\partial k}{\partial x_j}\frac{\partial \omega}{\partial x_j} \tag{24}$$

The model constants are [10]:
$\alpha_{k,1} = 1.176$, $\sigma_{\omega,1} = 2.0$, $\alpha_{k,2} = 1.0$, $\sigma_{\omega,2} = 1.168$, $a_1 = 0.31$, $\beta_{i,1} = 0.075$, $\beta_{i,2} = 0.0828$. All additional model constants ($\alpha_\infty^*, \alpha_\infty, \alpha_0, \beta_\infty^*, R_\beta, R_k, R_\omega, \varsigma^*$ and M_{t0}) have the same values as for the standard $k-\omega$ model.

4.1.4 Wall condensation using fully resolved boundary layer approach

The basic assumption in the implementation of this approach can be found in [11]. In this approach it is assumed that the condensation rate is governed by the rate of diffusion of condensable gases toward the cold surface. In case of water vapor as the condensable species, the mass fluxes for the non-condensable gas and water vapor at the liquid-vapor interface include both convective and diffusive components. Hence, :

$$\dot{m}_{nc}^{"} = \rho W_{nc} v - \rho D \frac{\partial W_{nc}}{\partial n} \tag{25}$$

$$\dot{m}_{s}^{"} = \rho W_{s} v - \rho D \frac{\partial W_{s}}{\partial n} \tag{26}$$

Where W are the mass fractions, v the mixture velocity, ρ is the mixture density, D is the mass diffusion coefficient, and n the normal direction to the wall (liquid film). Using the fact that the mass fractions of the mixture add up to unity, the mixture mass flux at the liquid–vapor interface can be written as:

$$\dot{m}^{"} = \dot{m}_{nc}^{"} + \dot{m}_{s}^{"} = \rho v \tag{27}$$

Since the interface is impermeable to the non-condensable gas:

$$\dot{m}_{nc}^{"} = 0 \tag{28}$$

Hence the mass flux of water vapor condensing at the wall is:

$$\rho v = \dot{m}_{s}^{"} = \frac{1}{\left(W_s - 1\right)} \rho D \frac{\partial W_s}{\partial n} \tag{29}$$

The above equation can also be derived by a different way [12]. Using the mass balance of steam at the interface one can write:

$$\textit{condensation flux} \;=\; \textit{steam transported with bulk motion} + \textit{diffusive transport} \tag{30}$$

Assuming the wall condensation flux:

$$\textit{condensation flux} \;=\; n_i \tag{31}$$

The bulk motion of the gas to the interface is also equal to n_i . The flux of steam that is transported with the bulk motion is:

$$\textit{steam transported with bulk motion} \;=\; n_i x_i \tag{32}$$

Where, x_i is the steam mass fraction at the interface. In a stagnant fluid, the diffusive mass transfer between mass fractions x and x_i is equal to:

$$\textit{diffusive transport} \;=\; g_m\left(x - x_i\right) \tag{33}$$

Where, g_m is the mass transfer coefficient. Substituting these equations in the mass balance results in

$$n_i = n_i x_i + g_m \left(x - x_i \right) \tag{34}$$

Rearranging this equation results in

$$n_i = g_m \frac{x - x_i}{1 - x_i} \tag{35}$$

Consequently, the driving force (B_D) for steam condensation is equal to

$$B_D = \frac{x - x_i}{1 - x_i}$$

The mass transfer coefficient (g_m) is a function of the turbulence near the wall, and is calculated as:

$$n_i = g_m \frac{x_{cell} - x_{wall}}{1 - x_{wall}} \tag{36}$$

If the cells near the walls are sufficiently narrow, the mass transfer coefficient reduces to laminar transport:

$$g_m = \frac{\rho D}{y} \tag{37}$$

The mass fraction x_{wall} of steam at the surface of the condensate film (or possibly water strokes) at the wall is calculated from the vapor pressure at the surface. The Antoine equation is used to describe the vapor pressure as a function of the surface temperature:

$$\ln\left(\frac{P}{1Pa} \right) = A + \frac{B}{T + C} \tag{38}$$

The coefficients A, B and C are fitted on data from steam tables. The result of this fitting process is A= +23.1512, B= −3788.02 K, and C= −47.3018 K. In condensation mass flux calculation, ρ and D are the mixture density and diffusion coefficient, respectively.

The condensation rate can be implemented as a sink in the continuity equation of cells adjacent to the cold wall:

$$\dot{m}'' = \dot{m}_s'' \frac{A_{cell-wall}}{V_{cell}} \tag{39}$$

Where, $A_{cell-wall}$ is the area of the cell on the wall and V_{cell} is the cell volume. In the simulation algorithm, it is assumed that condensation takes place if the wall temperature is less than or equal to the saturation temperature corresponding to the partial pressure of water vapor at the wall-adjacent cell. If the wall temperature is above the saturation temperature for given partial pressure of the vapor, the water vapor mass fraction at the wall is set to a value equal to the value in the wall adjacent cell. The partial pressure of the vapor in a mixture can be calculated using the following equations:

$$P_v = P_{mix} \frac{M_{mix} Y_v}{M_v} \tag{40}$$

Where, M_{mix} is the mixture molar mass, Y_v is the mass fraction of water vapor and M_v is the water vapor molar mass. In order to satisfy the local equilibrium assumption above, if the temperature is less than or equal to the saturation temperature, the water vapor mass fraction at the wall is assigned a value corresponding to the vapor saturation pressure at the local wall temperature. To close the problem, it requires that the rate at which species enters (or leaves) the computational domain is identical to the net rate at which mass enters (or leaves) the computational domain. In order to achieve this, the source term in the species equations at the wall adjacent cell must take the diffusive flux into account:

$$\dot{m}_s'' V_{cell} = \rho v W_s A_{cell-wall} - \rho D \frac{\partial W_s}{\partial n} A_{cell-wall} \tag{41}$$

Hence the sink term in the continuity equation for the cells adjacent to the walls is:

$$\dot{m}'' = \frac{1}{(W_s - 1)} \rho D \frac{\partial W_s}{\partial n} \frac{A_{cell-wall}}{V_{cell}} \tag{42}$$

A corresponding sink term needs to be included in the water vapor species equation:

$$\dot{m}_s'' = \dot{m}'' W_s \tag{43}$$

$$\dot{m}_s'' = \frac{W_s}{(W_s - 1)} \rho D \frac{\partial W_s}{\partial n} \frac{A_{cell-wall}}{V_{cell}} \tag{44}$$

The other volumetric sinks terms include velocity, energy and turbulence sink terms for the cells adjacent to the condensing walls:

$$S_{j-mom} = U_j \frac{\dot{m}_s''}{W_{s,i}} \tag{45}$$

$$S_E = h_{fg} \frac{\dot{m}_s''}{W_{s,i}} \tag{46}$$

$$S_k = k_{cell} \frac{\dot{m}_s''}{W_{s,i}} \tag{47}$$

$$S_\omega = \omega_{cell} \frac{\dot{m}_s''}{W_{s,i}} \tag{48}$$

$$S_\varepsilon = \varepsilon_{cell} \frac{\dot{m}_s''}{W_{s,i}} \tag{49}$$

Where, S refers to the volumetric sinks, U_j to the mixture velocity in the jth direction, h_{fg} to the vapor latent enthalpy and k, ε and ω are the turbulent kinetic energy, dissipation and dissipation rate. It should be pointed out that the energy sink term is applied on the near-wall cells in the cases of adiabatic walls.

4.1.5 Key Parameters and Conditions for TMC CFD Simulation

The simplified numerical model for simulation and heat and mass transfer inside a TMC unit is developed in this section. The modeling method is based on the condensation model on a solid wall, in which some correction factor has been implemented for applications in TMC tubes. These correction factors are obtained based on the previous lab-scale experimental results.

a) Key dimensions and schematic of the experimental apparatus:

The experimental setup for the lab scale TMC unit was equipped with pressure, humidity, temperature, flow rate measurements and complete gas analysis [3]. The measured data during the experiments were collected and stored using the data acquisition system in the setup. The amount of recovered water was obtained from the difference between the inlet and outlet humidity of the flue-gas as it passes through the TMC module. The TMC unit was installed horizontally and the flue-gas was flowing upward through the TMC tubes banks. The TMC unit has 78 identical TMC tubes with a length of 18 inches. The schematic and key dimensions of the test section with the symmetry plane is shown in Figure 4-1 and Table 4-1. Moreover the tube sizes and pitches for the lab scale TMC is shown is Table 4-2.

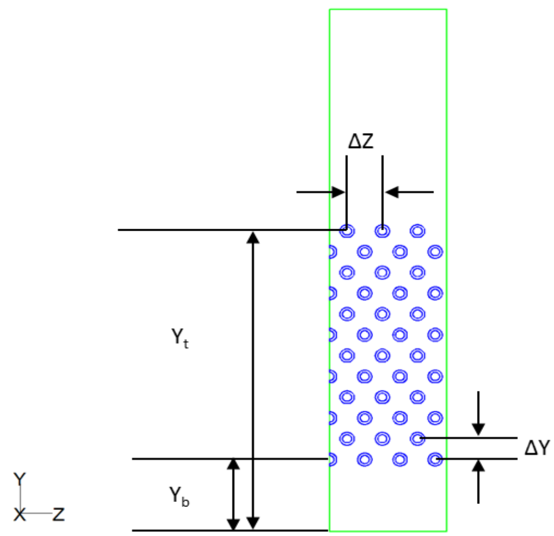

Figure 4-1. Schematic of the tube arrangement.

Table 4-1. Key dimensions of the test section.

Coordinate	Direction	Dimension (inch)
X	Water flow direction	17
Y	Flue gas flow direction	8.7
Z	From the center symmetric plane to the side wall	1.7875

Table 4-2. Key dimensions of the tubes and bundle arrangement.

		Dimension (inch)
The ceramic tube	Inside Diameter (ID)	0.138
	Outside Diameter(OD)	0.216
	The thickness of the tube wall	0.039
The arrangement of the tubes	Tube spacing in Y direction ΔY (center to center)	0.346
	Tube spacing in Z direction ΔZ (center to center)	0.536
	The bottom row of tubes location Y_b from inlet	1.200
	The top row of tubes location Y_t from inlet	5.006

b) Boundary conditions and thermodynamic properties:

Table 4-3 shows the boundary condition list for the numerical simulation setup. A single phase multi-species transport model [13] was used to predict the heat and water transfer inside the TMC unit.

Table 4-3. Summary of the different zones and boundary conditions in the numerical setup.

Location	Zone name	Zone type
Flue-gas zone	Flue-gas	Mixture
Water zone	Water	Mixture
Membrane zone	Porous	Mixture-porous
Flue-gas flow inlet	Inlet flue-gas	Velocity-inlet
Flue-gas flow outlet	Outlet flue-gas	Pressure-outlet

Water flow inlet	Inlet water	Velocity-inlet
Water flow outlet	Outlet water	Pressure-outlet
Central symmetric surface	Symmetry-porous Symmetry-water Symmetry flue-gas	Symmetry
Tube inside surface	Porous-water-interior	Interior
Tube outside surface	Flue-gas porous wall	Wall (conjugate boundary condition)
Side Wall	Side wall flue-gas Side wall porous	Wall (Adiabatic thermal condition)

The interface wall between the porous and zones are changed to the interior type to make the water transfer from the Flue-gas zone to the porous zone and from that to the water zone possible. The date related to a typical experimental setup for the TMC module test at GTI's lab is shown in Table 4-4.

Table 4-4. Typical experimental results for the lab scale TMC rig.

Case No.	48	
Gas Flow rate (SCFH)	201.6	
O_2 at stack (%)	3.84	F_{o2}
Vacuum(psi)	-3	P_{vacuum}
Flue gas flow rate(SCFH)	2551	RF_{flue}
Water flow rate(gpm)	0.34	RF_{water}
Flue Inlet Temp (^oF)	200	T_{fluein}
Flue Outlet Temp (^oF)	137.6	$T_{flueout}$
Water Inlet Temp (^oF)	100.2	$T_{waterin}$
Water Outlet Temp (^oF)	129.3	$T_{waterout}$
Vapor Transportation Rate (%)	24.4	
Flue inlet dew point(^oF)	134.75	T_{din}
Flue inlet relative humidity (%)	21.93	V_{in}
Flue outlet dew point(^oF)	124.8	T_{dout}
Flue outlet relative humidity (%)	69.9	V_{out}

The flue-gas flow inlet temperature T_{fluein} is obtained from experimental data, and velocity U_{flue} is calculated using the following equation, from the volume flow rate of the flue-gas RF_{flue}.

$$U_{flue} = \frac{\dot{V}}{Area} = \frac{RF_{flue}(SCFH)}{2\times 3600} \times \frac{(460+T_{fluein})}{(460+80)} \times \frac{1}{1.7875/12\times 17/12} \tag{50}$$

The inlet velocity of water U_{water} is calculated using the following equation RF_{water}.

$$U_{water} = \frac{\dot{V}}{Area} = \frac{RF_{water}(GPM)\times 3.785\times 10^{-3}(m^{-3}/gallon)}{60\times 78\times \pi \times (3.5\times 10^{-3}/2)^2} \times 3.2808(ft/meter) \tag{51}$$

The outlet pressure for the water and the flue gas are P_{vacuum} and atmosphere, respectively. The flue-gas inlet species mass fraction is shown in Table 4-5. There are four species in the flue gas, vapor, O_2, CO_2

and N_2. The vapor fraction of vapor F_{vapor} is calculated from the flue inlet dew point T_{din}. The O_2 fraction comes from the experimental data, and the mass fraction of N_2 can be calculated by subtracting the sum of the specified mass fractions from 1.

Table 4-5. Inlet mass fraction of different species for the flue-gas.

Species	Mass Fraction
H_2O (vapor)	F_{vapor}
O_2	F_{o2}
CO_2	9%
N_2	Balance of 100%

As mentioned previously, the thermodynamic properties of the mixture are calculated based on the thermodynamic properties of each species and the mass fraction for them in the mixture. The thermodynamic properties of the water vapor has already been implemented in the numerical setup and been used for validation of the condensation model on the solid wall. Thermodynamic properties of the other non-condensable species, i.e. N_2, O_2 and CO_2 are obtained from the NIST data base [14]. These properties have been implemented in the numerical method using 5 point piecewise-linear function for the temperature variation range of the experiment. The temperature range for the experimental data is between 68 to 200 (^oF) which are the maximum flue-gas inlet and minimum cooling water inlet temperatures.

The other important property in simulation of condensation process is the diffusion coefficient of different species including the condensing species. The condensation rate on a solid wall is directly related to the diffusion coefficient of the condensing species. For the condensation of water vapor in a multi-species mixture the kinetic theory was used to calculate the diffusion coefficient.
The thermophysical properties of the TMC tubes need to be calculated and applied in the numerical simulation. Table 4-6 [1] [15] show the thermophysical properties of the TMC tubes.

Table 4-6. Dimensions and physical properties of different types of TMC tubes.

Material	**Ceramic**
ID (inch)	0.138
OD (inch)	0.216
Density (kg m^{-3})	3790
heat capacity (J K^{-1} kg^{-1})	775
Solid material thermal conductivity (W m^{-1} K^{-1})	30
Porosity	20%
Porous substrate pore size	$4\mu m$

The effective thermal conductivity for the TMC tube will be obtained based on the following equation:

$$k_{eff} = \gamma k_f + (1-\gamma) k_s \tag{52}$$

Where γ is the porosity of the medium, k_f is the fluid phase thermal conductivity and k_s is the solid medium thermal conductivity. Viscous resistance coefficient ($1/\alpha$) is one of the parameters which needs to be determined in the Fluent setup and α is the permeability of the porous medium. Permeability of the porous medium can be calculated using the following equation:

$$\alpha = \frac{\gamma d_p^2}{72(1-\gamma)^2 \tau} \tag{53}$$

where, τ is the tortuosity of the porous medium and can be obtained using the following equation [16]:

$$\tau = 1 - \frac{1}{2}\ln(\gamma) \tag{54}$$

By using the specification of the TMC tubes the value of viscous resistance coefficient is $3.24{\times}10^{11}$.

4.1.6 Validation studies for TMC CFD simulations

a) Model implementation

One of the options for modeling the condensation processes on the TMC tube surface is to use the solid wall based condensation model, with appropriate correction factors that are determined based on the lab-scale experimental data. The data series based on the lab scale TMC heat exchanger setup is shown in Figure 4-2. As seen in the figure the heat and mass transfer coefficients for the lab scale TMC and stainless-steel heat exchangers follow the same trend. For both types of tubes the mass transfer (condensation rate) and heat transfer coefficients are decreasing as the average cooling water or interface temperature increased. By comparison of the performance of the TMC unit with the stainless-steel heat exchanger it can be concluded that using the solid wall condensation model by incorporating some correction factors is feasible.

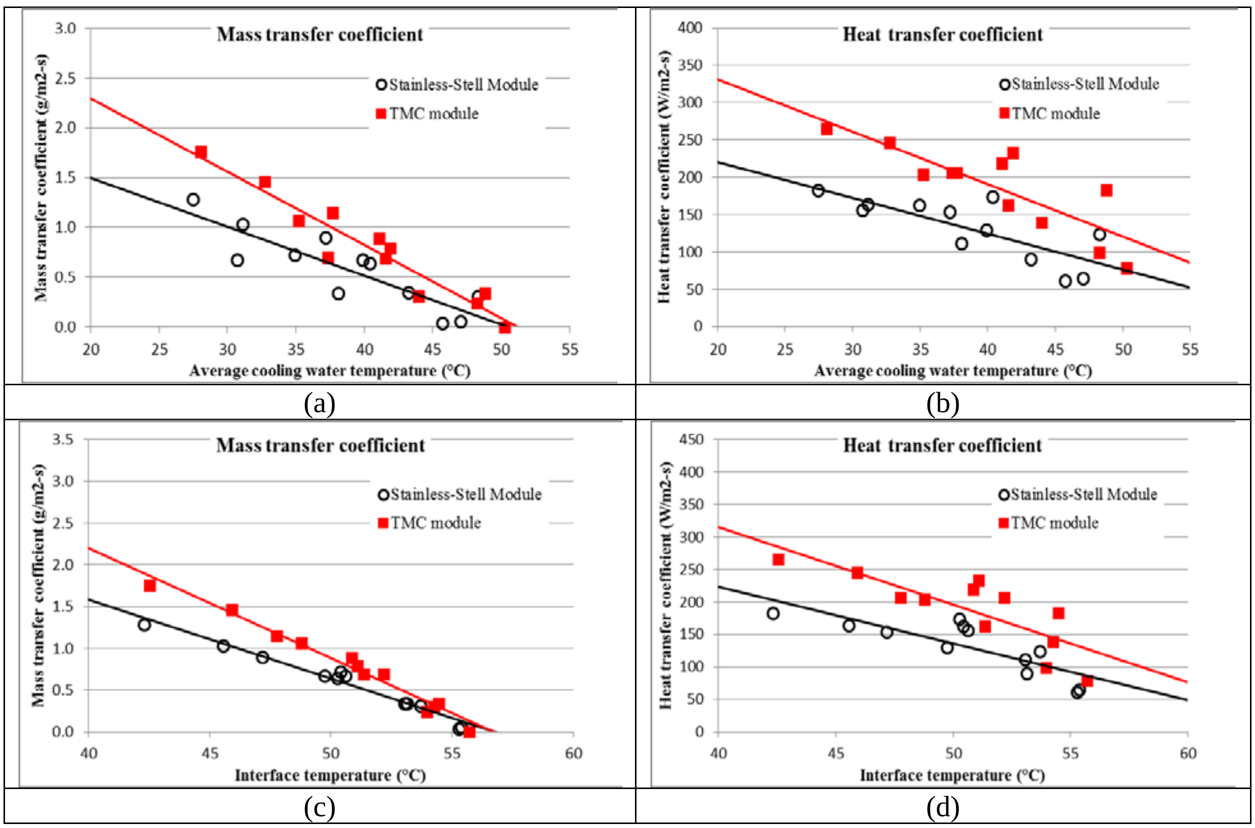

Figure 4-2. Heat & mass transfer coefficient for a lab scale TMC and a SS heat exchanger

To adapt the solid wall condensation model for the TMC tubes the following points need to be taken into the account:

1- Based on the Kelvin equation, condensation in nano-pores occurs for partial pressure of the condensing species lower than its vapor pressure.

2- The condensation rate on the surface of the TMC tubes needs to be adjusted based on the available experimental data points.

To address the aforementioned points the condensation rate has been modified using the following equation:

$$\dot{m}'' = C_1 \frac{1}{(W_s - 1)} \rho D \frac{\partial W_s}{\partial n} \frac{A_{cell-wall}}{V_{cell}} \quad (55)$$

Where, the constant C_1 is obtained from the available experimental results. Moreover the criteria for the starting point of condensation rate (vapor saturation pressure at the local wall temperature) have been modified by implementing the second correction factor C_2. Figure 4-3 shows the schematics of different zones and domains which have been used for the numerical setup. The condensation rate in the flue-gas side is calculated using the modified equation which includes the correction factors. The sink terms which have been used for the condensation rates in the flue gas domain include the mass, species, momentum and turbulent sinks.

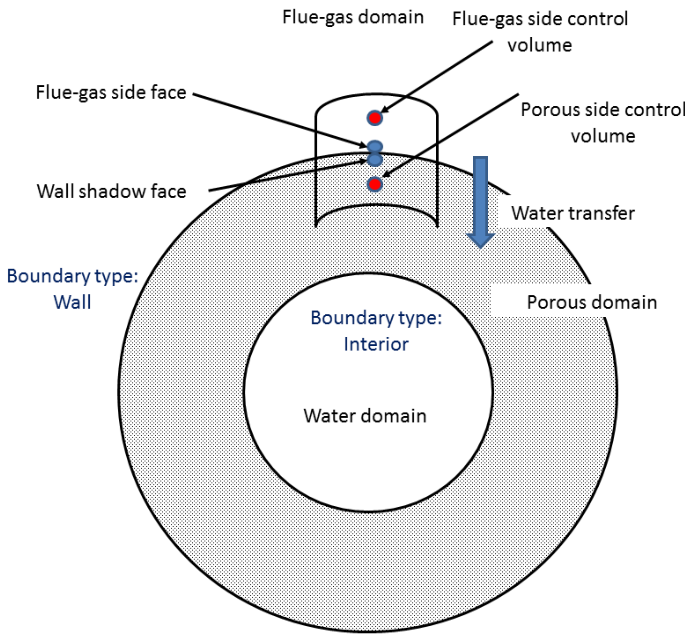

Figure 4-3. Schematic of different zones and domains specified in the numerical setup

To apply the water and energy transfer from the flue-gas side to the porous wall in the numerical setup, the pertinent source terms need to be applied on the cells adjacent to the wall in the porous zone. The source terms include mass, species and energy sources. It should be noted the species sources has been added to the liquid water transport equation, while in the flue-gas side the species sink term was applied on the water vapor equation. Moreover the heat source has been applied only on the porous wall side. This is consistent with using the wall as an infinite reservoir [17]. User Defined Functions (UDFs) have been used in the numerical simulations, and transport of the condensed water from the porous domain to the cooling water domain is implemented by converting the interface type of the two domains from the wall to interior.

Simulation of the heat and mass transfer inside the TMC has been done using ANSYS Fluent V16. A single multi-species transport model was used to model the transport equations of different species in the computational domain. The second order upwind discretization scheme is used for the special discretization for all of the governing equations except the turbulent equations. The coupled algorithm is used for pressure velocity coupling with appropriate Courant number and under relaxation. The convergence criteria are set to 10^{-8} for the scaled residual of all transport equations. The outlet parameters, i.e. the cooling water outlet temperature, flue-gas outlet temperature and condensation rate are monitored to confirm the solution convergence. The User Defined Functions (UDFs) are mounted to the solution setup to account for the condensation and water transfer process and the User Defined Memories (UDMs) are used to store the calculated values between the UDFs. The boundary conditions (inlet velocity, temperature, species mass fraction) and material properties are the same as the lab scale experimental setup. Figure 4-4 shows the geometry and computational grid for the numerical setup. The symmetry plane is used to reduce the computational time due to the symmetric pattern of the boundaries and geometry in all of the simulations.

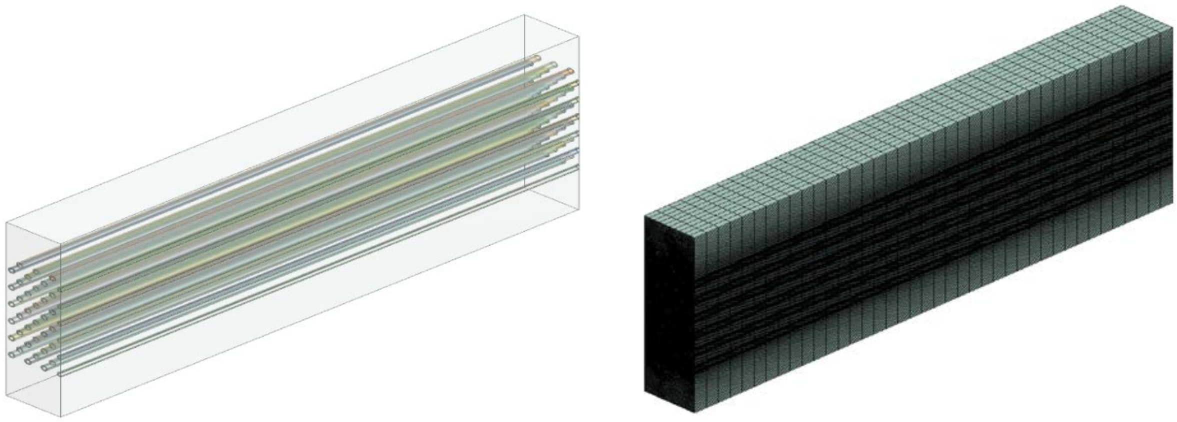

Figure 4-4. Geomety and computational grid for the lab scale TMC module

The grid independency study is conducted for the case which has the closest inlet values to the averaged inlet condition of the experimental cases. Also, study is carried out for the case without condensation. Different species are calculated from the volume fraction in the experimental data.
Table 4-7 shows the boundary and working conditions for the experimental case, which has been used for the grid independency study and the calculation of the model constants. The inlet mass fractions of different species are calculated from the volume fraction in the experimental data.

Table 4-7. Boundary and working conditions for the base case

Natural gas flow rate	SCFH	201.35
Flue inlet T	°F	179.0
Flue inlet dew point	°F	132.4
Flue inlet Humidity	%	32.3
Flue outlet T	°F	129.2
Flue outlet Humidity	%	87.7
Flue outlet dew point	°F	124.3
Water inlet FR	gpm	0.339
Water inlet T	°F	89.4
Water outlet T	°F	124.1
TMC vacuum	"Hg	-5.93
CALCULATED PARAMETERS		
Flue Gas SCF/SCF Gas (based on fuel and O_2 reading)		
O_2		0.0945
N_2		7.82
CO_2		0.965
H_2O		2.11
Total Flue Gas Flow	SCFH	2216.0
Inlet Mass Fraction of Species		
O_2		0.04
N_2		0.756
CO_2		0.09

H_2O		0.114
Water transferred	lb/h	3.187
Water transferred	%	19.4

Variation of the outlet flue gas and water temperatures has been plotted in Figure 4-5. As seen from the figures, a total number of 2.9 million control volume ensures the grid independency of the numerical simulations.

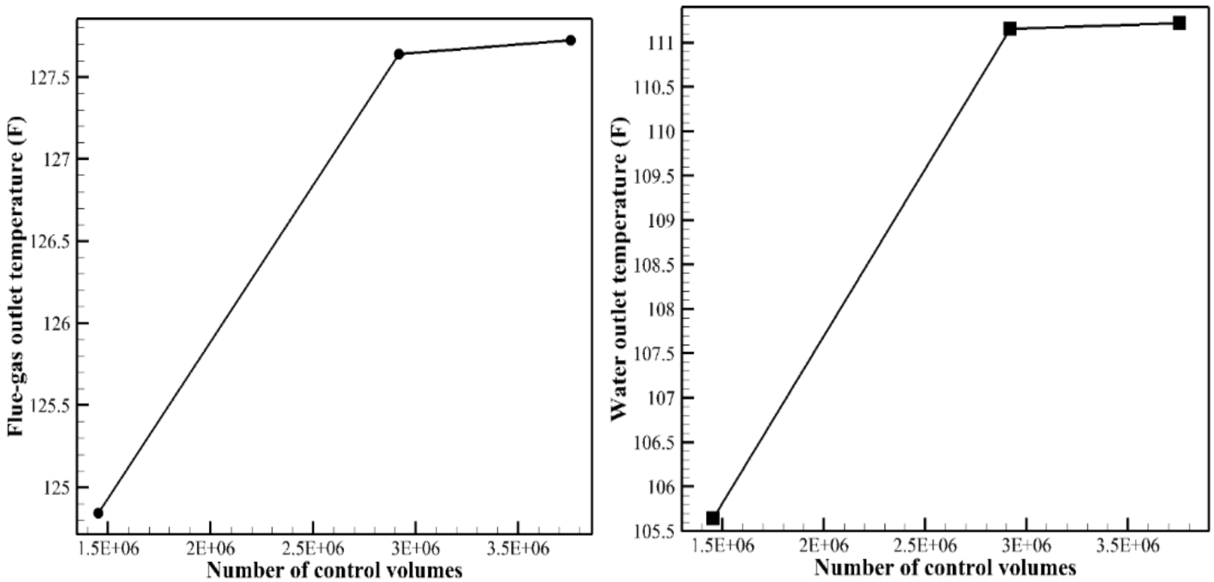

Figure 4-5. Grid independence study for the cross-flow TMC module modelling

b) Comparisons between modeling and experimental data

To validate the proposed simulation algorithm for modeling TMC, the numerical results are validated against the available experimental data from a lab scale TMC test rig. The data series for 11 test cases are presented in Table 4-8 and Table 4-9.

Table 4-8. Inlet and outlet conditions for the experimental cases 1-6.

Test case		**1**	**2**	**3**	**4**	**5**	**6**
Natural gas flow rate	SCFH	201.2	201.2	200.4	201.4	201.2	200.8
Flue inlet T	°F	179.3	179.6	180.3	179.0	179.8	180.9
Flue inlet dew point	°F	132.6	132.7	131.8	132.4	132.7	132.8
Flue inlet Humidity	%	32.3	32.1	30.8	32.3	31.9	31.2
Flue outlet T	°F	127.3	122.1	134.2	129.2	124.4	121.4
Flue outlet Humidity	%	105.1	107.2	87.3	87.7	87.6	102.0
Flue outlet dew point	°F	129.2	124.6	129.1	124.3	119.6	122.1
Water inlet FR	gpm	0.1997	0.2047	0.31907	0.339218	0.3279	0.5059
Water inlet T	°F	90.9	69.4	108.5	89.40	70.2	89.8
Water outlet T	°F	131.3	129.02	129.2	124.1	120.6	122.0
Flue Gas SCF/SCF Gas (based on fuel and O_2 reading)							
O_2		0.0945	0.0945	0.0945	0.0945	0.0945	0.0945
N_2		7.8263	7.8263	7.8263	7.8263	7.8263	7.8263
CO_2		0.9655	0.9655	0.9655	0.9655	0.9655	0.9655

H_2O		2.1195	2.1195	2.1195	2.1195	2.1195	2.1195
Total Flue Gas Flow	SCFH	2214.7	2214.7	2206.061	2216.0	2215.3	2210.9
Flue-gas inlet velocity	(ft/s)	1.7256	1.7267	1.7218	1.7259	1.727	1.7271
Water inlet velocity	(ft/s)	0.0550	0.0564	0.0879	0.093552	0.0904	0.1395
*VOLUME FRACTION_FG_IN							
O_2		0.0085	0.0085	0.0085	0.0085	0.0085	0.0085
N_2		0.711	0.711	0.711096	0.71	0.7110	0.7110
CO_2		0.087	0.087	0.087725	0.08	0.0877	0.0877
H_2O		0.192	0.192	0.192585	0.19	0.1925	0.1925
Water transferred	lb/h	1.408	3.21	1.12296	3.1	4.9	4.1
Water transferred	%	8.5	19.5	7.01	19.4	29.819	24.9
Deviation from the ACR		2.5377	0.7328	2.8230	0.7586	-0.9712	-0.174
Full geometry condensation rate (kg/s)		0.000177	0.000405	0.000141	0.0004	0.00062	0.00051
Half geometry condensation rate (kg/s)		8.87E-05	0.000202	7.07E-05	0.0002	0.00031	0.00026

Table 4-9. Inlet and outlet conditions for the experimental cases 7-11.

Test case		7	8	9	10	11
Natural gas flow rate	SCFH	201.7	201.4	201.7	201.0	201.7
Flue inlet T	°F	179.1	180.3	178.5	161.2	161.0
Flue inlet dew point	°F	133.2	132.5	132.7	133.2	133.0
Flue inlet Humidity	%	32.9	31.4	32.9	49.6	49.6
Flue outlet T	°F	118.9	123.7	113.2	128.4	126.9
Flue outlet Humidity	%	87.9	85.5	87.1	102.9	91.9
Flue outlet dew point	°F	114.4	118.1	108.4	129.512	123.8023
Water inlet FR	gpm	0.496	1.01	1.04	0.335	0.332
Water inlet T	°F	68.2	89.9	69.4	109.8	89.0
Water outlet T	°F	113.5	109.6	95.5274	129.8911	125.7128
Flue Gas SCF/SCF Gas (based on fuel and O2 reading)						
O_2		0.094	0.094	0.094	0.094	0.094
N_2		7.8	7.8	7.8	7.8	7.8
CO_2		0.96	0.96	0.96	0.96	0.96
H_2O		2.11	2.11	2.11	2.11	2.11
Total Flue Gas Flow	SCFH	2220.4	2217.7	2220.3	2213.236	2220.6
Flue-gas inlet velocity	(ft/s)	1.72	1.73	1.72	1.67	1.68
Water inlet velocity	(ft/s)	0.136	0.279508	0.289	0.092	0.091
*VOLUME FRACTION_FG_IN				1		
O_2		0.0085	0.0085	0.0085	0.0085	0.0085
N_2		0.711	0.711096	0.711	0.711	0.711

CO_2		0.087	0.087	0.087	0.087	0.087
H_2O		0.192	0.192	0.192	0.192	0.192
Water transferred	lb/h	6.738	5.33	8.11	1.58	3.66
Water transferred	%	40.25	32.45	49.04	9.495	22.00
Deviation from the ACR		-2.792	-1.385	-4.168	2.360	0.279
Full geometry condensation rate (kg/s)		0.000849	0.000672	0.001022	0.0002	0.000462
Half geometry condensation rate (kg/s)		0.000425	0.000336	0.000511	9.99E-05	0.000231

The inlet and working boundary conditions are set the same as that in the experimental setup for all of the 11 cases. Figure 4-6 shows the comparison between the numerical results and the experimental ones. As shown in this figure the numerical results obtained using the present model are in very good agreement with the experimental results.

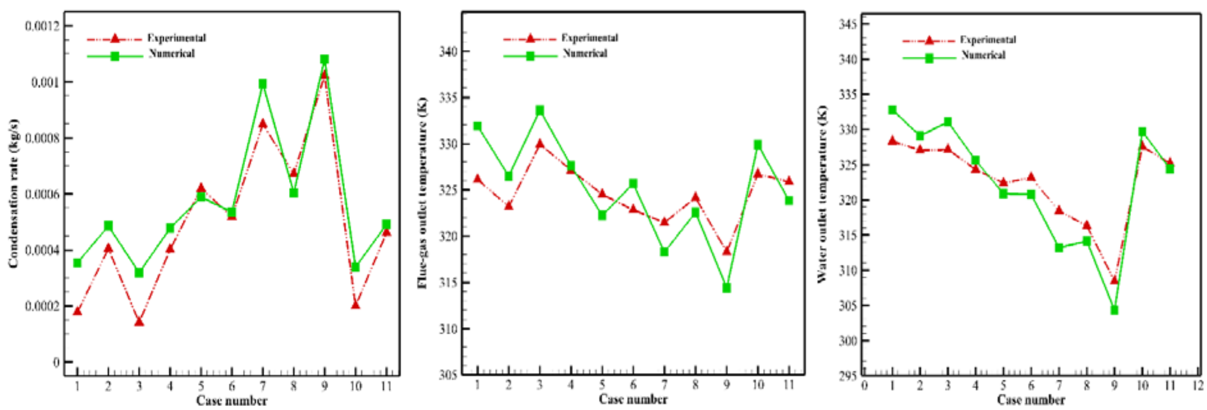

a) Condensation rate b) Outlet flue-gas temperature C) Outlet water temperature.

Figure 4-6. comparision between the CFD simulation of TMC with the experimental data.

To briefly demonstrate the effect of the inlet conditions, the temperature and H_2O mass fraction contours for cases 1, 5 and 9 are shown in Figure 4-7. As seen from the figures, the water mass fraction along the cross flow TMC unit decreases as the cooling water temperature decreases (or mass flow rate increases).

Mass fraction ***Temperature***

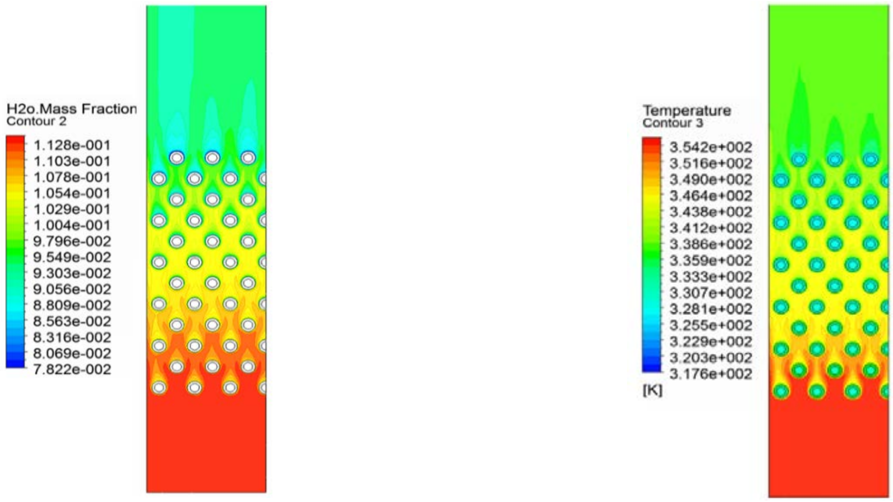

a) Case 1

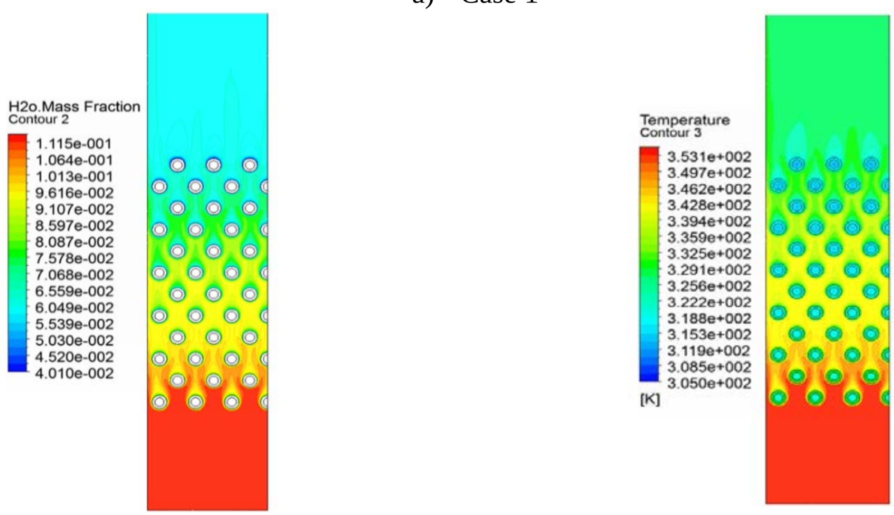

b) Case 5

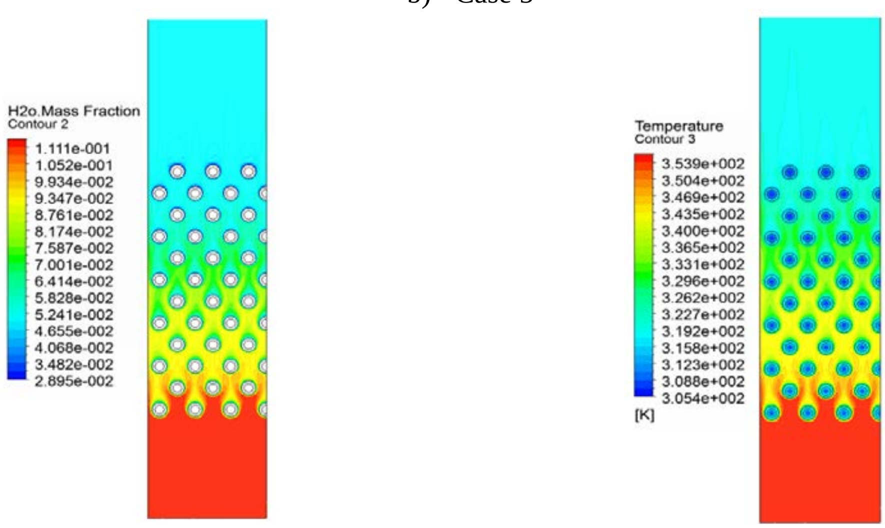

c) Case 9

Figure 4-7. Temperature and water vapor mass fraction contours for selected cases

Figure 4-8 shows the deviation of the numerical results from the experimental data in terms of condensation rate. This figure further supports the previous observation that the numerical results generally agree with the experimental data. The computational condensation rate deviates from the experimental data and over predicts them to certain degrees, mostly for the cases with lower condensation rate (higher surface temperature).

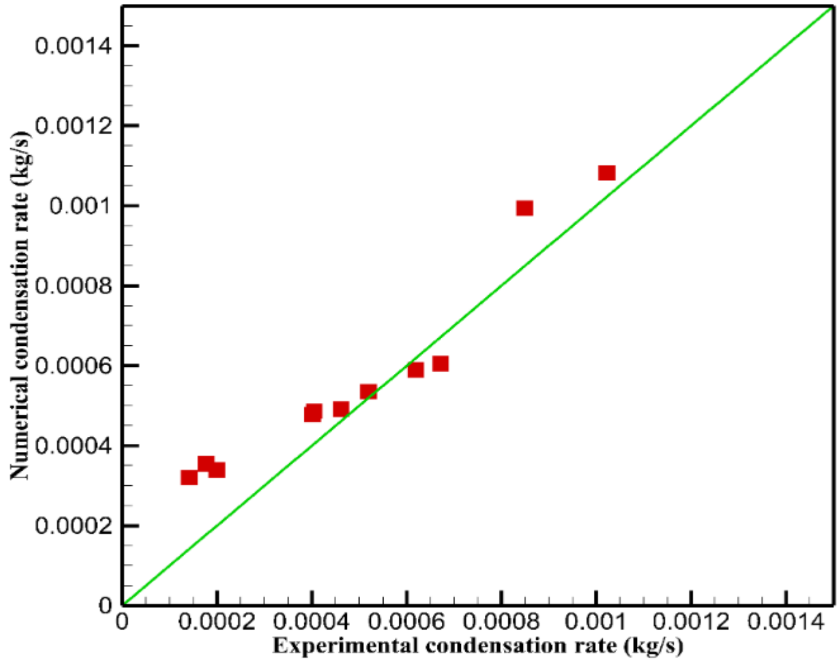

Figure 4-8. Deviation of numerical prediction from the experimental results.

4.2 Results and Discussion

In this section, numerical modeling and parametric study of the effective parameters on the performance of a pilot scale TMC unit have been conducted. The main objective of this section is to optimize the performance of a TMC unit to obtain maximum heat transfer rate while using reasonable number of membrane tubes. Then select the best performance TMC configuration and tube arrangement patterns for next step real pilot scale TMC unit design.

4.2.1 Effects of different tube numbers on the performance of a TMC

Figure 4-9 shows the geometry of a complete pilot scale TMC module. The computational domain is divided into three zones: the cooling water zone, the flue gas zone and the TMC tube zone. In the pilot scale TMC unit design, the inner and outer tube diameters and the length of each TMC membrane tube are 0.1536, 0.232 and 34 inches, respectively. As shown in Figure 4-9b, B_t and B_l are the transversal and longitudinal pitches respectively, which determine the number of TMC tubes in the corresponding directions for a fixed TMC module overall dimensions.

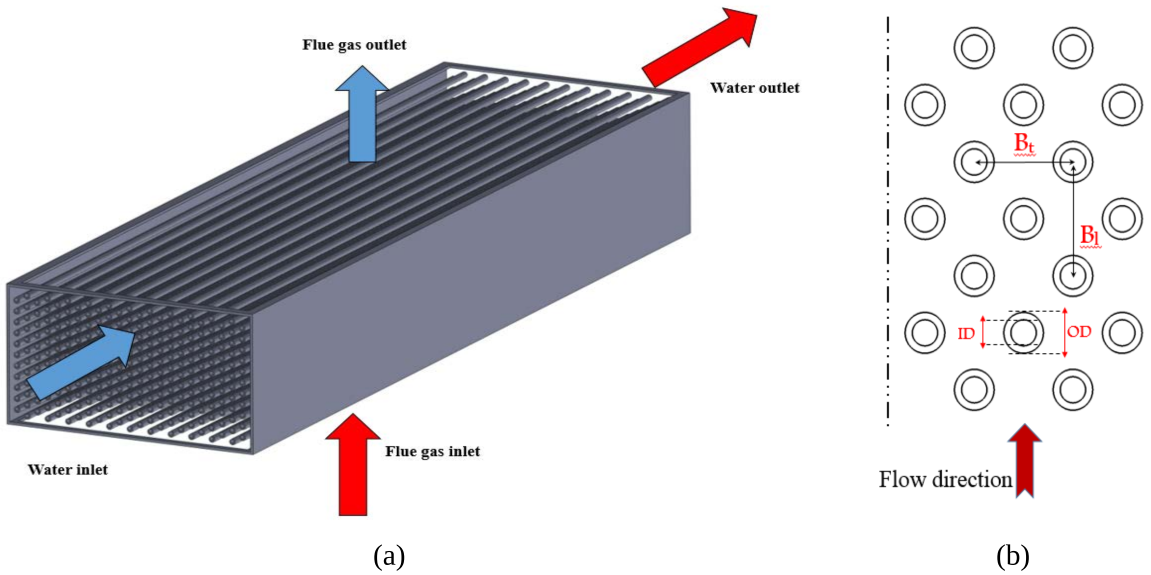

Figure 4-9. Schematic of a TMC module

To understand how each parameter will affect the final design, a series of numerical simulations have been conducted for a wide range of governing parameters to assess the heat and water recovery of the pilot scale TMC unit. Figure 4-10 shows a sample of mesh generated for the computational domain. In this study, a single column of the pilot scale TMC unit with two symmetry boundaries was considered for actual numerical simulation. As seen in this figure, a structured grid is used for the TMC tube walls, top and bottom parts of the flue gas zones, and hex-dominant meshes are used for the cooling water and the central flue gas zones. A total number of about 2 million control volumes is selected for the whole computation domain after the grid study.

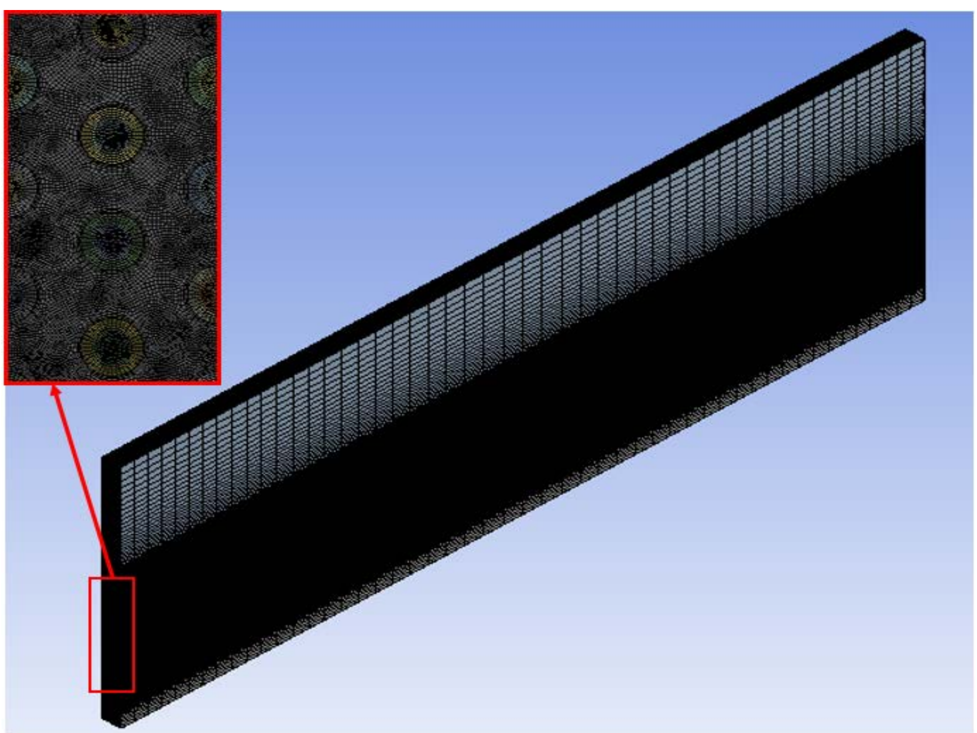

Figure 4-10. 3-D grid generated for the TMC module.

The inlet velocity and temperature of the flue gas were set at T_{fg_in}=355.2 K, V_{fg_in}= 1.83 m/s and 3.68 m/s. The cooling water inlet temperature was T_{w_in} = 310.7 K and the water flow rate for a single stage module was 21.2 liter/min. For each arrangement of the TMC unit with different number tubes in longitudinal and transversal directions, the inlet velocity is obtained based on this constant flow rate. Generally for industrial applications, a matrix of TMC unit with several TMC modules in the cross section or along the flow direction is necessary. Considering the above points, different arrangement of TMC modules can be selected for an industrial application such as in power plants, hence the TMC matrix can be designed to have different tube numbers and various dimensions. The simulations have been carried out for the longitudinal pitches of B_l = *0.35*, *0.432* and *0.55*, which corresponds to 15, 12 and 9 TMC tubes in the streamwise direction, and transversal pitches B_t = *0.3*, *0.35*, *0.4* and *0.45*,which corresponds to 34, 29, 25 and 22 TMC tubes in the spanwise direction, respectively.

Figure 4-11(a) shows variation of cooling water outlet temperature for different values of transversal and longitudinal pitches, inlet water vapor mass fractions, and flue gas inlet velocities. As expected the cooling water outlet temperature is higher for higher flue-gas inlet velocity (V_{fg_in}=3.68 m/s). The cooling water outlet temperature increases as the water vapor mass fraction is increased for the inlet flue-gas. The higher water vapor mass fraction in the flue gas, the higher the condensation rate. As the condensation rate increases, the transferred latent heat to the cooling water increases, which increases the cooling water outlet temperature. Figure 4-11(b) also shows that the cooling water outlet temperature change is almost linear with respect to the transversal pitches. Increasing of either transversal or longitudinal pitches decreases the cooling water outlet temperature at both flue gas inlet velocity conditions, namely V_{fg_in}=1.83 m/s and 12 m/s.

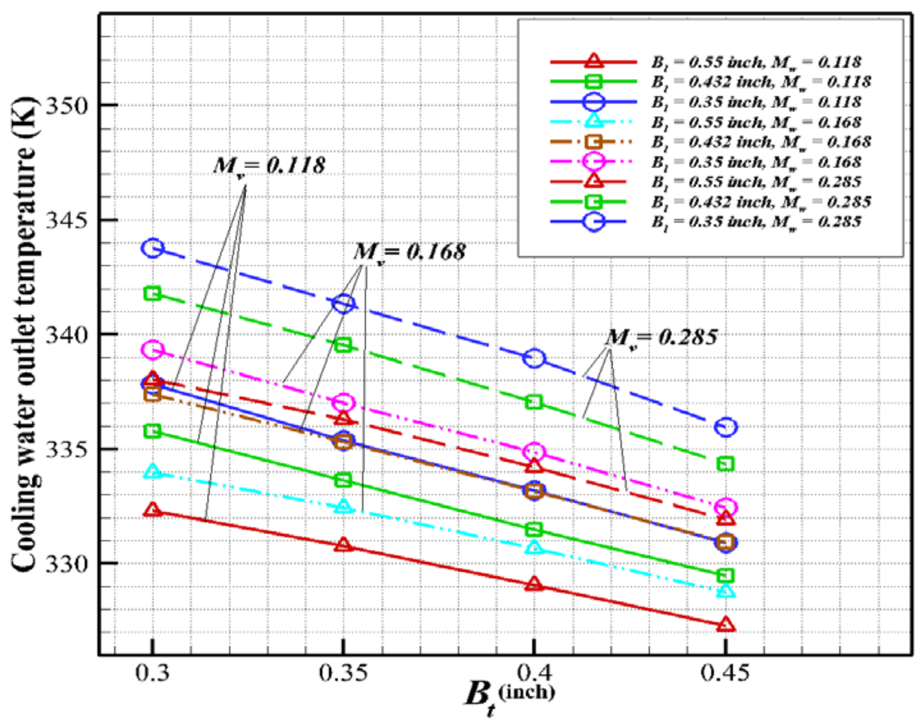

(a) V_{fg_in}=1.83 m/s

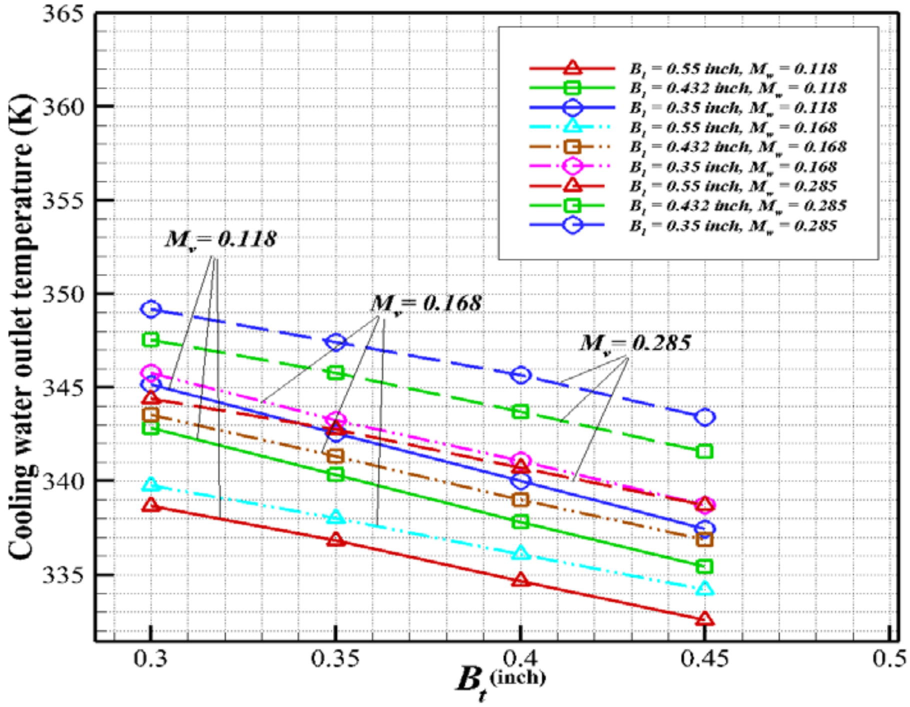

(b) V_{fg_in}=3.68 m/s

Figure 4-11. TMC cooling water outlet temperature for various inlet conditions and configurations.

Variation of the flue-gas outlet temperature with respect to different transversal and longitudinal pitches, inlet water vapor mass fractions and flue gas inlet velocities is shown in Figure 4-12. As seen in this figure, the flue gas outlet temperature has the opposite trend compared with outlet cooling water temperature. As the longitudinal and transversal pitches increases (i.e. the number of TMC tubes decreases) the outlet flue-gas increases. The figure shows that the effect of longitudinal pitches on the flue gas outlet temperature is more pronounced for smaller value of transversal pitches. For different arrangements of TMC tubes, increase of water vapor mass fraction results in decrease in outlet flue-gas outlet temperature because of the increase in condensation rate and transfer of the latent heat. Figure 4-12 also indicates that the variation of flue-gas outlet temperature for different values of governing parameters (i.e. water vapor mass fractions, longitudinal and transversal pitches) is more significant for the smaller inlet flue-gas velocity. The flue-gas outlet temperature has an important role in the design and performance of two or multi-stage TMC unit.

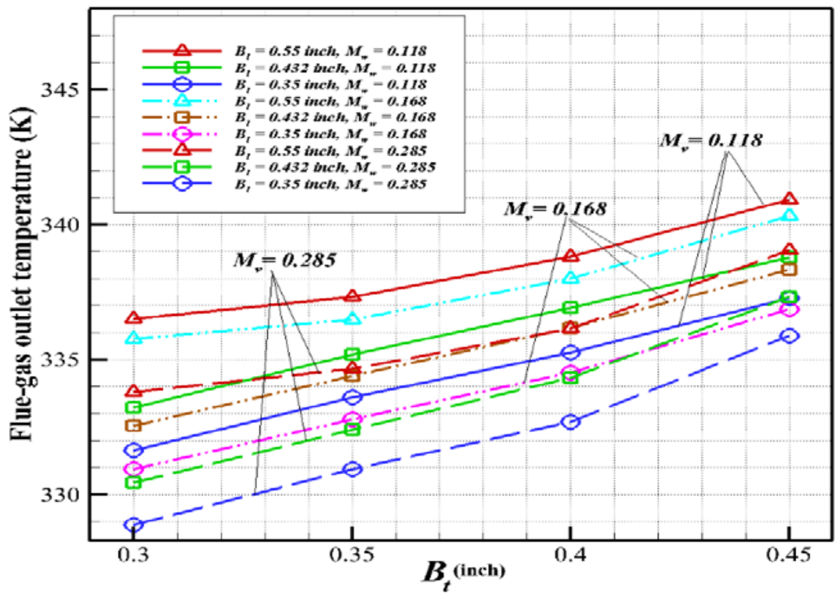

V_{fg_in}=1.83 m/s

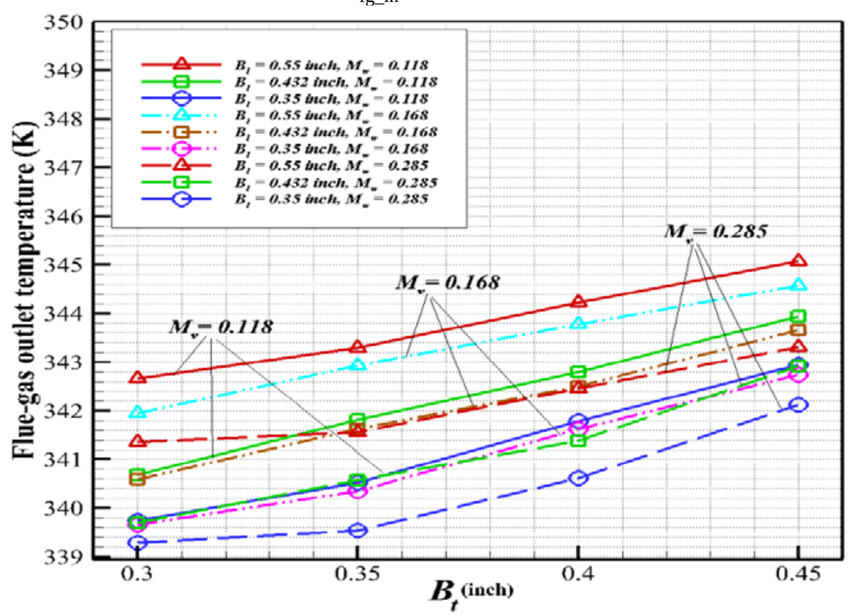

V_{fg_in}=3.68 m/s

Figure 4-12. TMC flue gas outlet temperature for various inlet conditions and configurations.

Effects of different arrangements of TMC tubes and inlet water vapor mass fractions for two different inlet velocities on the inlet to outlet enthalpy change in the flue-gas zone are shown in Figure 4-13. Similar to the outlet cooling water temperature, the enthalpy change decreases as the longitudinal and transversal pitches increases.

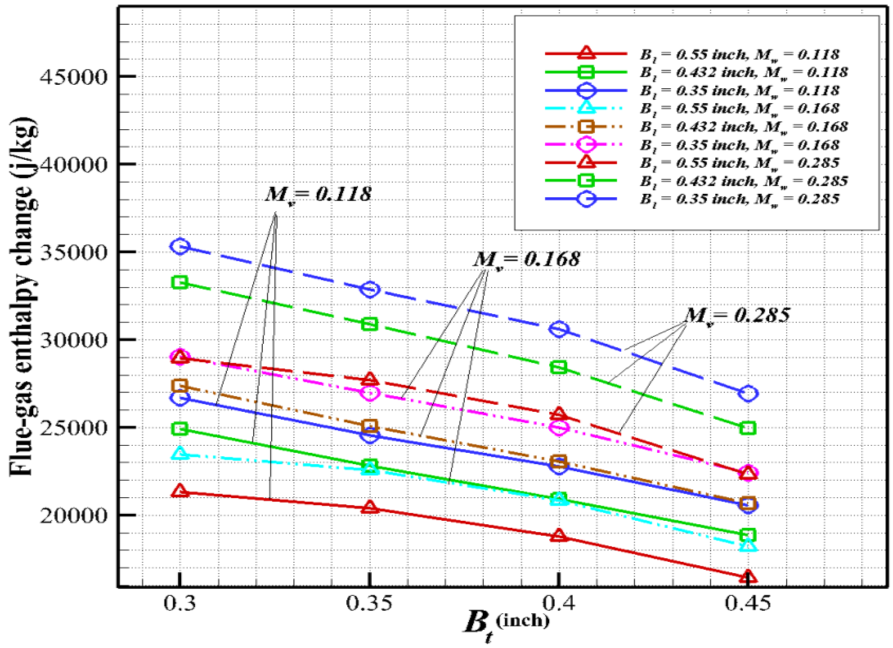

(a) V_{fg_in}=1.83 m/s

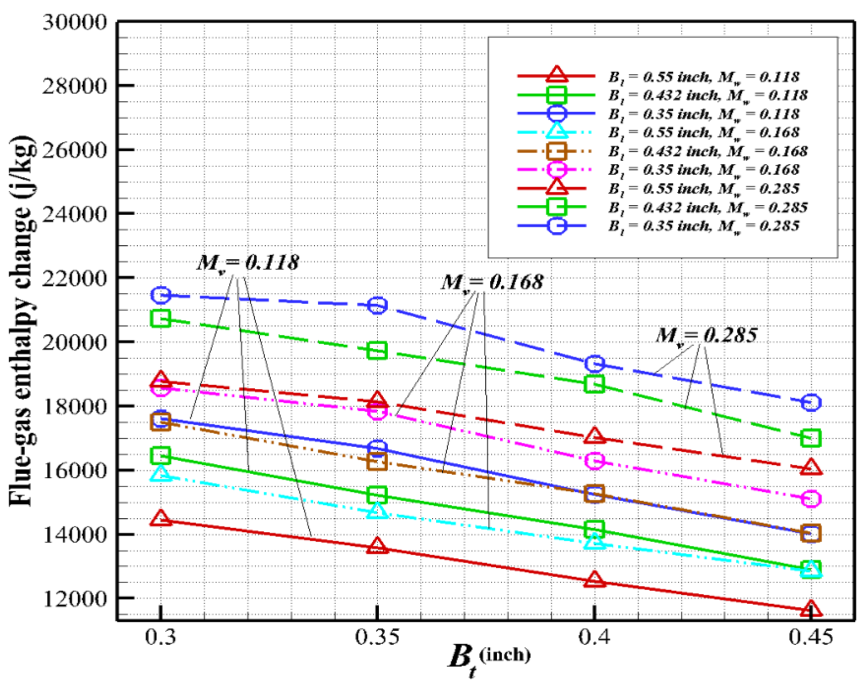

(b) V_{fg_in}=3.68 m/s

Figure 4-13. TMC flue gas enthalpy decrement for various inlet conditions and configurations.

Figure 4-14 shows the effects of different values of transversal and longitudinal pitches, inlet water vapor mass fractions and flue-gas velocities on the condensation rate of the TMC unit. As seen in this figure the condensation rate does not show a linear trend as the arrangement of TMC tubes and water vapor mass fraction change. The condensation rate depends on different parameters such as surface temperature, free stream water vapor mass fraction and pressure of the flue-gas and the condensing surface or number of TMC tubes in TMC unit. In the present work, a constant total cooling water rate is used for different number and arrangements of TMC tubes, and based on this cooling water rate the inlet velocity is calculated. As the number of TMC tubes increases the water flow rate in each TMC tube decreases, therefore the outlet temperature and average surface temperature of the TMC tubes increases which has a negative effect on the condensation rate. On the other hand as the number of TMC tubes increases, the total condensing area increases, which has a positive effect on the condensation rate. The above points indicate that design of a TMC unit for recovering both water and heat from the flue-gas is a multi-objective task, which needs more consideration compared to a non-condensing heat exchangers.

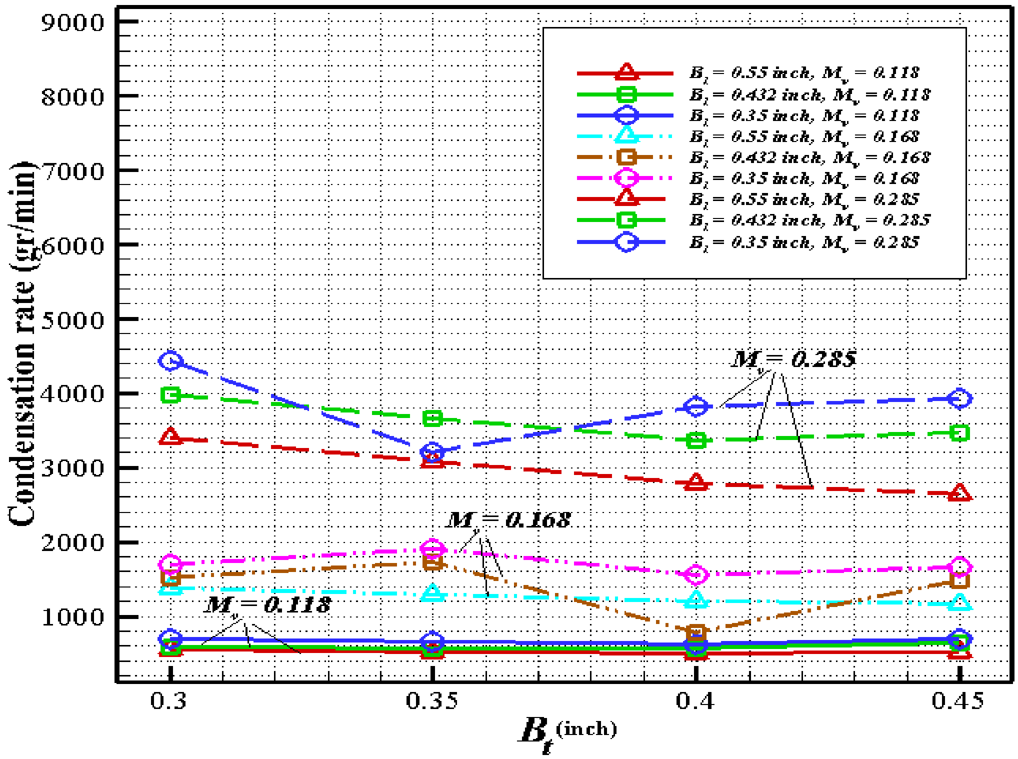

(a) V_{fg_in}=1.83 m/s

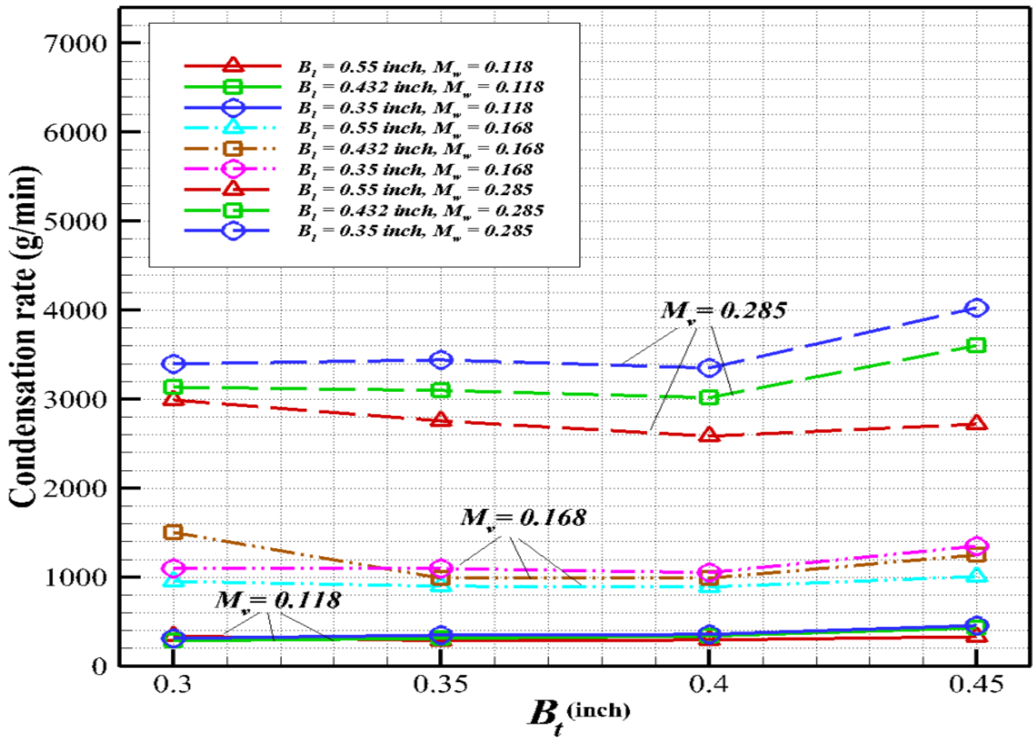

(b) V_{fg_in}=3.68 m/s

Figure 4-14. TMC condensation rate for various inlet conditions and configurations.

Effects of different tube numbers and arrangement of TMC tubes and water vapor mass fraction on the pressure drop along the industrial TMC unit is shown in Figure 4-15 for the flue-gas inlet velocities 1.83 m/s and 3.68 m/s. The pressure drop decreases as the longitudinal and transversal pitches increases. Moreover the pressure drop is lower for higher inlet water vapor mass fraction. This is due to the fact that for higher inlet water vapor mass fraction the condensation rate and flue-gas mass flow depletion rate are higher, which decrease the negative pressure gradient along the TMC units. The figure also clearly indicates the importance of the number of tubes and their arrangements for high velocity flue-gas flow as the maximum pressure drop for an inlet velocity of 3.68 m/s is about four times of that for inlet velocity of 1.83 m/s. Figure 4-15 also shows that for larger values of longitudinal pitches the pressure changes linearly with respect to transversal pitches.

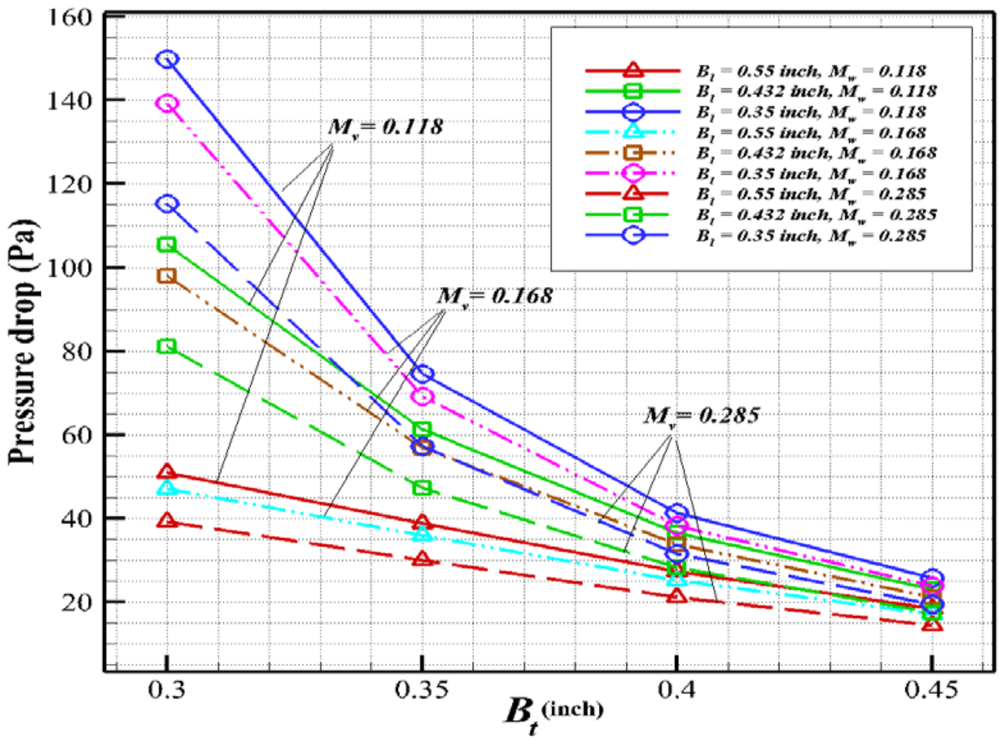

(a) V_{fg_in}=1.83 m/s

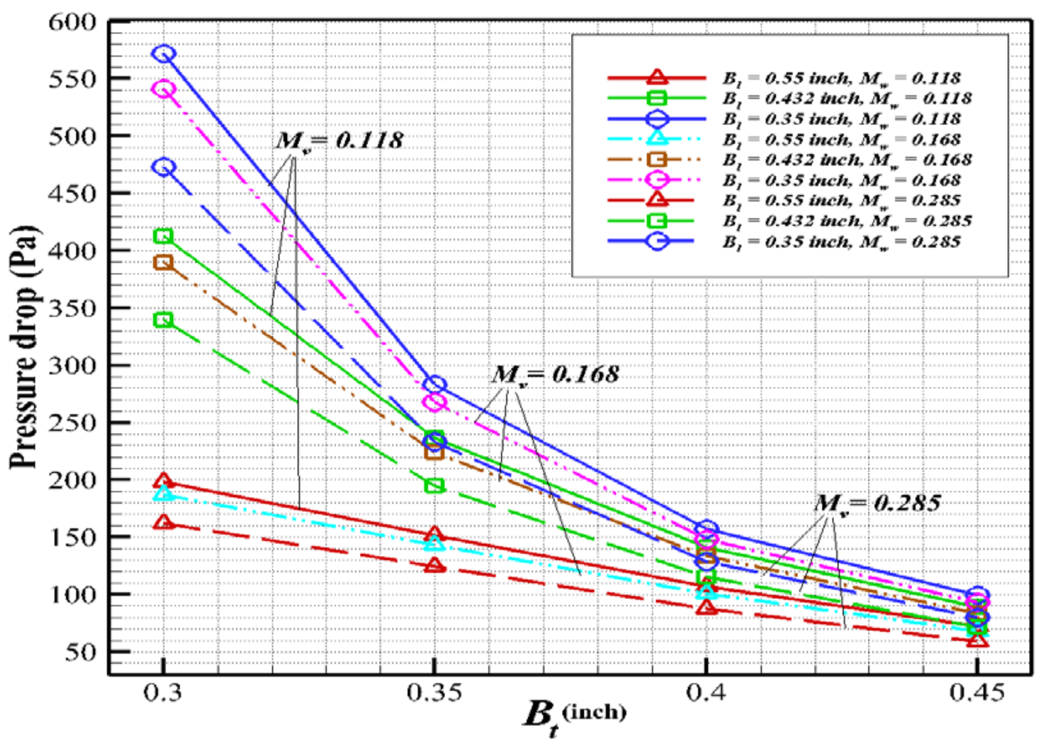

(b) V_{fg_in}=3.68 m/s

Figure 4-15. TMC flue gas pressure drops for various inlet conditions and configurations.

Figure 4-16 shows the effects of different inlet water vapor mass fractions and tube numbers in longitudinal direction on the contours of mass fraction and temperature distribution at $B_t = 0.3$ inch and V_{fg_in}=1.83 m/s. As seen in this figure, for different values of the inlet water vapor mass fraction and numbers of TMC tubes, the minimum values of the water vapor mass fraction decreases by increasing the number of TMC tubes. The region with low water vapor content is limited to the flue-gas near the cooling water inlet area. As the number of tubes increases and the water flows inside the TMC tubes toward the outlet of the tubes the cooling water temperature increases. As seen in this figures this increase in the average surface temperature suppresses the effect of increase of condensing area, and the water vapor content of the flue gas remains high for the given number of TMC tubes in the TMC unit.

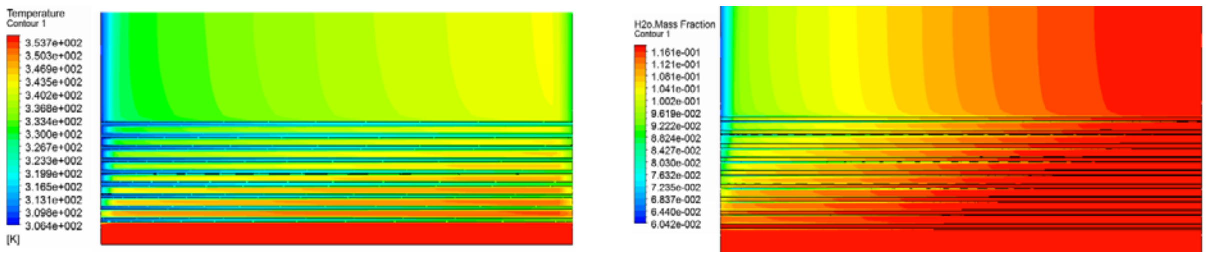

V_{fg_in}= 1.83 m/s, $B_l = 0.55$ inch and $M_w = 0.118$

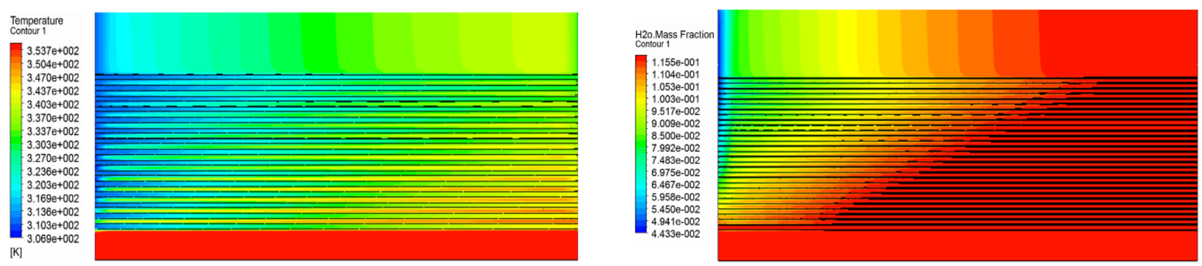

V_{fg_in}=1.83 m/s, $B_l = 0.35$ inch and $M_w = 0.118$

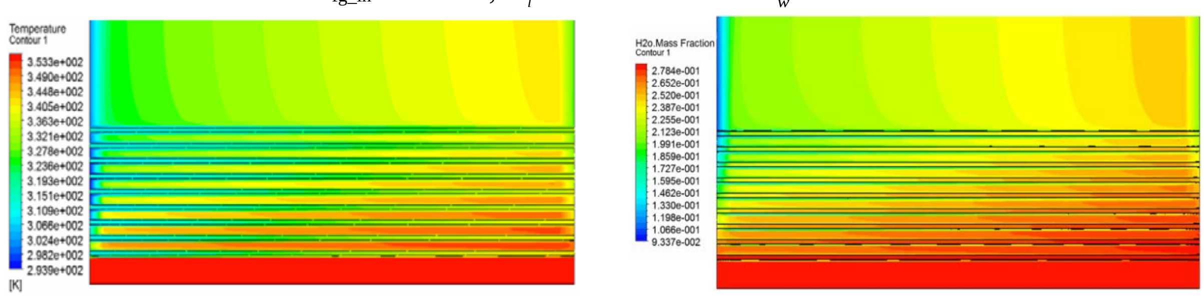

V_{fg_in}=1.83 m/s, $B_l = 0.55$ inch and $M_w = 0.285$

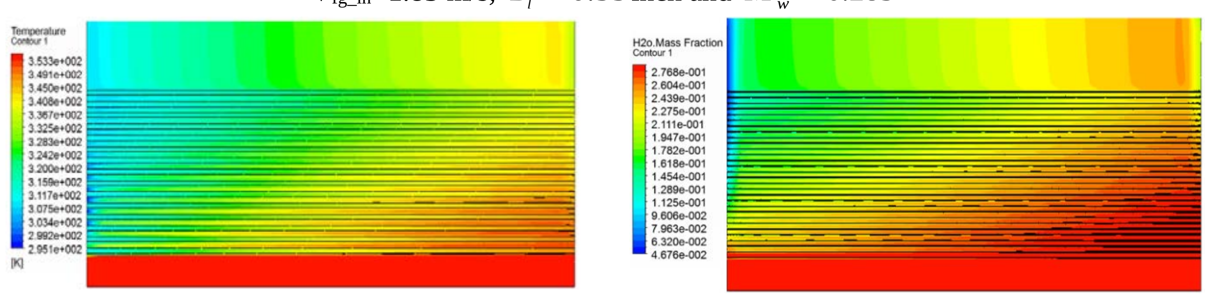

V_{fg_in}= 1.83 m/s, $B_l = 0.35$ inch and $M_w = 0.285$

Figure 4-16. Effects of different inlet water vapor mass fractions and number of tubes in longitudinal direction on mass fraction and temperature distribution

Figure 4-17 depicts the variation of non-dimensionalized parameters in a pilot scale TMC unit with the number of TMC tubes in the unit. The non-dimensionalized values are obtained by:

$$X_n = \frac{X - X_{\min}}{X_{\max} - X_{\min}} \tag{56}$$

where, X is the value of the parameter investigated, and min and max correspond to the maximum and minimum values of that parameter respectively. As seen in this figure, the non-dimensionalized parameters do not have a linear trend with respect to the total number of TMC tubes in a pilot scale TMC unit.

Figure 4-17 shows that in general the flue gas outlet temperature decreases with the increase of the number of TMC tubes, while the cooling water outlet temperature, pressure drop and enthalpy changes along the TMC unit decrease. The design objective of a TMC unit could be to minimize the pressure drop along the heat exchanger, minimize the number of TMC tubes, and maximize the condensation rate and heat transfer. The importance of each parameter depends on the different applications and real world restriction in industrial applications.

Figure 4-17 also suggests that by changing the arrangement of TMC tubes it is possible to achieve a better performance of TMC unit in terms of pressure drop, heat transfer and condensation rate without considerable addition of membrane tubes to the TMC unit.

As seen in Figure 4-17 for different values of inlet velocities and water vapor inlet mass fractions, for a predetermined overall TMC unit dimension, the TMC units with tube numbers of 250 to 350 have better performance in terms of heat transfer and condensation rate.

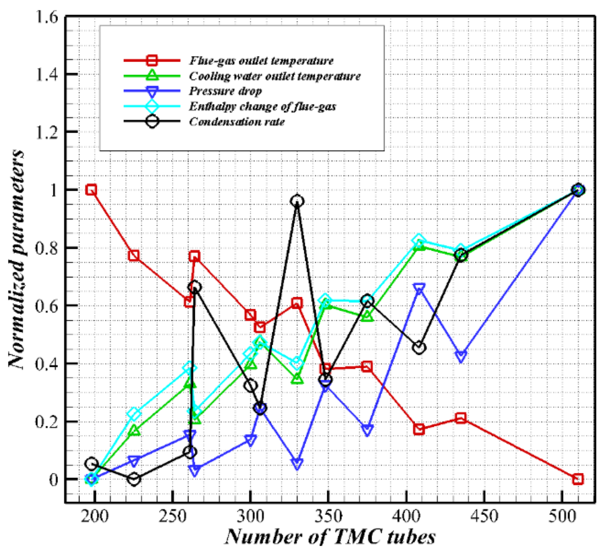

V_{fg_in}=1.83 m/s, M_w=0.118
(a)

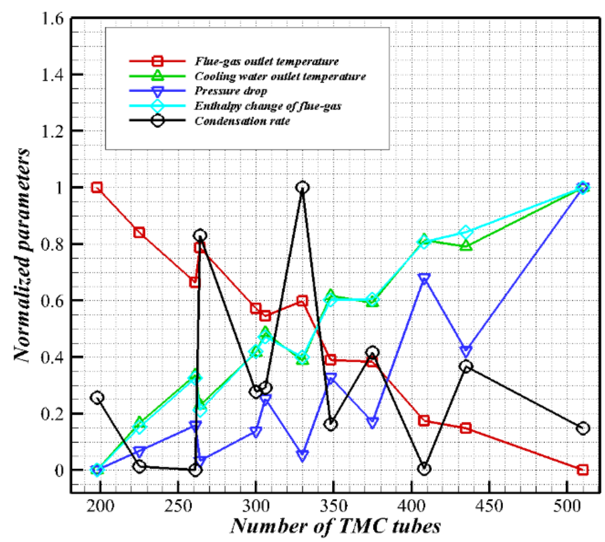

V_{fg_in}=3.68 m/s, M_w=0.118
(b)

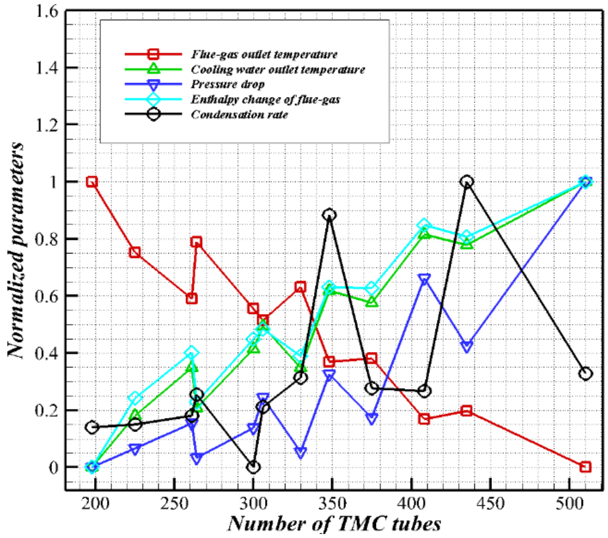

V_{fg_in}=1.83 m/s, M_w=0.168
(c)

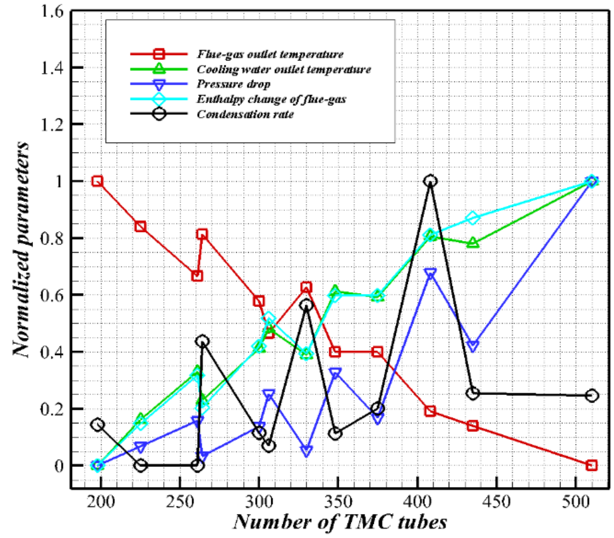

V_{fg_in}=3.68 m/s, M_w=0.168
(d)

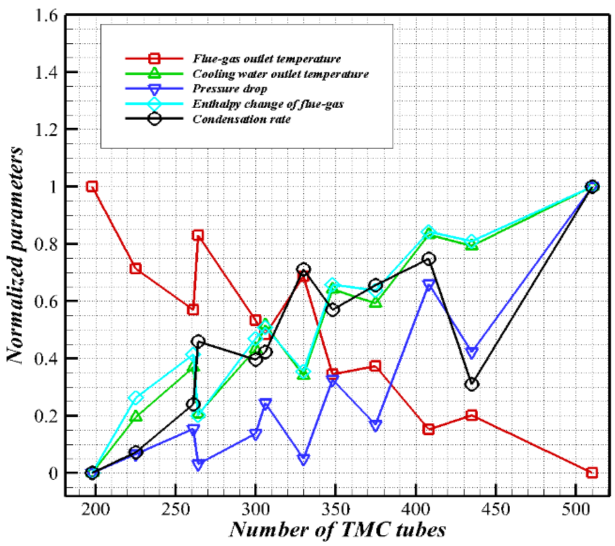

V_{fg_in}=1.83 m/s, M_w=0.285
(e)

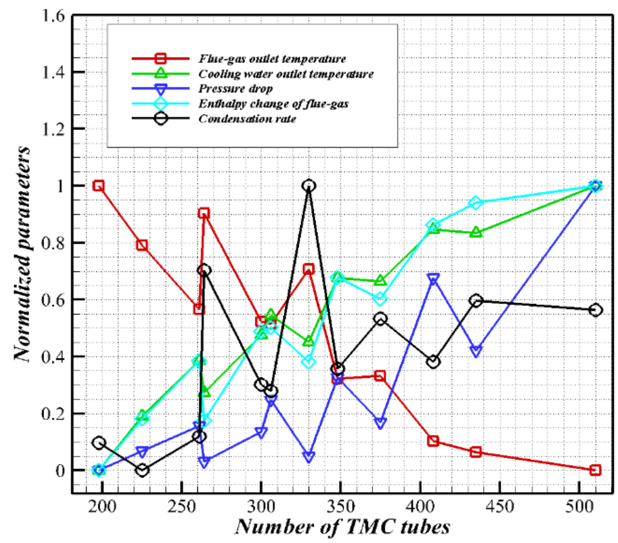

V_{fg_in}=3.68 m/s, M_w=0.285
(f)

Figure 4-17. Non-dimensionalized parameters for various TMC performance

4.2.2 Single TMC Module Performance Study

One of the main objectives of this task is to obtain the maximum performance of a TMC unit in terms of overall heat transfer while the total number of TMC tubes in each stage is reasonable. Based on the original design of the cross-flow TMC unit, the overall heat transfer duty expected, and the numerical results from the previous studies, a tube number at around 300 for each membrane module was chosen for the final design.

To study different membrane tube arrangement effect on the performance of a single membrane module TMC unit with the tube number of about 300, the following cases (Cases 1 to 6) have been considered and compared with the baseline arrangement (Case 0):

Case 0: Inline arrangement with 300 tubes: 12×25 =300: B_t =0.402, B_l =0.432

Case1: Staggered arrangement with 294 tubes: 25×6+24×6=294: B_t=0.402, B_l =0.864

Case 2: Staggered arrangement with 311 tube: 14×12+13×11=311: B_t=0.742, B_l =0.432

Case 3: Staggered arrangement with 311 tubes: 12×14+11×13=311: B_t=0.877, B_l =0.3656

Case 4: Staggered arrangement with 288 tubes: 12×13+11×12=288: B_t=0.877, B_l =0.39608

Case 5: Staggered arrangement with 301 tubes: 22×7+21×7=301: B_t=0.45938, B_l =0.73122

Case 6: Staggered arrangement with 299 tubes: 12×13+11×13=301: B_t=0.8778, B_l =0.38024

Schematic drawings of the 6 different cases and the baseline arrangements are shown in the following Figure 4-18.

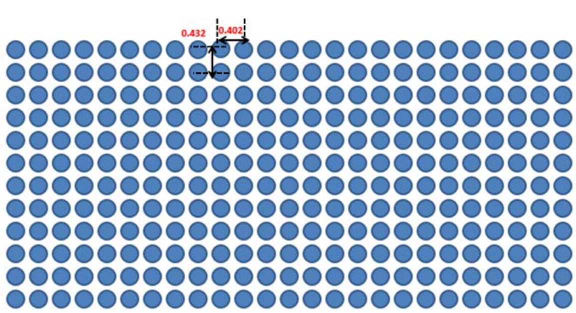

Baseline

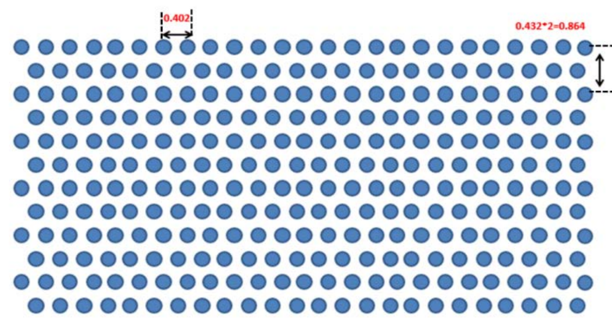

Case 1

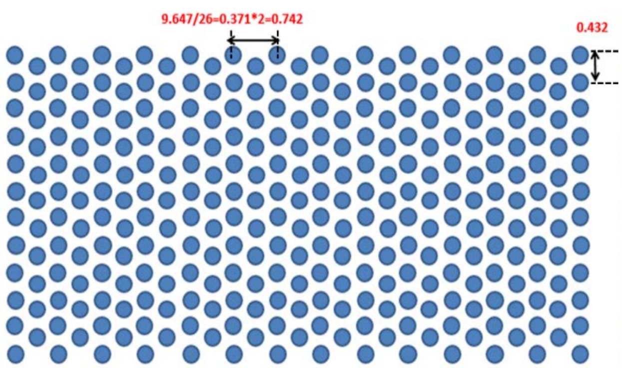

Case 2

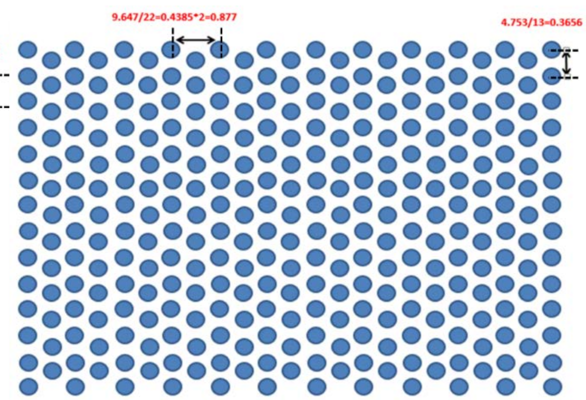

Case 3

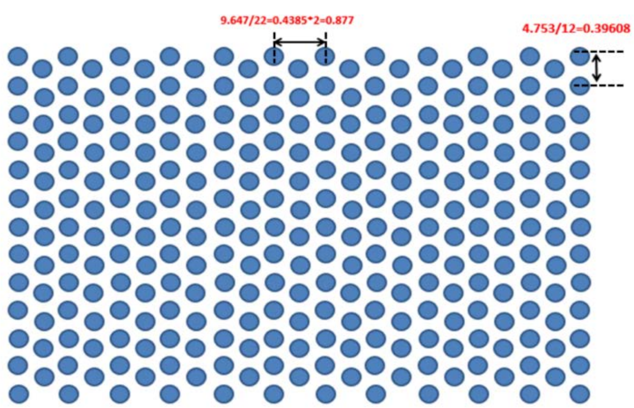

Case 4

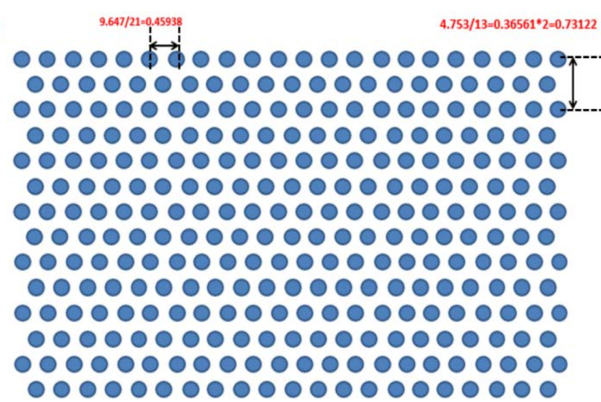

Case 5

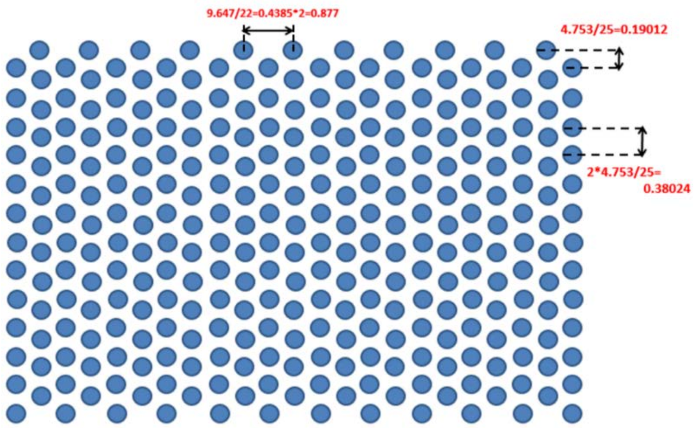

Case 6

Figure 4-18. Schematic of different arrangements for a TMC module

Figure 4-19 shows the performance of the TMC units for different arrangements in terms of outlet temperatures of the cooling water and flue-gas, enthalpy change, pressure drop and condensation rate. As can be seen in this figure, **Case 1** has the maximum heat transfer rate (enthalpy change) compared to the other cases. Although Case 1 also has the maximum pressure drop, such pressure drop level is manageable when considered for actual cross flow heat exchanger applications. Case 1 also has very low number of membrane tubes in a module, which means lower cost for constructing the TMC module. Therefore, this arrangement has been chosen for the next step lab pilot scale TMC unit design, fabrication, and performance testing.

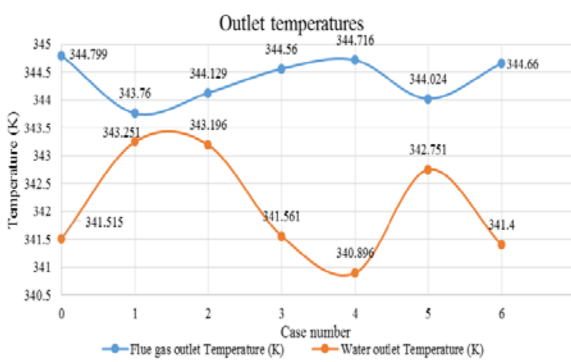

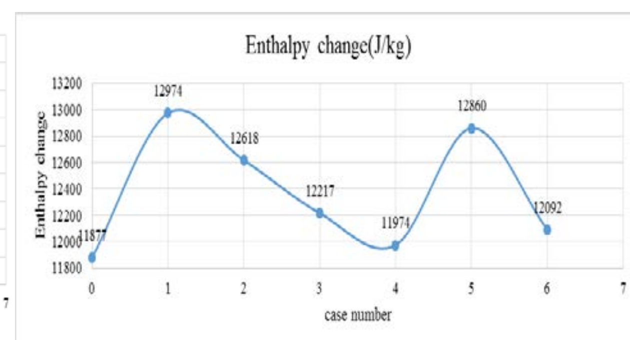

(a) (b)

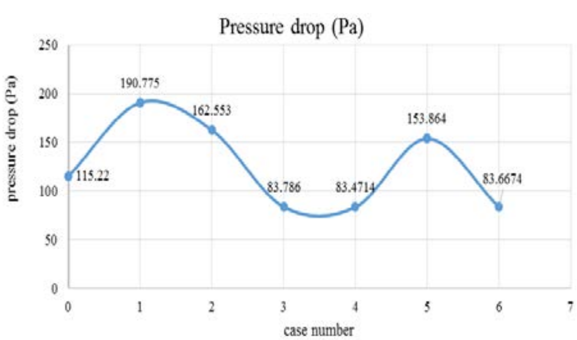

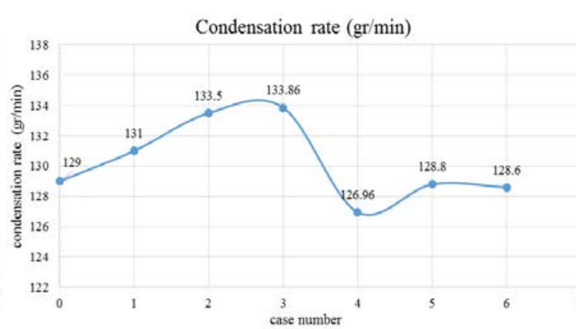

(c) (d)

Figure 4-19. Performance of the cross-flow TMC module for different tube arrangements.

4.2.3 Streamlines and Flow Patterns

One of the parameters in design and evaluation of the performance for different heat exchanger is the amount of pressure drop along the heat exchangers. To better understand the pressure drop variations, GTI investigated the pressure drops at different pitches. Figure 4-20 shows the effect of vertical pitches on the total pressure drop along the cross-flow TMC unit. As seen from the figure, the change in the pressure drop for the vertical pitches less than 0.4 inches is not noticeable while the pressure drop decreases sharply for greater values of vertical pitches.

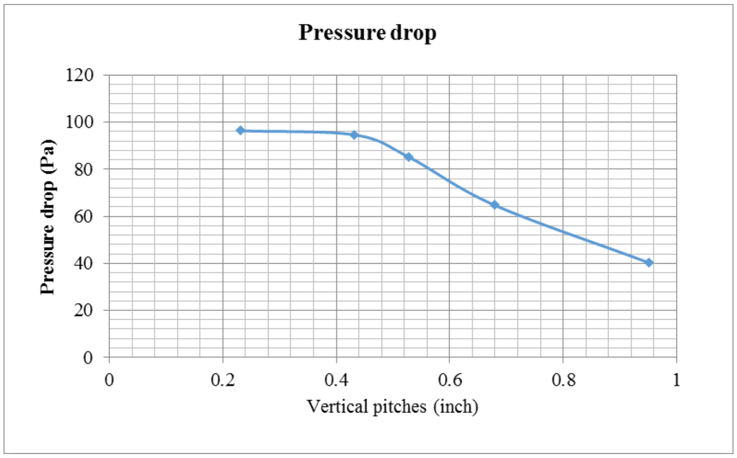

Figure 4-20. Effect of vertical pitches on the pressure drop along a TMC

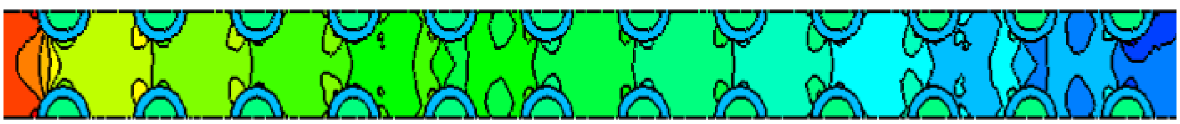

(a) Pressure contour.

(b) Streamlines.

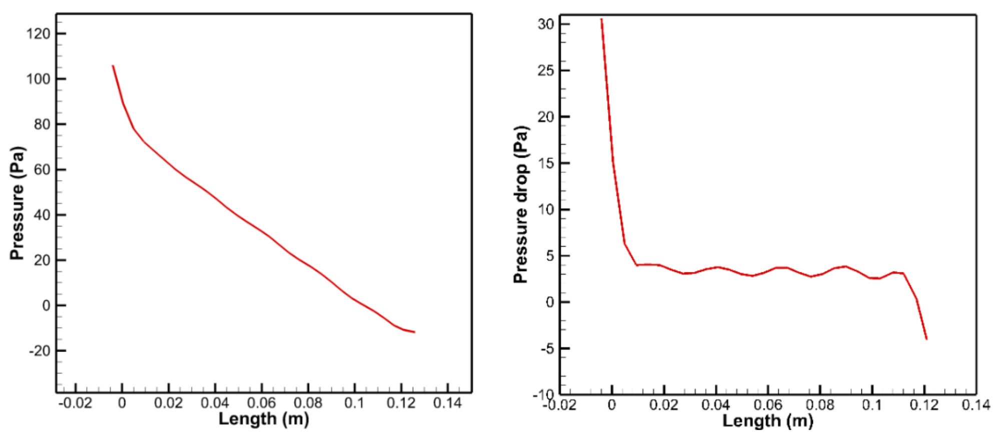

(c) Graph of pressure along TMC.

Figure 4-21. Streamlines, pressure contour and the graphs of pressure and pressure drop for baseline arrangement (Case 0).

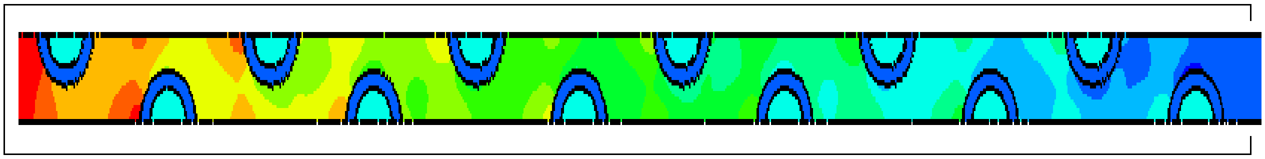

(a) Pressure contour.

(b) Streamlines.

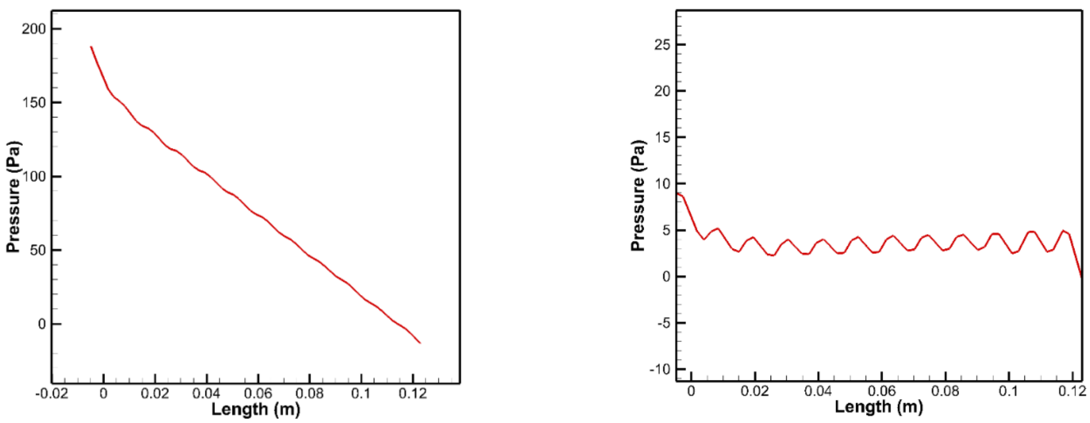

(c) Graph of pressure and pressure drop.

Figure 4-22. Streamlines, pressure contour and the graphs of pressure and pressure drop for optimum arrangement (Case 1).

Figure 4-21 and Figure 4-22 show the streamlines and pressure contours as well as the graphs of gauge pressure and pressure drop along the cross-flow TMC unit for Case 0 (baseline) and Case 1 (optimum arrangement). For both cases, pressure changes linearly except at the entrance region of the TMC module where the entrance effect occurs. Thereafter, the pressure drop does not change much or remains near constant for both cases.

The streamline patterns in these two figures show that the fluid flows in a straight path for Case 0, while in Case 1, the serpentine pattern of the flow results in a considerable increase in the pressure drop.

4.2.4 Two Stage TMC Unit

Generally for industrial applications, a matrix of TMC units with several TMC modules in the cross section or along the flow direction is necessary[3]. Considering the above point, a different arrangement of the TMC unit can be selected for an industrial application, such as in power plants, since the TMC matrix can be designed to have different numbers and various dimensions. In this section, the performance of a two-stage TMC was studied numerically and the outlet parameters of the TMC unit for various values of longitudinal and transversal pitches as well as number of TMC tubes in each stage was reported. Figure 4-23 shows the schematic arrangement for a two-stage TMC unit.

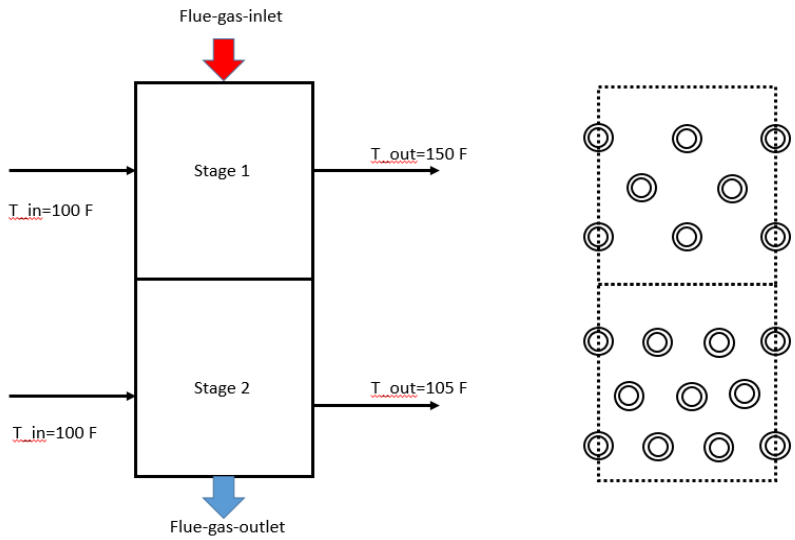

Figure 4-23. Schematic of a two-stage TMC unit.

As shown in Figure 4-23 the outlet flue-gas of the first stage feeds the inlet of the second stage TMC. The cooling water at constant temperature enters the TMC separately. The mass flow rate in the first and second stages are adjusted to obtain the outlet temperatures 150ºF and 105ºF as the requirement of the operating conditions for the unit when the same design is used for both stages (B_t=0.402 and B_l=0.0.432 inches). These water mass flow rates were also used for other numerical simulations with different longitudinal and transversal pitches.

Numerical simulations have been carried out for total TMC tubes of 528 to 816 in the two-stage TMC units and different tube pitches. As seen in Table 4-10, 20 different cases have been studied corresponding to different arrangements and numbers of TMC tubes in different stages.

Table 4-10. Different arrangements and tube numbers of a TMC unit

Case#	**B_t(Nx)**	**B_l(Ny), Stage1**	**B_l(Ny), Stage2**	**Total Tubes**
1	B_t=0.3, (Nx=34)	B_l=0.55, (Ny=9)	B_l=0.35,(Ny=15)	816
2	B_t=0.3, (Nx=34)	B_l=0.45, (Ny=11)	B_l=0.4, (Ny=13)	816
3	B_t=0.3, (Nx=34)	B_l=0.432, (Ny=12)	B_l=0.432, (Ny=12)	816
4	B_t=0.3, (Nx=34)	B_l=0.4, (Ny=13)	B_l=0.45, (Ny=11)	816
5	B_t=0.3, (Nx=34)	B_l=0.35, (Ny=15)	B_l=0.55, (Ny=9)	816
6	B_t=0.35, (Nx=29)	B_l=0.55, (Ny=9)	B_l=0.35, (Ny=15)	696
7	B_t=0.35, (Nx=29)	B_l=0.45, (Ny=11)	B_l=0.4, (Ny=13)	696
8	B_t=0.35, (Nx=29)	B_l=0.432, (Ny=12)	B_l=0.432, (Ny=12)	696
9	B_t=0.35, (Nx=29)	B_l=0.4, (Ny=13)	B_l=0.45, (Ny=11)	696
10	B_t=0.35, (Nx=29)	B_l=0.35, (Ny=15)	B_l=0.55, (Ny=9)	696
11	B_t=0.402, (Nx=25)	B_l=0.55, (Ny=9)	B_l=0.35, (Ny=15)	600
12	B_t=0.402, (Nx=25)	B_l=0.45, (Ny=11)	B_l=0.4, (Ny=13)	600
13	B_t=0.402, (Nx=25)	B_l=0.432, (Ny=12)	B_l=0.432, (Ny=12)	600
14	B_t=0.402, (Nx=25)	B_l=0.4, (Ny=13)	B_l=0.45, (Ny=11)	600
15	B_t=0.402, (Nx=25)	B_l=0.35, (Ny=15)	B_l=0.55, (Ny=9)	600
16	B_t=0.45, (Nx=22)	B_l=0.55, (Ny=9)	B_l=0.35, (Ny=15)	528
17	B_t=0.45, (Nx=22)	B_l=0.45, (Ny=11)	B_l=0.4, (Ny=13)	528
18	B_t=0.45 , (Nx=22)	B_l=0.432, (Ny=12)	B_l=0.432, (Ny=12)	528

19	B_t=0.45, (Nx=22)	B_l=0.4, (Ny=13)	B_l=0.45, (Ny=11)	528
20	B_t=0.45, (Nx=22)	B_l=0.35, (Ny=15)	B_l=0.55, (Ny=9)	528

For all of the cases the inlet temperature of the cooling water for the first and second stages are the same, 100ºF. The flue-gas inlet temperature is 180ºF and the inlet water vapor mass fraction is 0.118. The inlet velocity of flue-gas is set to 12.1 ft/s. The longitudinal and transversal pitches were varied in the range of (B_l= 0.35 to 0.55 inches) and (B_t=0.3 to 0.45 inches), which correspond to (N_x=34 to 22) and (N_y= 15 to 9) tubes in horizontal and vertical directions respectively. The effects of the longitudinal and transversal pitches on the total pressure drop are shown in Figure 4-24. As seen from this figure, the pressure drop decreases with an increase in the number of transversal pitches for all cases. For a constant transversal pitch, it was observed that the minimum pressure drop is obtained for longitudinal pitches of 0.402 or 0.45 inches. Moreover the figure indicates that the effects of transversal pitches on the pressure drop are more pronounced as compared to that of longitudinal pitches.

Figure 4-25 shows the variation of cooling water outlet temperature in the first and second stage TMC units for various values of transversal and longitudinal pitches. As seen the cooling water outlet temperature decreases as the transversal pitch increases. The figure also indicates that the longitudinal pitches have opposite effects on the water outlet temperature of the first and second stages. The more TMC tubes in the first stage (the smaller longitudinal pitches), the higher the cooling water outlet temperature. The higher outlet temperature of the cooling water in the first stage is the result of higher heat transfer rate in the first stage which leads to lower heat transfer rate in the second stage hence the lower cooling water outlet temperature at this stage.

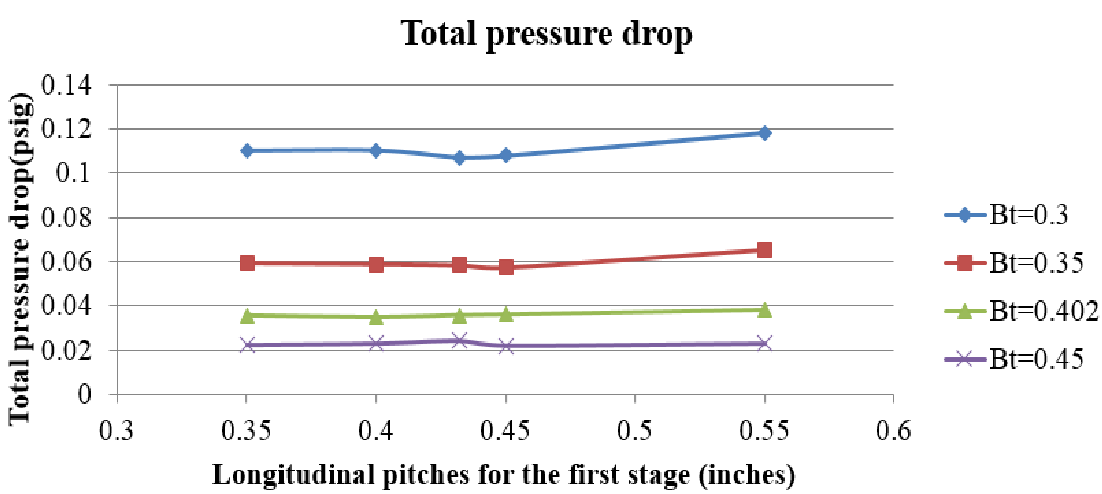

Figure 4-24. Effect of longitudinal and transversal pitches on the total pressure drop.

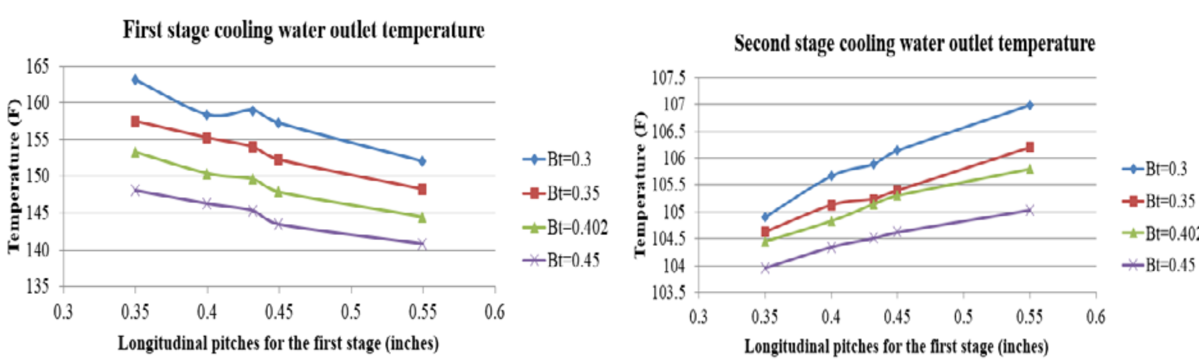

Figure 4-25. Effect of longitudinal and transversal pitches on cooling water outlet temperatures.

Figure 4-26 indicates that the flue-gas outlet temperature has the same trends as the transversal and longitudinal pitches of the TMC tubes vary. Increase of the transversal pitches has a negative effect on the heat transfer rate and increases the flue-gas outlet temperature, while with the increase of longitudinal pitches in the first stage the total heat transfer increases.

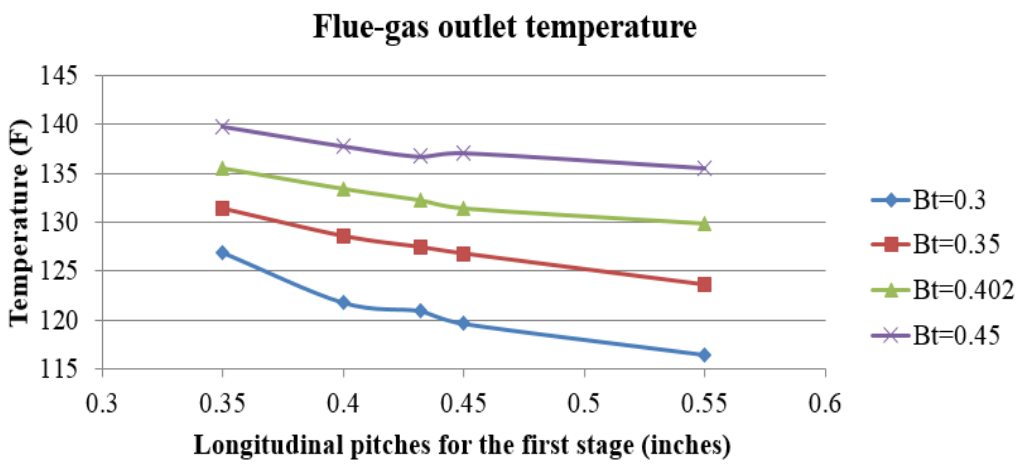

Figure 4-26. Effect of longitudinal and transversal pitches on the flue-gas outlet temperature.

The effect of different tube pitches on the outlet water vapor mass fraction for a two stage TMC unit is shown in Figure 4-27. As seen in this figure the outlet water vapor mass fraction change is similar to the outlet flue-gas temperature. The similar trends of water vapor outlet mass fraction and flue gas outlet temperature is due to the effect of latent heat on the total heat transfer inside the TMC unit. As the condensation rate of the water vapor on the surface of TMC tubes increases, the heat transfer rate was enhanced and the flue-gas outlet temperature drops.

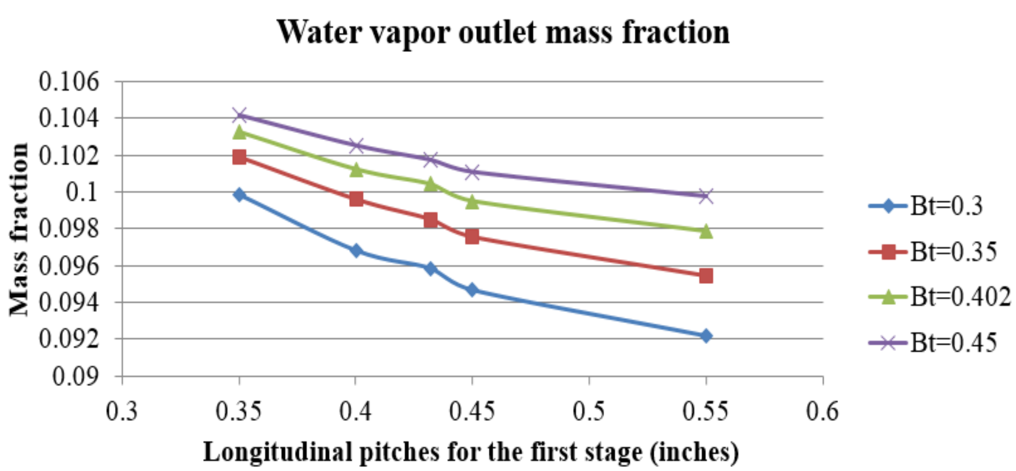

Figure 4-27. Effect of longitudinal and transversal pitches on the water vapor outlet mass fraction.

4.3 TMC Pilot Scale Unit Design Suggestions

In this section, the numerical simulation and optimization of TMC modules and units were conducted at the pilot scale for a coal power flue gas waste heat and recovery application. Using a modified condensation model based on the condensation over a solid wall, heat and mass transfer inside TMC units were studied systematically to support the design of a pilot scale TMC unit. The parametric study is focused on the effects of number of tubes, transversal and vertical pitches on the total heat transfer and condensation rate under various inlet conditions.

The numerical study was divided into two steps. In the first step the effects of number of TMC tubes on the heat transfer and condensation rate inside the TMC units were investigated. Simulations showed that for various values of inlet conditions, i.e. water vapor mass fraction and the flue-gas inlet velocity, 250 to 350 membrane tubes in a TMC unit results in a high heat transfer rate while the number of TMC tubes are acceptable economically. Based on the results of the first step of simulation a tube number of around 300 was considered for the final design of the pilot scale TMC unit. In the second step of numerical simulations, the effects of different arrangements and tube pitches in vertical and horizontal directions were studied. Six different staggered arrangements were considered and the performance of them were compared. Based on the numerical results, an optimum arrangement and tube number for the pilot scale TMC unit was determined for the final design, manufacturing, and prototyping.

The effects of longitudinal and transversal pitches of TMC tubes on the performance of a two-stage TMC unit have also been studied. The results obtained indicated that the cooling water outlet temperature decreases as the transversal pitch increases. Moreover, the longitudinal pitches have the opposite effect on the water outlet temperature of the first and second stages. In terms of condensation rate the results indicate that the outlet water vapor mass fraction changes is similar to that of the outlet flue-gas temperature, which is due to the great effect of latent heat transfer on the total heat transfer. The total heat transfer and condensation rate indicate that for the arrangements with more tubes in the second stage, the total heat transfer is higher.

Reference:

1. D. Wang, “Final technical report, Advanced Energy and Water Recovery Technology from Low Grade Waste Heat,” GTI, 2011.
2. U. S. Dept. of Energy (DOE), “Energy Intensive Processes (EIP) Portfolio - Waste Heat Minimization and Recovery Platform,” 2011.
3. D. Wang, “Transport Membrane Condenser for Water and Energy Recovery from Power Plant Flue Gas,” GTI, 2012.
4. H. Strathmann, B. Bauer, and J. Kerres, “Polymer membranes with selective gas and vapor permeation properties,” *Makromol. Chemie.*, 1990.
5. J. Randon and R. Paterson, “Preliminary studies on the potential for gas separation by mesoporous ceramic oxide membranes surface modified by alkyl phosphonic acids,” *J. Memb. Sci.*, 1997.
6. R. Noble and S. Stern, *Membrane separations technology: principles and applications*. 1995.
7. C. C. Lin, “Imece2011-63530 Nanoporous Membrane Tube Condensing Heat Transfer,” pp. 1–7, 2011.
8. R. Benelmir, S. Mokraoui, and A. Souayed, “Numerical analysis of filmwise condensation in a plate fin-and-tube heat exchanger in presence of non-condensable gas,” *Heat Mass Transf. und Stoffuebertragung*, vol. 45, no. 12, pp. 1561–1573, 2009.
9. F. Menter, “Two-equation eddy-viscosity turbulence models for engineering applications,” *AIAA J.*, 1994.
10. F. R. Menter, “Two-equation eddy-viscosity turbulence models for engineering applications,” *AIAA J.*, vol. 32, no. 8, pp. 1598–1605, 1994.
11. A. Dehbi, F. Janasz, and B. Bell, “Prediction of steam condensation in the presence of noncondensable gases using a CFD-based approach,” *Nucl. Eng. Des.*, vol. 258, pp. 199–210, 2013.
12. M. Houkema, N. B. Siccama, J. A. Lycklama à Nijeholt, and E. M. J. Komen, “Validation of the CFX4 CFD code for containment thermal-hydraulics,” *Nucl. Eng. Des.*, vol. 238, no. 3, pp. 590–599, 2008.
13. C.-X. Lin, D. Wang, and A. Bao, “Numerical modeling and simulation of condensation heat transfer of a flue gas in a bundle of transport membrane tubes,” *Int. J. Heat Mass Transf.*, vol. 60, pp. 41–50, 2013.
14. “NIST webbook.” [Online]. Available: http://webbook.nist.gov/chemistry/.
15. B. Bischoff et al., *Advanced Membrane Seperation Technologies for Energy Recovery from Industrial*

Process Steeams, 2013.
16. H. Weissberg, “Effective diffusion coefficient in porous media,” *J. Appl. Phys.*, 1963.
17. Ansys, Inc.[Online]. Available: http://www.ansys.com/.
18. H. Sun, G. Lauriat, and X. Nicolas, “Natural convection and wall condensation or evaporation in humid air-filled cavities subjected to wall temperature variations,” *Int. J. Therm. Sci.*, vol. 50, no. 5, pp. 663–679, May 2011.
19. D. R. Lide and H. V. Kehiaian, *CRC Handbook of Thermophysical and Thermochemical Data*. CRC Press, 1994.
20. V. Dharma Rao, V. Murali Krishna, K. V. Sharma, and P. V. J. M. Rao, “Convective condensation of vapor in the presence of a non-condensable gas of high concentration in laminar flow in a vertical pipe,” *Int. J. Heat Mass Transf.*, vol. 51, no. 25–26, pp. 6090–6101, 2008.
21. M. Saraireh, “Heat transfer and condensation of water vapour from humid air in compact heat exchangers,” 2012.
22. H. A. McGee, *No Title*. New York: McGraw-Hill, 1991.
23. K. K. Kenneth, *Principles of combustion*. New York: John Willey & Sons, 1986.

5. Membrane Development for High TMC Performance

The primary objectives of this section are conducting membrane development work to improve the water transport properties of the TMC membrane tubes, explore strategies to reduce the membrane cost, and prepare 1,000 membrane tubes for the pilot scale TMC testing later in this project. The project activity and results are discussed below and are organized as follows:

- Development of the ZrO2 membrane surface layer for low pH resistance
- Development of larger pore size membranes for higher water flux
- Development of low cost TMC membrane tubes
- Preparation of 1,000 finished TMC tubes for pilot TMC unit testing

5.1 Development of the ZrO2 surface membrane layer for low pH resistance

During this project, preparation and testing of zirconia based membrane surface layers as improved TMC coatings for enhanced performance and performance stability was required. In particular, it was necessary to develop a low pH resistant membrane top layer that could handle exposure to coal derived flue gas acid gas contaminants. The commercially available membrane tubes used in natural gas flue gas processing was based upon the γ-alumina membrane coating which is not stable at pH value below about 4 to 5 (temperature dependent). Small pore size ceramic membrane coatings based upon zirconia and titania have been demonstrated to be stable at these low pH values. During this project, we successfully prepared at the bench and then at the pilot production scales high quality zirconia based membranes in the target pore size range of 100 to 200Å.

At the end of this development, GTI manufactured 1,000 full length (36”) TMC membrane tubes as required for the pilot TMC test system. Quality Control (QC) testing of three of the finished membrane tubes prepared as part of this production batch showed good agreement with parts prepared during the scale-up development from the 10” to 36” membrane tubes. Table 5-1 shows a summary of the He and N_2 permeance and %IF (initial flow) of the parts prepared in this project (Production Membranes) compared with the shorter length development membranes. For reference, performance of some of the standard MPT γ-alumina based membranes at 40, 100, and 500Å are included. He and N_2 permeance are in-line with previous data. %IF measurements are slightly lower, indicating slightly better defect control and/or slightly smaller pore size than previous parts.

Table 5-1. Performance of the various ZrO_2 membrane tubes prepared during the project period

Membrane ID	N_2	He	He/N_2	% IF
2Q 2015 Membranes (10")				
ZrO2(50/14)-10-01	46.7	83.9	1.80	55.0
ZrO2(50/14)-10-02	76.5	131	1.71	50.3
2Q 2015 Membranes (36")				
ZrO2(50/14)-36-#2	32.2	57.3	1.78	61.5
3Q 2015 Membranes (36")				
ZrO2(50/14)-01	39.55	74.44	1.88	46.0
ZrO2(50/14)-02	39.55	72.61	1.84	43.7
ZrO2(50/14)-03	29.19	52.73	1.81	46.5
ZrO2(50/14)-04	31.46	61.65	1.96	44.4
ZrO2(50/14)-05	34.33	63.69	1.86	37.4
ZrO2(50/14)-06	33.62	63.98	1.90	39.6
ZrO2(50/14)-07	32.10	60.29	1.88	40.9
ZrO2(50/14)-08	33.55	59.51	1.77	40.3
ZrO2(50/14)-09	33.53	64.31	1.92	33.6
4Q 2015 Membranes (36"). Production Membranes				
ZrO2(50/14)-01P	36.82	71.48	1.94	15.5
ZrO2(50/14)-02P	35.75	67.18	1.88	14.3
ZrO2(50/14)-03P	34.22	64.49	1.88	18.2
Standard MPT Alumina Membranes				
MPT 40Å Gamma Alumina	25 to 30	50 to 60	>2.2	<1
MPT 100Å Gamma Alumina	35 to 45	65 to 80	~2	<3
MPT 500Å Alpha Alumina	60 to 70	100 to 130	<1.7	98.0

Table 5-1 shows the QC testing results of the full length 1,000 tube production batch of ZrO_2 membranes prepared during this project. These results show performance consistent with the 10" and 36" membranes prepared in the development phases. Interestingly, the production batch tubes exhibit superior initial flow measurements in the 14 to 22% range compared with the 33 to 46% range for the membranes (36" length) prepared during the development phase (3Q2015). This data shows that the modifications made to the deposition process as developed in this project, with a focus on avoiding excess slip accumulation at the drain ends of the tubes during slip casting, significantly improved membrane quality. This resulted in a steady decrease in the %IF of the membranes, indicating a steady increase in the membrane quality throughout the project.

Table 5-2. Water permeance at room temperature and 2 bar for different membranes.

Membrane ID	H_2O [liter/m2/hr/bar]
4Q 2015 Membranes (36"). Production Membranes	
ZrO2(50/14)-01P	228
ZrO2(50/14)-02P	235
ZrO2(50/14)-03P	211
Standard MPT Alumina Membranes	
MPT 40Å Gamma Alumina	8 to 15
MPT 100Å Gamma Alumina	80 to 110
MPT 500Å Alpha Alumina	220 to 280

Table 5-2 shows the water permeance of the three production ZrO_2 membranes pulled for QC testing. These values are compared with water permeance of various MPT alumina based substrates. The water permeance of these membranes is in the range of 211 to 235 liters/m^2/hr/bar. This value is consistent with the 500Å alumina support membrane. Hence, the ZrO_2 layer deposited during this production batch must be (i) high quality based upon the %IF data in Table 5-1 and (ii) very thin since the water permeance is very close to the underlying support membrane. Figure 5-1 shows the SEM photomicrographs of the surface and cross section of a typical ZrO_2 deposited membrane prepared during the project. The surface ZrO_2 layer is relatively defect free. The cross section image shows the ZrO_2 layer to be ultrathin at <2 micron thick which explains the very high water permeance of the finished membrane.

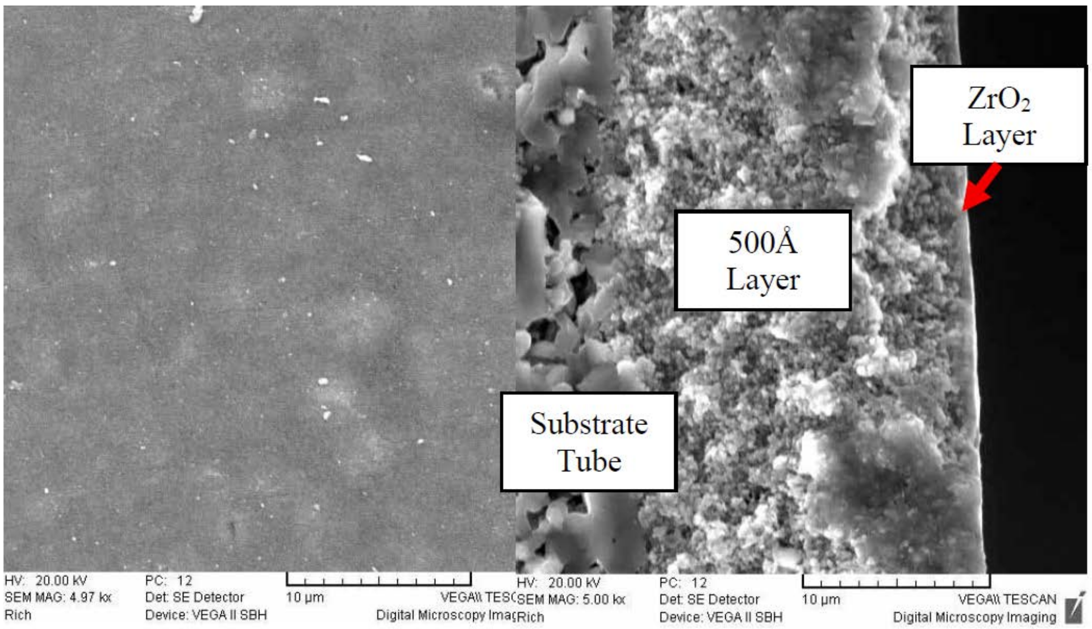

Figure 5-1. SEM photomicrographs of the surface and cross section of a ZrO2 modified TMC membranes

Overall, GTI successfully developed a full scale TMC membrane with an ultrathin ZrO_2 membrane layer at the production scale level. This layer offers far superior acid resistance than MPT's commercial γ-alumina based top layer, a requirement for exposure to coal derived flue gas containing far higher levels of sulfur and other inorganic acid sources. Approximately 1,000 of these ZrO_2 modified membranes were prepared, QC tested, and delivered for pilot scale TMC module preparation and testing.

5.2 Development of larger pore size membranes for higher water flux

GTI began preparation of larger pore size membranes to boost the overall membrane permeance and deliver product that meets the reduced membrane area and lower cost requirements. In general, larger pore sizes can be prepared using larger particles in the preparation of the base membrane tubes. For instance, the size of the alumina particle used in the current commercial tube is on average about 2μm in diameter which yields an average interstitial "hole" of about 0.3 to 0.4μm diameter as per our pore size analysis. Similarly, the lower cost substrates were prepared from lower cost alumina with particle diameters in the range of our current substrate material. Again, these yielded pore sizes in the range of our current substrate and further the slightly smaller pore size of the LP807 material could be attributed to the smaller average diameter of this starting precursor material.

To deliver increased pore size then requires as a first step a larger particle diameter. However, larger particle sizes require higher firing temperature (cost) to deliver comparable strength of the smaller diameter analogs. Further, if the pore size is increased beyond a critical size, it may be necessary to add an additional ceramic layer coating to modify the surface pore size and permit TMC layer deposition, also increasing cost and complexity. Consequently, there is a tradeoff that needs to be made between increased flux (reduced TMC cost) and higher fabrication costs. In this project, GTI prepared discs and tubes using an alumina powder with a nominal particle size of ca. 5µm, targeting a pore size in the 1 to 1.5µm range. Since flux is nominally proportional to pore size squared, it was expected that the flux should increase by ca. 4 to 6-fold over the current substrate tube.

Initially, this work was conducted using discs so that rapid prototyping of the proper body formulation, firing temperature, and preliminary characterization could be conducted. The as prepared discs were approximately 1" in diameter and 2mm thick. This thickness is about double the nominal 1mm wall thickness in our standard commercial tube but is necessary for green (pre-fired part) handling of the as pressed bodies. Discs were prepared from powders formulated with proprietary binders and pressed using a piston and die hydraulic ram press. Following pressing, the discs were dried at room temperature and then calcined at several temperatures. GTI targeted a minimum calcination temperature that yielded a disc that was unbreakable by hand. Discs prepared at this target temperature yielded clean water permeance of 850 to 900 liters/m^2/hr/bar (lmhb). For a 1mm thick tube, this would be equivalent to about 1,700 to 1,800 lmhb or about 7 to 8-fold higher than the 220 to 250 lmhb of our standard pore size commercial tube used by us commercially in our current product.

Table 5-3. Performance of the low purity alumina substrates and large pore size substrates

Part ID	Water Permeance [liter/m^2/hr/bar]	N_2 [m^3/m^2/hr/bar]	Bend Strength [psi]
Low purity substrates from 1Q2016 (this reporting period)			
SubAL-LPTC15.01	233	62	44
SubAL-LPTC15.02	221	60	42
SubAL-LPTC15.02	245	71	46
Low purity substrates from 2Q2015			
SubAL-LP807.02	142	27	48
SubAL-LP807.06	155	33	46
MPT Standard Substrate	220 to 250	75 to 90	40 to 45
MPT LPS Batch #1	2,150	NA	37 to 40
MPT LPS Batch #2	1,640	NA	44 to 49

Based upon the disc work, GTI followed up with the preparation of several tubes via extrusion. Fifteen tubes were prepared using a slightly modified disc formulation to permit lower pressure extrusion and good tube morphology development. The tubes were calcined following the procedure developed for the "optimized" disc above. Table 5-3 shows the permeance and strength testing results for these tubes labeled MPT LPS Batch #1 and similar data for the low purity and commercial substrates (MPT standard substrate) for comparison. As shown, the average water permeance of these tubes was determined to be ca. 2,150 lmhb, slightly higher than the disc permeance noted above for a nominal 1mm thick body. Three point bend testing (destructive) was also conducted with six of these tubes and the bend strength was determined to be ca. 37 to 40 psi, which was slightly below the target 40 to 45 psi observed with our standard substrate. Given the lower strength and exceptionally high water permeance, the remaining tubes in this batch were calcined again at slightly higher temperature to improve the strength to at least the commercial body strength. The results for the higher firing temperature are also shown in Table 5-3 for MPT LPS Batch #2. As can be seen, it is possible to develop slightly higher strength at 44 to 49 psi relative to the commercial substrate and still maintain water permeance that are exceptionally higher.

Overall, GTI demonstrated that it is possible to prepare larger pore size substrates with strength comparable to an existing commercial product, but display ca. 7-fold higher water permeance. As the next phase of this development process, it is necessary to prepare both the 50 and 8nm pore size surface layers to qualify this substrate as a potential membrane for the TMC application.

5.3 Development of low cost TMC membrane tubes

Reducing the cost of the membrane tube was also a primary objective of this project. Initially, a small batch of 30 TMC membrane tubes was prepared using a lower cost “low purity” alumina. The primary difference between our standard alumina and the newer variant is the soda (NaO) content. The low soda (high purity) material used as a standard product is qualified for nuclear service. However, this level of quality is unnecessary for this TMC application. Further, the tube cost reduction can be expected to be on the order of at least 20 to 25% using a lower cost alumina.

Table 5-4. Performance of the low purity alumina substrates and the MPT standard substrate tube.

Part ID	**Water Permeance [liter/m^2/hr/bar]**	**N_2 [m^3/m^2/hr/bar]**	**Bend Strength [psi]**
Low purity substrates from 1Q2016 (this reporting period)			
SubAL-LPTC15.01	233	62	44
SubAL-LPTC15.02	221	60	42
SubAL-LPTC15.02	245	71	46
Low purity substrates from 2Q2015			
SubAL-LP807.02	142	27	48
SubAL-LP807.06	155	33	46
MPT Standard Substrate	220 to 250	75 to 90	40 to 45

The initial set of tubes (SubAL-LP807 series) showed considerably lower N_2 and water permeance than the standard high purity alumina membrane we prepare commercially as shown in Table 5-4. This has been attributed to the smaller average pore size, due to the smaller average particle diameter relative to our commercial part. Figure 5-2 shows the percentage contribution to flow (air testing) versus pore size for the SubAl-LP807 alumina membrane using MPT liquid displacement porometer. In brief, this unit is used to measure the flow contribution at various pore sizes by comparing the gas permeation rate of the membrane at a given pressure (which is proportional to pore size) with the dry membrane versus the membrane wetted with isopropanol. At low transmembrane pressure, the gas permeance of the *wetted membrane* is essentially zero. As the pressure is increased, it eventually becomes high enough to begin displacing the wetting fluid from the largest pores. This is the “breakthrough” pressure of the membrane and in an immersion bubble test, this would be observed as the first instance of bubbles emerging from the part (below this pressure, the membrane is impermeable to air when wetted with isopropanol). For reference, in isopropanol for our standard substrate, this breakthrough pressure is 16 to 18 psig and corresponds to a pore size of ca. 0.6 micron. At higher pressures above the breakthrough pressure, the wetting fluid is displaced from progressively smaller pores. Hence, a flow contribution from pores of various sizes can be determined. Figure 5-2 shows that there is a considerable shift to lower average pore size for the LP807 material versus the MPT standard material. This shift is consistent with the lower average water and gas permeance of this style of tube.

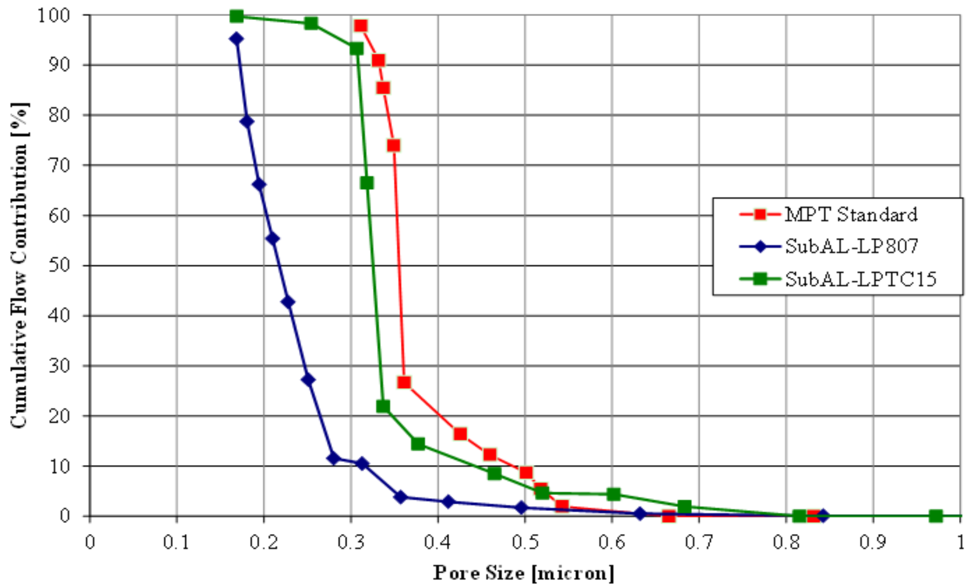

Figure 5-2. Percent of flow contribution versus pore size for air with the two lower purity alumina substrates compared with MPT's standard substrate

Following the disappointing results with the SubAl-LP807 membranes, a new set of membranes was prepared from a different source of lower purity alumina designated SubAL-TC15 series. The water and N_2 permeance of a sample of these membranes is presented in Table 5-4, which shows this material has comparable permeance to the high purity alumina membrane and displays considerably better performance than the previously prepared batch (SubAl-LP807). Also, the membrane strength is comparable to the high purity standard. In addition, the pore size distribution for the SubAL-TC15 material is also shown in Figure 5-2. As can be seen, this material more closely tracks the pore size distribution of MPT standard substrate and this result is consistent with the water and gas permeance data shown in Table 5-4.

Overall, GTI has prepared reasonably high quality membrane supports from low purity alumina that show water and gas permeance similar to the high purity alumina standard support previously prepared. Furthermore, the part strengths are indistinguishable between the various styles. Hence, it is reasonable to expect that high quality TMC membranes can be prepared using lower cost alumina.

<u>Completed the Production Cost Estimates for the Lower Purity Alumina:</u> Based on successful testing of the two lower cost tubular substrates, GTI prepared a preliminary cost estimate to fabricate tubes for a standard low pressure TMC unit. The specifications for the tubes are as follows:

<u>OD/ID:</u> Nominal 3.5mm/5.7mm ID/OD ceramic TMC membrane tubes.
<u>OD Spec:</u> OD spec is 0.2205 to 0.2245".
<u>Length:</u> 38" (977.7mm)
<u>Length Spec:</u> ± 1/16"
<u>Nominal Pore Size:</u> 100Å Alumina or 200Å zirconia modified active layer

Table 5-5 shows the estimated single tube cost breakdown between the standard and low cost alumina materials. The LP807 and LPTC15 materials are similar in cost, so only one line item is generated for this material. The table is broken down by production volume on a yearly basis and reflects levels at which improvements in bulk material pricing, labor utilization, automation, and other cost savings can be introduced to further decrease the tube production cost. At volumes above ca. 750,000 parts per year, it is possible to take advantage of the full pricing impact of the low cost tubes and at this level it is estimated that the cost savings over the standard substrate will be substantial and on the order of 30%. Further, at these larger volumes, considerable economy of scale is introduced as suggested above. Hence, the overall cost reduction from the current substrate at small volumes (~$3.21 per tube) versus the new substrate at high volumes (~$1.69 per tube) would be nearly 50%.

Table 5-5. Estimated TMC tube production cost based upon MPT standard and the newly developed

Production Quantity (parts/year)	<150,000	>150,000	>750,000
Substrate Material			
MPT commercial substrate	$3.21	$2.88	$2.41
LP807/LPTC 15 substrate (low purity substrates)	$2.88	$2.32	$1.69

5.4 Preparation of 1,000 finished TMC tubes for pilot TMC testing

Based on the membrane development work GTI completed to improve the membrane water vapor transport flux and low pH resistance shown at the end of this task, more than 1,000 36" long TMC membrane tubes with the newly developed ZrO_2 top layer coating were produced for the pilot scale TMC unit fabrication and testing.

6. Low Cost TMC Fabrication and Assembly Method Evaluation

Besides the cost of membrane tubes in the TMC module, GTI evaluated in the last section, there are another two parts having major cost implications on the TMC module. They are the two tube sheets, which hold the membrane tubes together by epoxy, and the two end caps which form the integrated water inlet/outlet chambers for the TMC module. They are made from engineering plastic material that can withstand high temperature, as well as resist corrosion. They are currently machined from existing Garolite® sheet material that costs about $200 for each piece required for fabrication. For mass production, this machining method needs to be replaced with other low cost fabrication approaches to reduce the overall TMC module cost. In this section, GTI summarized the work on this topic with engineering plastic manufacturers to evaluate different fabrication methods, including injection molding and compression molding methods for TMC tube sheet and end cap fabrications. From these evaluations, GTI developed cost estimates for using the selected method compared with current machining approach. By using the molding methods, GTI estimates each part cost can drop to 1/10th of the machining part, which alone can result in a cost reduction by half for the overall TMC module. The TMC heat and water recovery system cost can be further reduced by simplifying design and control methods, which will be further evaluated in future development.

6.1 Low Cost TMC Module Parts Fabrication Methods Evaluation

Figure 6-1 shows a picture of current TMC membrane module at upper left. Based on which GTI generated a 3-D model at upper right, and a 3-D exploded drawing to show all the major parts at the bottom.

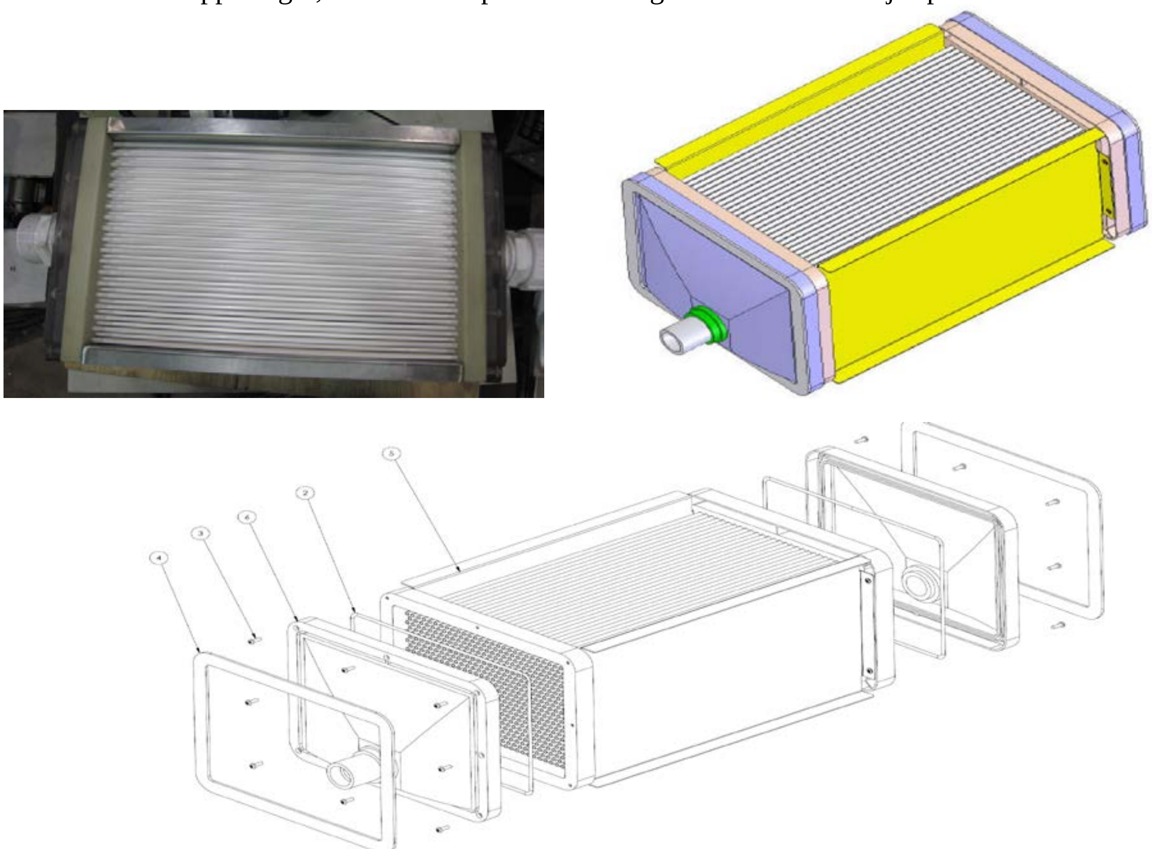

Figure 6-1. TMC membrane module and its exploded drawing

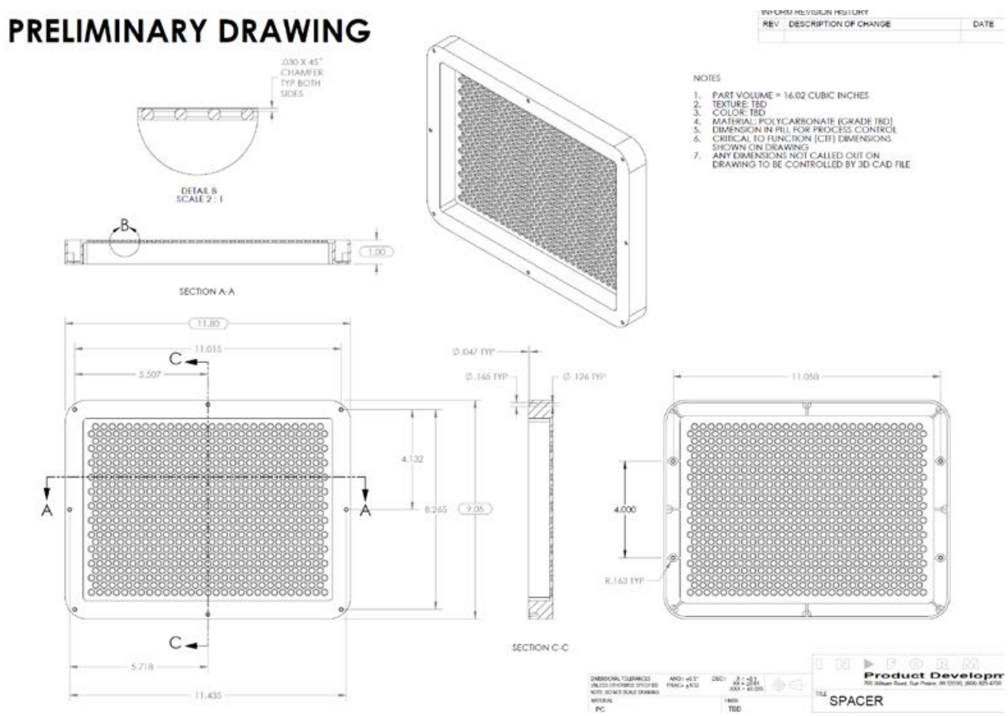

Figure 6-2. TMC module tubesheet drawing for compression molding

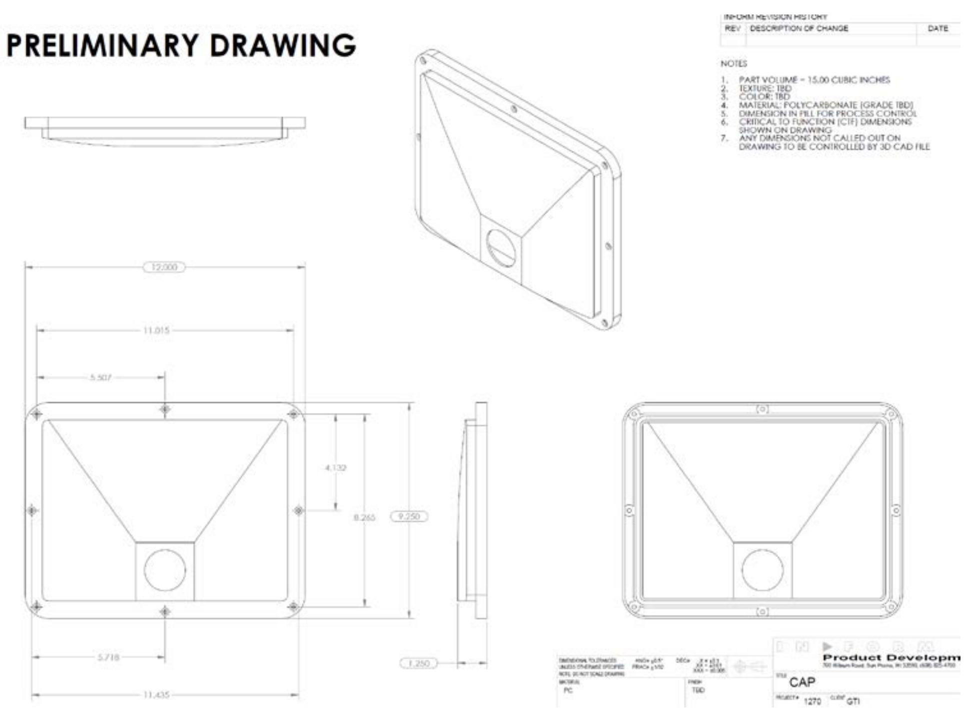

Figure 6-3. TMC module end cap drawing for compression molding

Two pair of major TMC module parts, namely TMC tubesheet and end cap, plus the membrane tubes, constituted of the most cost of the TMC module. GTI's efforts have been focused on reducing the fabrication cost of these two parts in this section.

By working with an independent consultant specialized on engineering plastic design and fabrication, the design of the TMC module tube sheet and end cap by using different molding methods and materials were evaluated, including injection molding, compression molding with thermoplastic material (e.g., polycarbonate) and thermoset Polyester and Phenolic material (e.g., epoxy with fiber re-enforcement). The following provides highlights of this evaluation:

1. Injection molding parts can't meet the strength requirement for the TMC module while the compression molding parts can. Therefore, GTI selected the compression molding method to mass produce for the TMC application requirement. This will reduce the end cap cost from about $200 down to $17. A similar price reduction has been confirmed for the tube sheet fabrication.
2. Selected a contractor, Innovation Mold & Design, to fabricate the tool (die) for a compression molding machine.
3. Selected a contractor, Dickten Masch Plastics, to manufacture the end caps and tube sheets using the compression mold. Drawings for the tubesheet and end cap are shown in Figure 6-2 and 6-3.
4. Selected two resins for testing of the new mold: a Thermoset Polyester and a Phenolic grade resin.
5. Fabricated 20 sample end caps and 20 tube sheets using equal portions of Polyester and Phenolic grade resins.
6. Completed a lab evaluation and confirmed the molded parts have comparable mechanical and thermal properties as the machined parts.

GTI's research into the molding method/regime and resin selection for the commercialization of the TMC end caps and tube sheets have resulted in GTI selecting the regime and resins, as well as contractors for making the tools and manufacturing the parts. Although the proposed scope of this task was to design and have a die made for injection molding the TMC end caps and tube sheets, and selection of the best resin, GTI learned from this research that injection molding was not the best value. GTI concluded that a compression-molded end cap and tube sheets is the best choice for the TMC in the long run.

Comparing the original plastic (polycarbonate resin or PC resin) that was employed and what GTI's design evolved to is revealing that the "Garolite" material GTI ultimately selected was a Phenolic resin. GTI tested Dickten's Phenolic resin #106472, similar to the Garolite. Phenolic resins have a crystalline lattice shape and are cross-linked across an oxygen molecule. This means there are no voids (interstitial interstices (vacancies) in the lattice structure) for movement or entrapment (of moisture, for instance). Therefore, there is no issue with moisture absorption and no negative Van der Wall's effect of slight warping during cooling of the part.

With this die, GTI can produce compression-molded end caps or tube sheets for a price of 8% of the current machined part. Note that the Phenolic resin we are using is not "Garolite", since Garolite is simply a trade name for a resin that each manufacturer assigns. On all significant properties, Phenolic resin far exceeds the PC resin, having 4-times the Compressive Strength that the PC has. Figure 6-4 shows both the 3-D drawings and the actual molded parts with the machined parts as comparison.

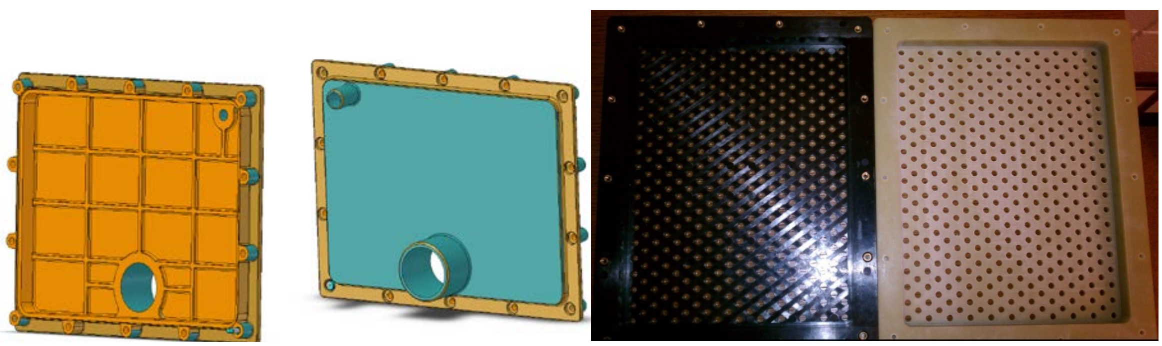

Figure 6-4. Compression molded end cap drawings, and pictures of molded tubesheet (black color) compared with machined tube sheet (yellow color)

Financial benefit of compression molded end cap and tubesheet:

Currently, it costs ~$200 to have an end cap made (machined part from an extruded or molded sheet). The new price of a compression molded end cap will be $17, a reduction of 92%. A similar price reduction can be achieved for a molded tube sheet. The side plates currently used are stainless steel sheet metal, which can be simply replaced with injection molded plastic plates. It will provide the same needed strength and anti-corrosion properties.

Besides reducing part fabrication costs, GTI also worked on a larger membrane module design to allow economical scale up of the TMC unit. Figure 6-5 shows one of the large TMC module GTI developed, which features a 34” long membrane tube module design instead of the current 18” long module design. This can significantly reduce the overall TMC unit cost for both reduced module cost and installation cost.

Figure 6-5. Long TMC module with higher capacity

6.2 Low Cost TMC Module Assembly Methods Evaluation

Besides the part fabrication cost, the TMC module assembly methodology is also very important to save labor costs on producing the TMC module. Working with our partner, GTI developed detailed procedures on how to assemble the TMC module. Figure 6-6 and Figure 6-7 show pictures on methods to improve current TMC module assembly and interconnection approaches, to achieve further cost reductions. A very important component in the TMC module assembly is the adhesive to be used for bonding the ceramic membrane tubes to the tubesheets at their two ends. It must have the following features to be qualified as the bonding adhesive for TMC modules:

1. adhesion to both alumina ceramic membrane tubes and the engineering plastic tubesheets,
2. flow characteristics to fill between tube and the holes on the tube sheets, but not leak through from the gap in-between (i.e., optimal viscosity),
3. withhold high temperature (>400ºF) at high moisture content,
4. flexibility after cured for thermal expansion/contraction cycles which it will experience during the TMC operation,
5. ability to be used in automated adhesive dispenser, and easy to be cured either by exposing to the atmosphere or by using UV lights or other approaches. Figure 6-8 gives some details of the setup on the automated adhesive dispenser for building a TMC module.

After experimenting with several adhesives, a two-part atmosphere cured adhesive was chosen for the TMC module assembly. The assembled TMC module with this method and the adhesive selected has been proved to be robost and feasible for the TMC application.

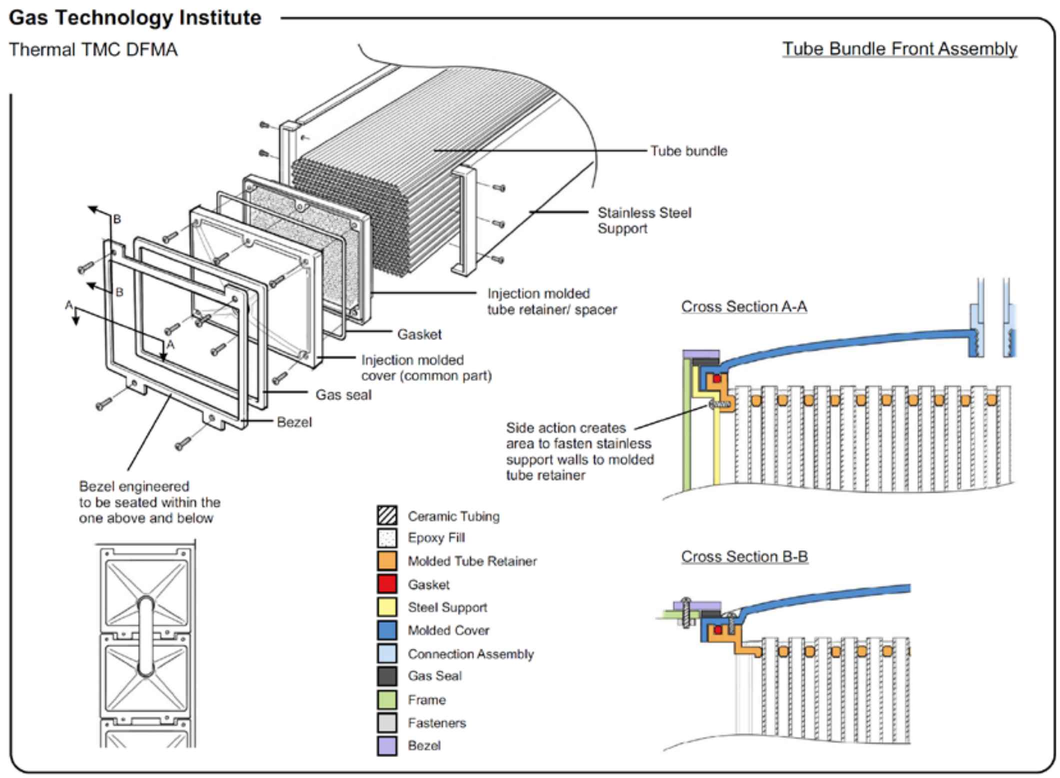

Figure 6-6. TMC module assembly details (front view)

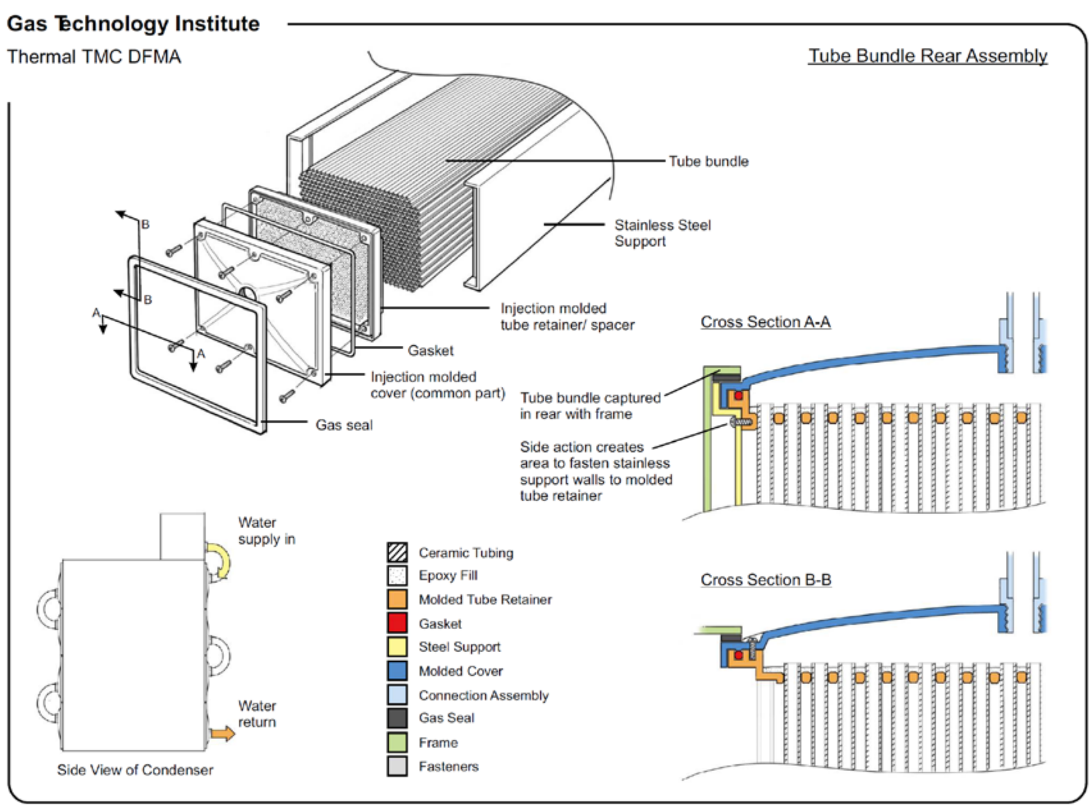

Figure 6-7. TMC module assembly details (rear view)

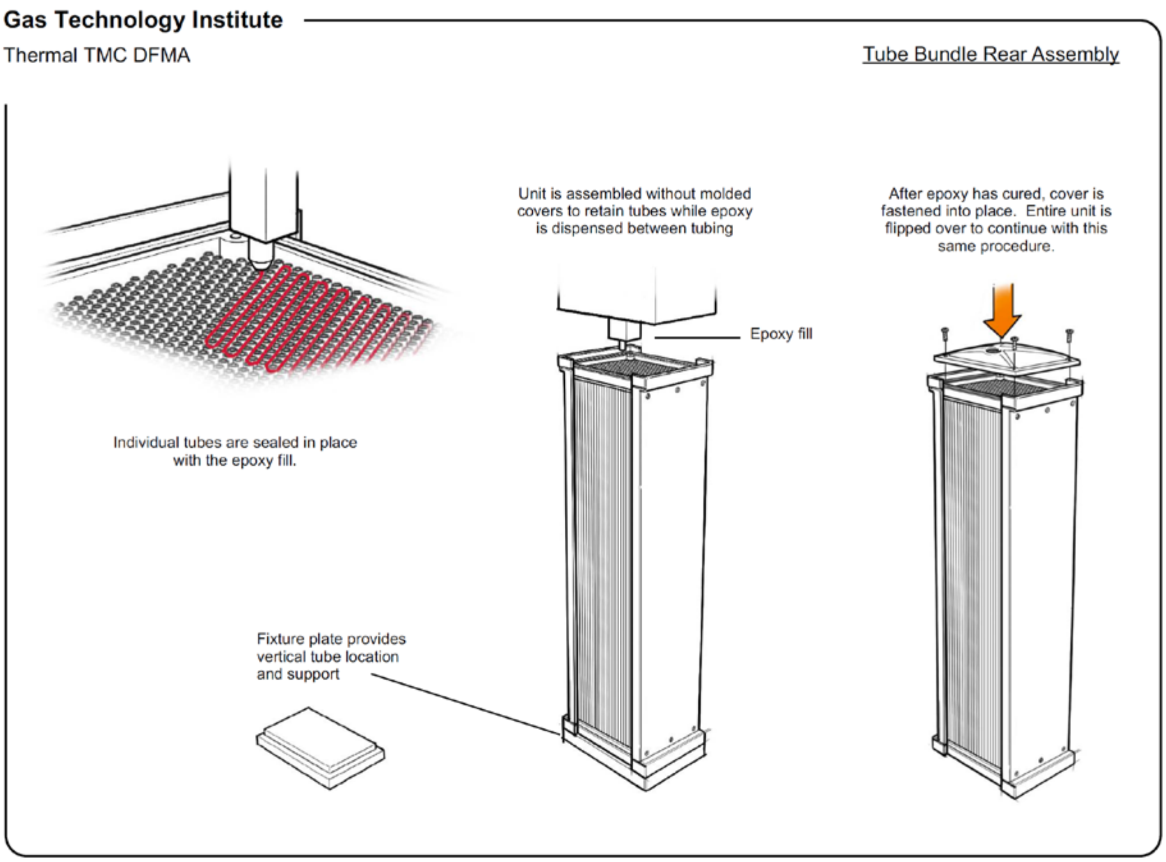

Figure 6-8. TMC module assembly details (automated adhesive distribution)

6.3 Cost Reduction Evaluation Summary

In summary, GTI has evaluated cost reduction methods on parts fabrication and TMC module assembly, which all contribute to the final TMC module cost reduction realized as shown in Table 6-1, which compares the current TMC module cost with the new design. The new design will provide approximately a 60% cost reduction compared to current costs.

Table 6-1. TMC Module Cost Review

Item	Supplier	Unit Cost($)	Number required	Present cost($)	Improvement	Future Cost($)
Tubes	M&PT	3.21	389	1249	$1.69	657
Tubesheets		230	2	460	Compression molded part at $17/each	34
End Caps		190	2	380	Compression molded parts at $10/each	20
Side plates		25	2	50	Injection molding at $2/each	4
Miscellaneous parts - 'O' ring, screws, etc.		50	1	50	None	50
Adhesive	Grainer	47	1	47	None	47

Assembly labor:1 hr for tube installation,1.5 hrs for assembly of endcaps/O ring/screws, total 2 hrs	$55/hr assembly facility	55	2.5	138	50% reduction due to higher production rates and process automation	119
Pressure test labor	$55/hr assembly facility	55	0.5	28	None	28
Total TMC Module Cost				**$ 2,402**		**$ 959**

7. TMC System Design and Performance Testing

The main objectives of this section are to develop the new pilot-scale TMC system design, prepare the lab test system for the TMC unit integration and testing, and carry out the TMC waste heat and water recovery system performance testing.

7.1 TMC Test System Design and Lab Setup

The TMC performance tests were completed in the GTI combustion lab. A schematic is shown in Figure 7-1, which is the test system setup specifically for the TMC performance testing. It consists of a 3-million-Btu/h boiler to provide the flue gas, a high pressure economizer (HPE) to lower the flue gas temperature to desired conditions, a flue gas conditioner to add in SO_2, water vapor and other components to simulate power plant flue gas conditions, the TMC test section, and associated pumps, ID fan, control valves, to complete the whole test system. Figure 7-2 shows the pictures of the installed system, with views for the boiler, HPE, flue gas conditioner, and the control panel. Figure 7-3 shows the TMC unit installed before and after the water connections, total 3 TMC modules installed in this pilot-scale TMC unit. With different water piping connections, a one- or two-stage TMC configuration can be formed to meet the desired flue gas waste heat and water recovery goals. Figure 7-4 shows one of the new TMC module picture, which features longer membrane tubes (34” long instead of regular 18” long) to save TMC module cost, as well as new tube arrangement pattern to enhance performance.

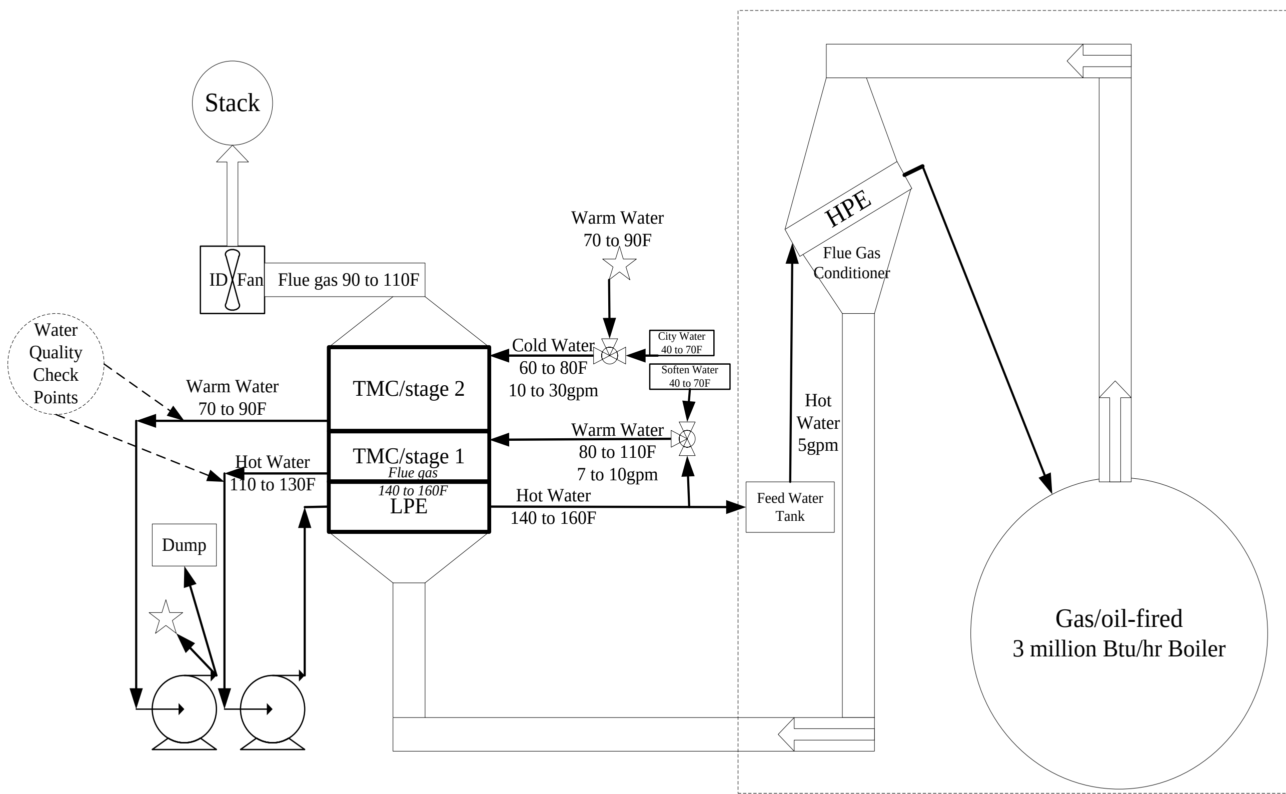

Figure 7-1. Schematic of the pilot-scale TMC lab test system setup

Figure 7-2. Pictures of the lab test system (left boiler, right control panel)

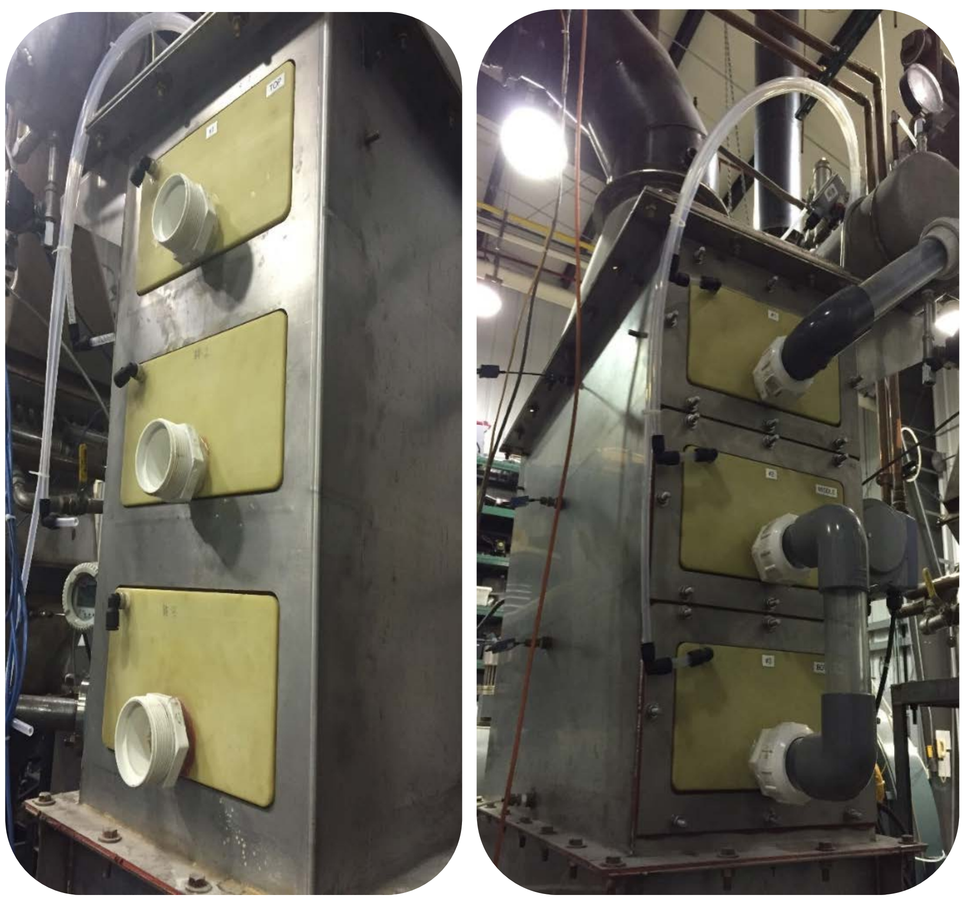

Figure 7-3. Lab TMC unit as installed with new TMC modules (left before water connections, right after water connections)

Figure 7-4. Picture of the new long TMC module as installed in Figure 7-3

7.2 TMC Pilot-Scale Unit Test at GTI lab

The design capacity of this pilot-scale TMC unit is to process all the flue gas coming out from the 3-million-Btu/h boiler, which is a significant enough scale to evaluate the TMC performance in real coal power plant flue gas. Different gas components can be added in the gas conditioner which includes SO_2, H_2O, NO_2 and others, to simulate coal combustion flue gas compositions from a power plant with or without a FGD. After shakedown to verify the whole system works properly, a series of baseline TMC unit performance tests were completed first with the original TMC modules. Next, GTI proceeded with the new TMC module testing at the same conditions. The new TMC module design uses the same amount of membrane tube surface area as the old one, to make sure it can be compared with the old TMC module performance objectively. The new TMC modules feature new arrangement patterns based on CFD simulation results in Chapter 4.

7.3 TMC Test Result Analysis

Several tests were done for both the old and new TMC module performances during this project. Figure 7-5 show the results on TMC cooling water inlet temperature effects on TMC heat transfer and water transport rates. The TMC heat transfer rate decreases as cooling water temperature increases, which is due to decreased temperature difference between the flue gas and cooling water sides in the TMC. The new TMC module shows about 30% heat transfer performance increase over the old TMC module, which is encouraging and favorable to prove the new design is effective. The TMC water transport rate shows a similar trend as the heat transfer rate, which is understandable because they are closely coupled. The condensed water vapor and transported water released latent heat, which contributes a great part of the TMC overall heat transfer rate. The new TMC module shows a 40% increase in water transport rate compared with the old TMC module.

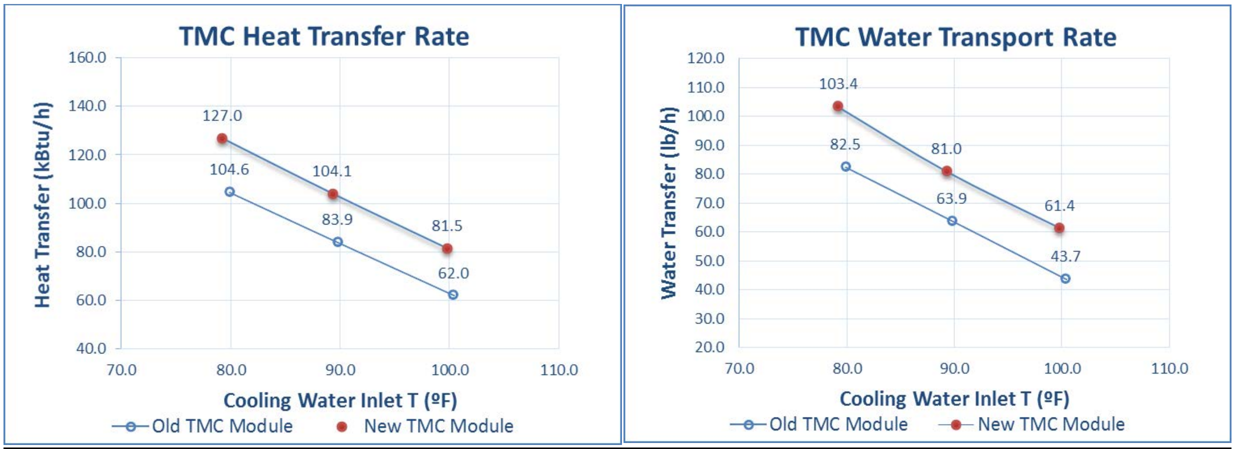

Figure 7-5. TMC cooling water inlet temperature effects on both old/new TMC performances

Figure 7-6 shows the TMC cooling water flow rate effects. Since the cooling water flow rate increase can effectively decrease the averaged cooling water side temperature, the heat transfer through the TMC increases as expected due to the resulted larger temperature difference between the flue gas and water sides. The same effect on TMC water transport rate, the more water vapor condensed and transferred, the more heat transfer can be achieved by the TMC. The new TMC module shows great improvement over the old TMC module on both heat transfer and water transport, by from 30 to 50% depending on the cooling water flow rates.

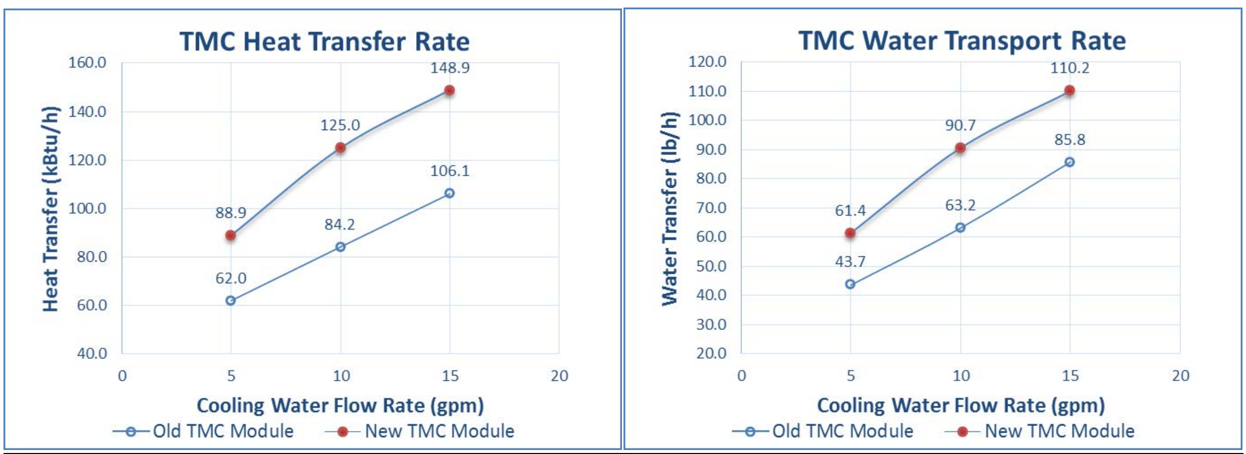

Figure 7-6. TMC cooling water inlet flow rate effects on both old/new TMC performances

TMC flue gas inlet temperature is another factor that affects the TMC performance. For the typical flue gas inlet temperature range designed for the TMC, from 150ºF to 180ºF, it only has a small effect on heat transfer and minimum effect on water transport as shown in Figure 7-7. Higher inlet flue gas temperature does increase heat transfer rate, but has minimum effect on water transport rate because the latter one is closely coupled with the flue gas moisture content, which was kept constant for these two cases. Without condensed water vapor latent heat contribution, total heat transfer rate does not change much which has proved vapor latent heat has a major contribution for overall TMC heat transfer. Again, the new TMC modules outperform the old TMC modules by 20 to 40% on heat transfer and water transport, which is very encouraging to prove the new TMC module was well designed with the higher water transport flux membrane and optimized membrane tube arrangement pattern.

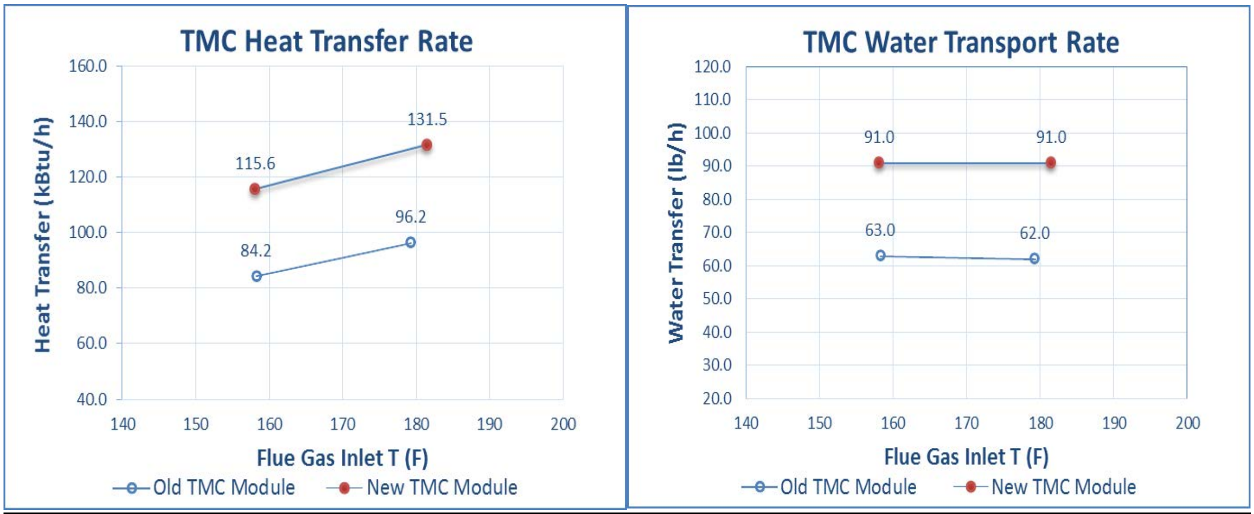

Figure 7-7. TMC flue gas inlet temperature effects on both old/new TMC performances

Several more tests were done for both the old and new TMC module performance during this project. Figure 7-8 shows results on TMC flue gas inlet moisture effects on TMC heat transfer and water transport rates. The TMC heat transfer rate increases as flue gas moisture content (dew point Td) increases, which is due to increased flue gas moisture content which increases water vapor partial pressure difference across the TMC membrane. The water vapor partial pressure difference is the major driving force for the membrane water vapor transportation. The new TMC module shows about 40% heat transfer performance increase over the old TMC module, which is encouraging and favorable. The TMC water transport rate shows a similar trend as the heat transfer rate, which is understandable because they are closely coupled. The condensed water vapor and transported water released latent heat, which contributes a great part of the TMC heat transfer rate. The new TMC module shows around 50% increase in water transport rate compared with the old TMC module.

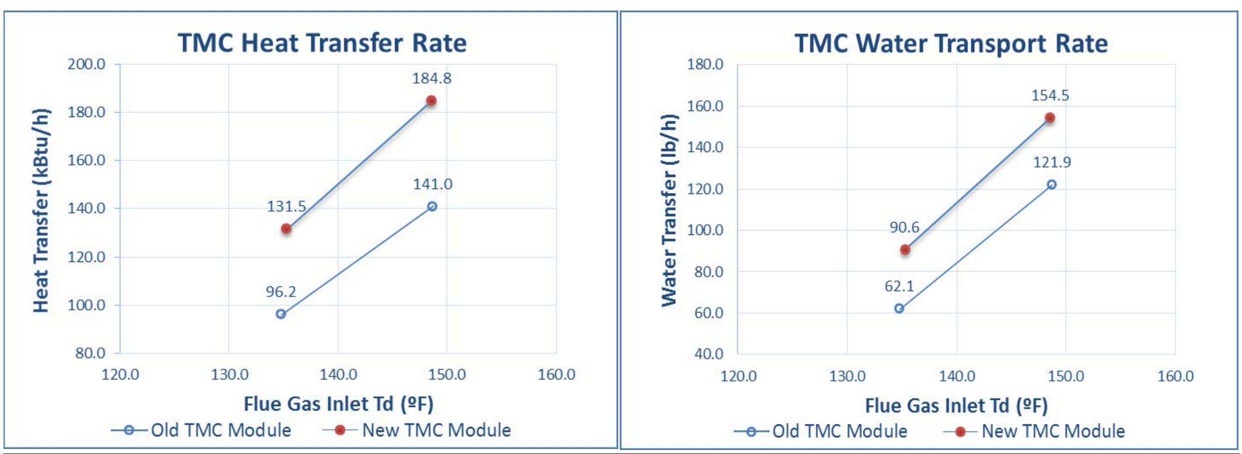

Figure 7-8. Flue gas inlet moisture effects on both old/new TMC performance

Figure 7-9 shows the cooling water flow rate effects for the TMC inlet flue gas at high moisture content. Because a water flow rate increase can effectively decrease the averaged cooling water side temperature, the heat transfer through the TMC increases as expected. The same effect on TMC water transport rate, the more water vapor condensed and transferred, the more heat transfer can be achieved by the TMC. The new TMC module shows great improvement over the old TMC module on both heat transfer and water transport, by about 25-35% depending on the cooling water flow rates.

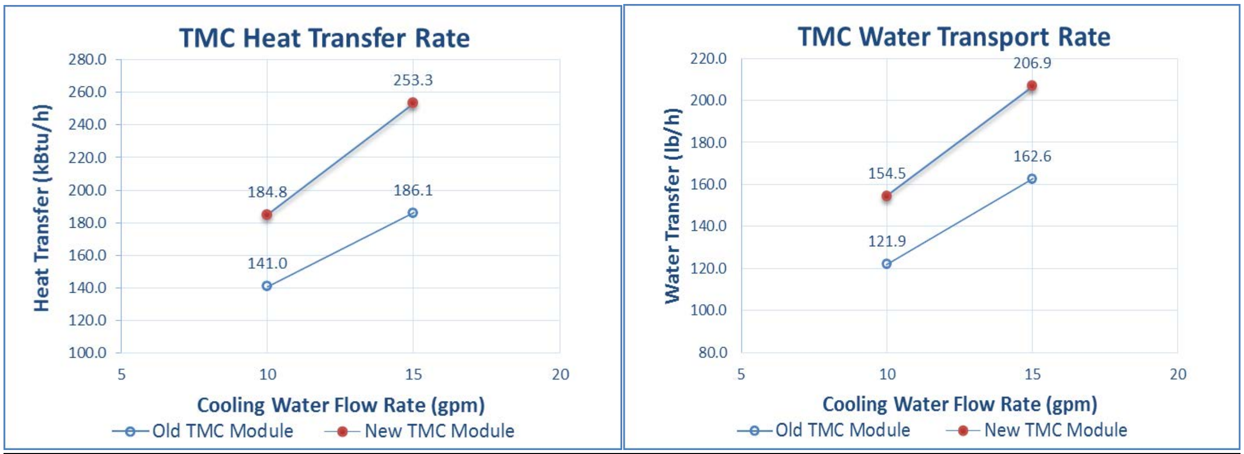

Figure 7-9. TMC cooling water inlet flow rate effects on both old/new TMC performance at high flue moisture content

7.4 TMC Test Summary

The newly designed TMC modules have been tested at the pilot scale in GTI's lab testing system for their performance to compare with existing TMC modules as a baseline. The new TMC modules are featured with high water transport flux and low pH resistant ZrO2 membrane, and new membrane tube arrangement patterns based on CFD simulations. The performance test results show that the new TMC module outperformed the baseline modules in all aspects of performance at various conditions, typically by 30 to 50%. The higher TMC performance and lower cost TMC development efforts together will contribute to a favorable prospective for the TMC future commercial applications in the power generation industry.

8. TMC Power Plant Integration Study and Economic Analysis

In this section, based on previous study and the pilot-scale test data, we have further evaluated the TMC power plant integration, and a preliminary scale-up design for a 550MW plant were developed. On this practical scale, GTI performed economic analysis to see if the TMC application is feasible on both technical and economic aspects. Previous analyses shows that the TMC system should perform well in terms of recovering waste water and heat simultaneously if integrated into a coal-fired power plant with a wet FGD system. However, it is still necessary to understand what extra impacts or expenses may be generated by using this technology.

8.1 Economic Analysis of Integrating TMC and FGD Systems

Wet FGDs have been successfully used for a complete range of coal types including anthracite, bituminous, sub-bituminous, lignite and brown coals. Wet FGD is also installed on systems that use heavy oil and Orimulsion for fuel. Conventional wet FGD systems utilize a wet limestone process with in situ forced oxidation to remove SO_2 and produce a gypsum byproduct [3]. Approximately 85% of the FGD systems installed in the US are wet systems, 12% are spray dry and 3% are dry systems [4]. Figure 8-1 and Figure 8-2 show the population of FGD systems and proportion of these different types in the U.S. Since wet FGD system is the most popular and adds the most water to the flue gas, the following sections focus on analyzing the integration of TMC with only wet FGD.

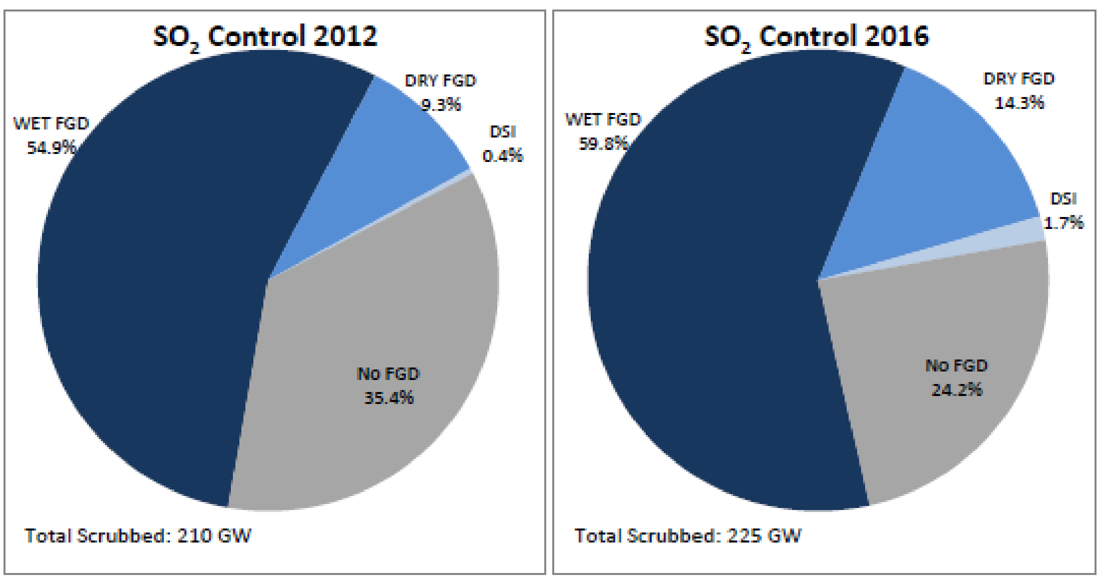

Figure 8-1. Population of FGD Systems in the U.S. in 2012 and Expected 2016 [5]

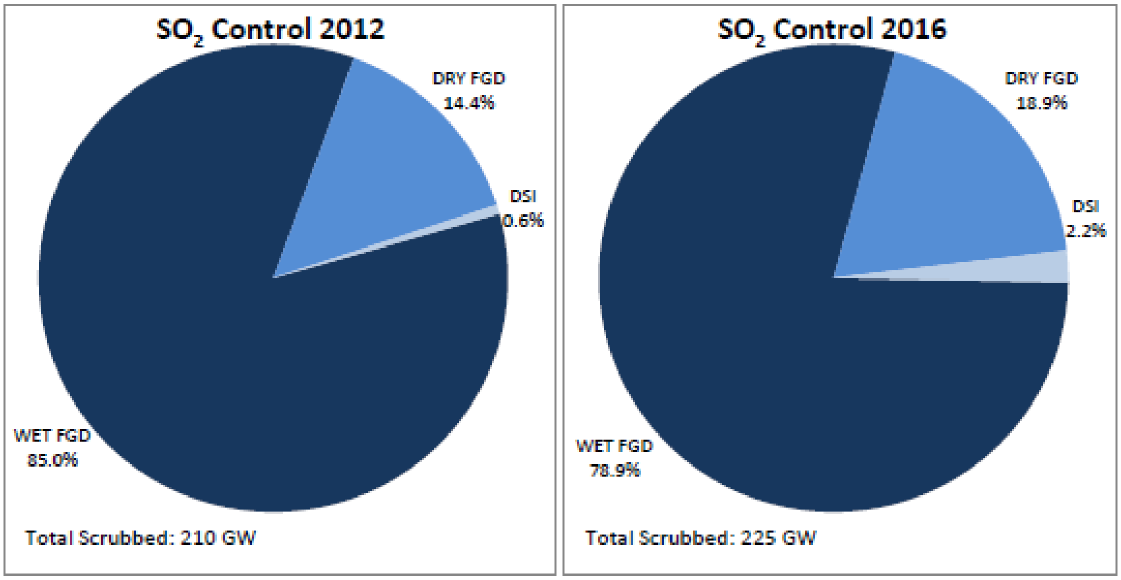

Figure 8-2. Proportion of FGD System Types in the U.S. in 2012 and Expected 2016 [5]

For those coal-fired plants without FGD systems or for new units, the capital costs and O&M costs (operations and maintenance) costs are shown in Table 8-1. This information shows that wet FGD systems typically have a lower cost in large units (>400 MW) than in small units (<400 MW). Among several wet FGD technologies, limestone-based (limestone with forced oxidation or LSFO) and lime-based (magnesium-enhance lime or MEL with forced oxidation) are the most popular ones and have both been successfully used in coal-fired power plants. Table 8-2 shows the detailed cost of a LSFO FGD system in a 500 MW power plant, which indicates that burning high-sulfur coal will result in higher cost. Also, installing a FGD system requires higher expenses in retrofit units than in new units.

Table 8-1. Cost Information of FGD Systems [4]

Scrubber Type	**Unit Size**	**Capital Cost**	**O&M Cost**	**Annual Cost**
	MW	**$/kW**	**$/kW**	**$/kW**
Wet	>400	100 - 250	2 - 8	20 - 50
	<400	250 - 1500	8 - 20	50 - 200
Spray Dry	>200	40 - 150	4 - 10	20 - 50
	<200	150 - 1500	10 - 300	50 - 500

Note: Data in 2001 dollars, and assumes capacity factor > 80%

Most of the retrofit units are equipped with booster fans to overcome the pressure drop across the FGD absorber. The booster fans are often installed behind the existing ID fans. On the other hand, new units are expected to be installed with ID fans that are large enough to overcome the pressure drop across the FGD absorber. This feature would typically result in a lower capital cost for the draft system on a new unit application in comparison with a retrofit application. To accommodate the saturated flue gas from a wet FGD system, wet stacks are typically designed using a highly corrosion-resistant material with lower gas velocity. This is required to prevent condensed moisture from being carried out the top of the stack. Most of the retrofit units are, therefore, required to have a new stack [2]. However, if TMC technology is applied in the system, some of the moisture will be recovered and a new stack may not be necessary since the corrosion risk would be mitigated. With that being said, the stack can be reused if the corrosion condition of the stack meets the standard, thus the cost of building a new stack can be saved.

Table 8-2. Detailed Cost of LSFO FGD System in 500 MW Coal-Fired Power Plants

		New Units		**Retrofit Units**	
		High-S Coal	**Low-S Coal**	**High-S Coal**	**Low-S Coal**
Capital Cost	US$	64,451,000	53,344,000	85,858,000	76,256,000
Capital Cost per kW	$/kW	125	107	172	152
Fixed O&M Cost	$/yr	3,929,000	3,514,000	4,470,000	4,055,000
Variable Operating Cost	$/yr	4,369,000	2,448,000	4,369,000	2,448,000
Total Yearly O&M Cost	$/yr	8,298,000	5,962,000	8,839,000	6,503,000
FGD System Life	years	30	30	20	20
Capital Cost Levelization Factor		14.50	14.50	15.43	15.43
Operating Cost Levelization Factor		1.30	1.30	1.22	1.22
Levelized Cost	MM$/yr	19.84	15.49	24.05	19.68
Total Cents/kW-hr	cents/kWh	0.57	0.44	0.69	0.56

Note: Data from [2], discount rate and inflation rate for levelized cost were set to 8.75%/yr and 2.5%.

8.2 Potential Impacts and Benefits of Integration TMC System

Integration of the TMC system will result in less than 1 inch-water pressure drop increase to the original system. With FGD system added, one of the major components of auxiliary power is the additional power required by ID fans to overcome the system pressure drop caused by the flue gas flow through the absorber. The pressure drop that the TMC system will bring to the gas path is much less than the total pressure drop that FGD system will bring to the gas path. That means the additional ID fan power for integrating the TMC system can be covered by the FGD booster ID fan power increase. The system pressure drop of the FGD was estimated and the results are shown in Table 8-3. The gas path of the system will start at the discharge of the existing ID fans, through the new booster ID fans and the FGD unit, and discharge into a new acid brick chimney. The draft requirements of the LSFO FGD system can be accommodated by the booster ID fans. The booster ID fan is sized to provide an additional 10" H_2O (9" operating) and 9" H_2O (8" operating) pressure drop through the FGD for high- and low-sulfur applications, respectively. The flue gas system for the MEL process will be identical to the LSFO process, with the exception that the draft requirements will be reduced to 8” H_2O (7” operating) [2]. Table 8-3 shows that the extra pressure drop that the TMC will add to the system is similar to a mist eliminator of an FGD. Therefore, if TMC is designed to replace the mist eliminator, the extra auxiliary power requirements on the ID fans could be eliminated.

There are different potential approaches with several benefits of integrating the TMC system in coal-fired power plants with wet FGD technology. First, TMC may work like a mist eliminator of the FGD system to collect moisture after the FGD system. It will not only improve the mist eliminating efficiency but also recycle the recovered water. This procedure will not require extra pressure drop and no extra load to the ID fans. Second, some FGD systems apply a Gas-to-Gas Heat exchanger (GGH) to reheat the exhaust and reduce visible stack plume. The GGH reheats the scrubbed gas using unscrubbed gas flow streams of the FGD system. If a TMC system was integrated, the moisture in the flue gas would be decreased and any visible stack plume would be reduced. Because of these benefits, the GGH may not need to be installed and therefore the capital cost and O&M cost of the GGH would be eliminated. Third, TMC systems can improve coal-fired boiler efficiency by recovering heat, which can lower the coal consumption and CO_2 emissions with the same power generation. As coal-fired power plants have to meet ever more stringent emissions regulations, it is significant that TMC is able to help reduce emissions and benefit coal-fired power plants in this way. Finally, TMC systems will save a lot of water consumption for coal-fired power plants which is important for maintaining water supplies, especially in drought-prone regions of the world. Recovered water from TMC can be used as boiler make-up water, cooling tower make-up water, FGD make-up water or RRI/SNCR dilute water. Detailed layout design and technology methods for incorporation of TMC modules are compared and summarized in the next sections.

Table 8-3. Estimated FGD System Pressure Drop in inch of H_2O

	LSFO High-S	**LSFO Low-S**	**MEL High-S**	**MEL Low-S**
Ductwork to FGD	1	1	1	1
FGD Inlet Expansion	0.5	0.5	0.5	0.5
FGD Spray	3.12	1.92	0.96	0.72
Mist Eliminator	0.8	0.8	0.8	0.8
FGD Outlet Contraction	0.5	0.5	0.5	0.5
Ductwork to Stack	0.2	0.2	0.2	0.2
Additional Stack Pressure Due to Wet Stack	2	2	2	2
Margin	1	1	1	1
Total Pressure Drop	9.1	7.9	7.0	6.7

8.3 Incorporation of TMC in a 550 MW Commercial Scale Power Plant

GTI has successfully demonstrated the use of the TMC in industrial gas-fired boilers. This section summarizes the results of a 550 MW scale coal-fired power plant with a TMC package installed. Based on the preliminary module arrangement for the commercial unit, AECOM provided a design for the TMC system installation. It was a two-train arrangement with the total flue gas flow split evenly between two identical trains.

PC-fired Rankine cycle power plant configurations were evaluated and used for TMC layout design and incorporation for a 550 MW (Gross generation is 583 MW) coal power plant. The power plant parameters are from NETL report Case 9 [6] and are based on a market-ready technology that is assumed to be commercially available. This case employs a one-on-one configuration comprised of a state-of-the art PC steam generator firing Illinois No. 6 coal and a steam turbine. Single-reheat steam condition is 16.5 MPa/556°C/556°C (2,400 psig/1050°F/1,050°F). Figure 8-3 shows the steam flow diagram of Case 9. The plant produces a net output of 550 MWe at a net plant efficiency of 36.8 percent (HHV basis).

The TMC system should be incorporated between the wet FGD and the stack in the plant, as marked in Figure 8-3. The inlet temperature of the flue gas to TMC system is 135°F with pressure of 14.8 psia. Total flue gas flow rate is 5 x 10^6 lb/h with moisture volume fraction of 0.1517, going to two (2) trains of the TMC system. With this input flue gas data, Cases S1, S2, S3 and S4 have been built and calculated using the SmartBurn efficiency analysis tool and also compared to the Aspen results by AECOM. The results are listed in Table 8-4. In Case S1, the steam condensate flow rate is 982,967 lb/hr which was provided by GTI, assuming that relative humidity is 91% and outlet steam condensate temperature is 119°F. Net water recovered is 45,099 lb/hr and 12.08 MW gross heat was recovered and added to the steam condensate system. In Case S2, the inlet water flow rate for one TMC train is 1,543,782 lb/hr which is half of the condenser water flow rate. In Case S3, the steam condensate temperature was assumed to be 125°F, and in Case S4 the inlet water flow rate was assumed to be cooled to 95°F to maximize benefits. In Case S4, the net recovered water is 92,756 lb/hr, which means 20% of the moisture in the flue gas is condensed, and about 30 MW gross heat can be recovered.

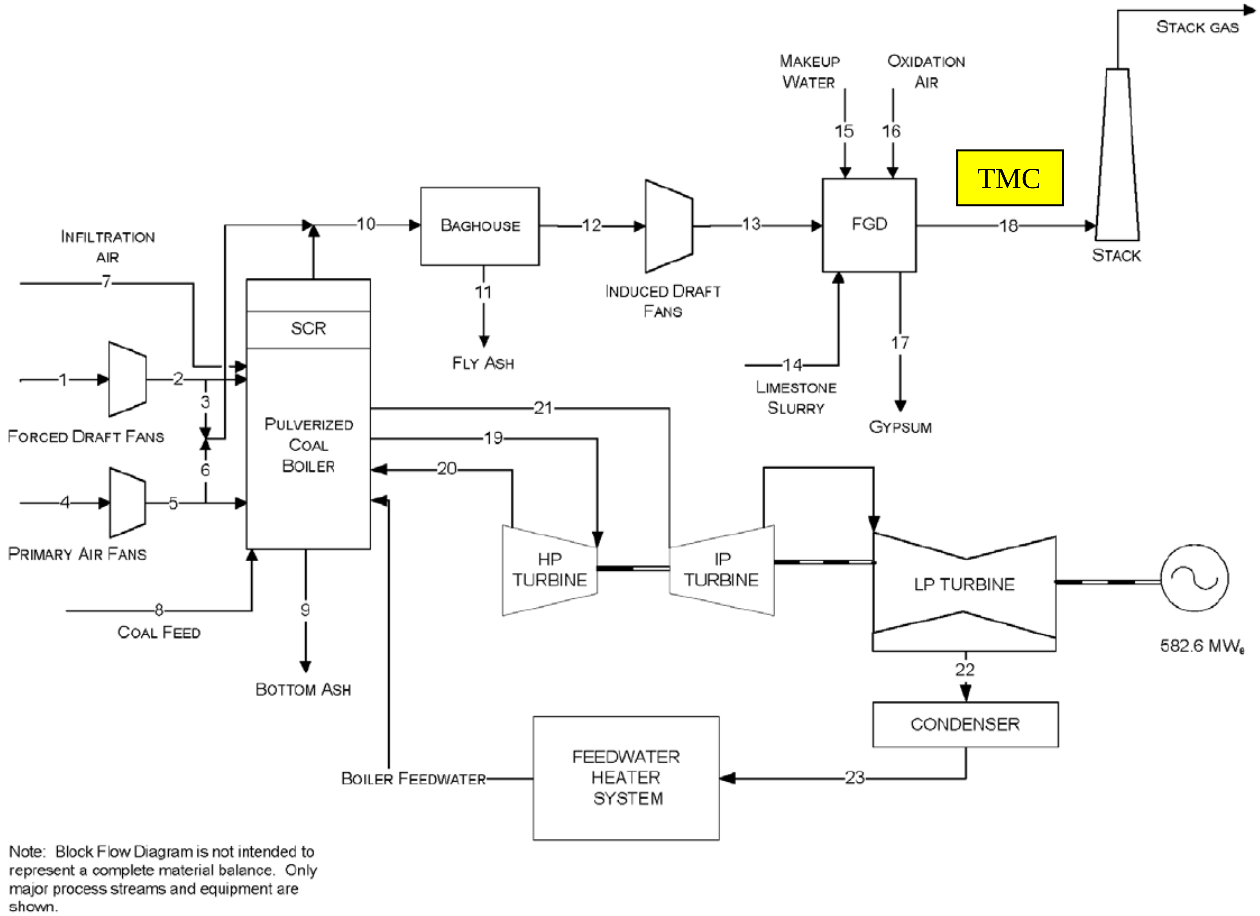

Figure 8-3. Block Flow Diagram of TMC Integration in a Subcritical Boiler

Table 8-4. Flue Gas and Water Condensate Conditions for TMC Design

	AECOM	S1	S2	S3	S4
Inlet					
Flue Gas Temperature (°F)	135*	135*	135*	135*	135*
Dew Point (°F)	N/A	130.1[S]	130.1[S]	130.1[S]	130.1[S]
Relative Humidity	N/A	88%[S]	88%[S]	88%[S]	88%[S]
Flue Gas Flowrate (lb/hr)	2,521,960*	2,521,960*	2,521,960*	2,521,960*	2,521,960*
Flue Gas H_2O Mole Fraction	0.1517*	0.1517*	0.1517*	0.1517*	0.1517*
Steam Condensate Temperature (°F)	100*	100*	100*	100*	95
Steam Condensate Flowrate (lb/hr)	982,967[#]	982,967[#]	1,543,782*	1,543,782*	1,543,782*
Outlet					
Flue Gas Temperature (°F)	132.68[+]	130[S]	128.3[S]	127.3[S]	126 [S]
Dew point (°F)	N/A	126.5[S]	124.8[S]	123.8[S]	122.5 [S]
Relative Humidity	N/A	91%[assumed]	91%[assumed]	91%[assumed]	91%[assumed]
Flue Gas Flowrate (lb/hr)	2,493,820[+]	2,499,463[S]	2,489,068[S]	2,483,073[S]	2,475,641 [S]
Flue Gas H_2O Mole Fraction	0.1377[+]	0.1377+	0.1316[S]	0.1281[S]	0.1236[S]
Steam Condensate Temperature (°F)	119	119	119	125	125
Steam Condensate Flowrate (lb/hr)	1,021,630[+Δ]	1,005,517[S]	1,576,731[S]	1,582,727[S]	1,590,160[S]

Condense Rate (% of Condensed Moisture in Flue Gas)	N/A	9.5%[S]	13.9%[S]	16.4%[S]	19.5%[S]
Net Water Recovered (lb/hr)	51,558[+]	45,099 [S]	65,898 [S]	77,891 [S]	92,756 [S]
Gross Heat Added to Steam Condensate (MW)	12.31[+]	12.08 [S]	18.85 [S]	24.71 [S]	29.64 [S]

* From DOE Case 9

[+] From Aspen simulation results

[Δ] Liquid flowrate going to deaerator (after entrained gases have been removed)

[#] Condition provided by GTI

[S] From SmartBurn Tool results

8.4 TMC Module Layout and Arrangement

The first version of the TMC system integration was envisioned by AECOM as shown in Figure 8-4. It is a two-train arrangement with the total flue gas flow split evenly between two identical trains. Due to the fact that the elevation of the TMC trains is lower than the outlet of the FGD vessel, a complicated ductwork is required, making the cost higher than expected. This is due to a separate structure that supports the ductwork extending from the FGD to the TMC and the length travelling back to the chimney breeching. Ductwork and the required support structure are site-specific and dictated by the site's layout and space constraints. For the purpose of this study, approximately 500 feet of duct and all necessary support frameworks were assumed to account for the FGD outlet to the TMC vessels and inlet to the chimney breeching. To decrease the duct length and cost, GTI designed a one train design for TMC system to be incorporated into the coal power plant. Figure 8-5 shows the general arrangement in which a single TMC train is placed on the top of the FGD unit. The flue gas flow enters into the one TMC train directly and then passes through a short outlet duct to the stack.

Figure 8-6 shows the TMC integration into the power plant with Rankine Cycle. A single-stage TMC design has been evaluated for this project, and only steam condensate from the plant condensate system was used at a design temperature of 100°F for the TMC inlet cooling water that runs inside the TMC membrane tubes. On the flue gas side, the TMC is positioned between the FGD unit and the stack with a flue gas design inlet temperature of 135°F.

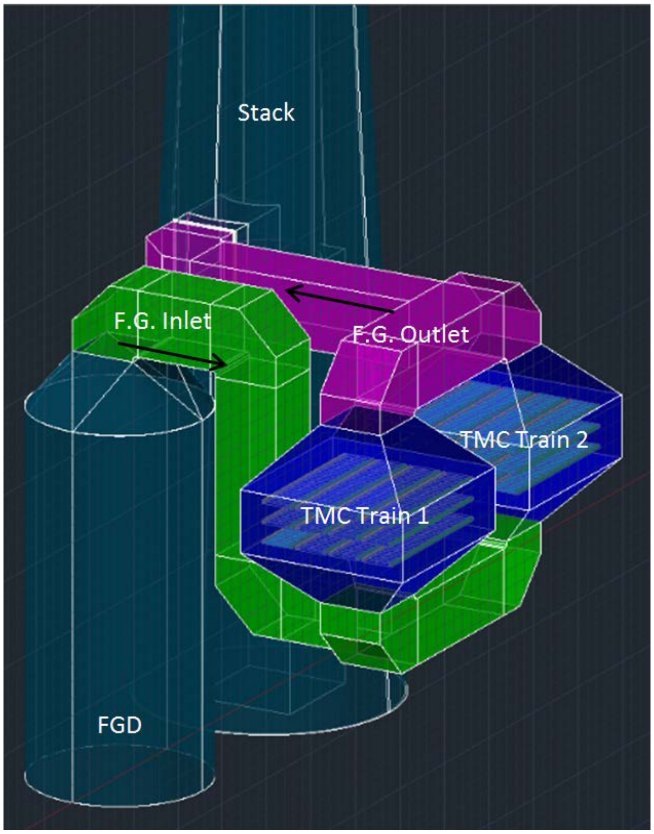

Figure 8-4. Two-Train Design TMC

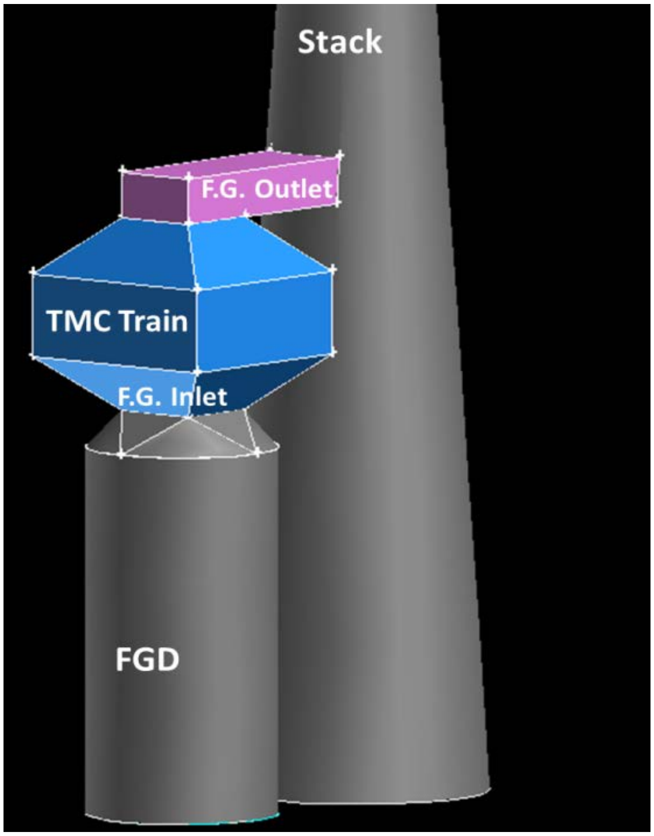

Figure 8-5. One-Train Design TMC

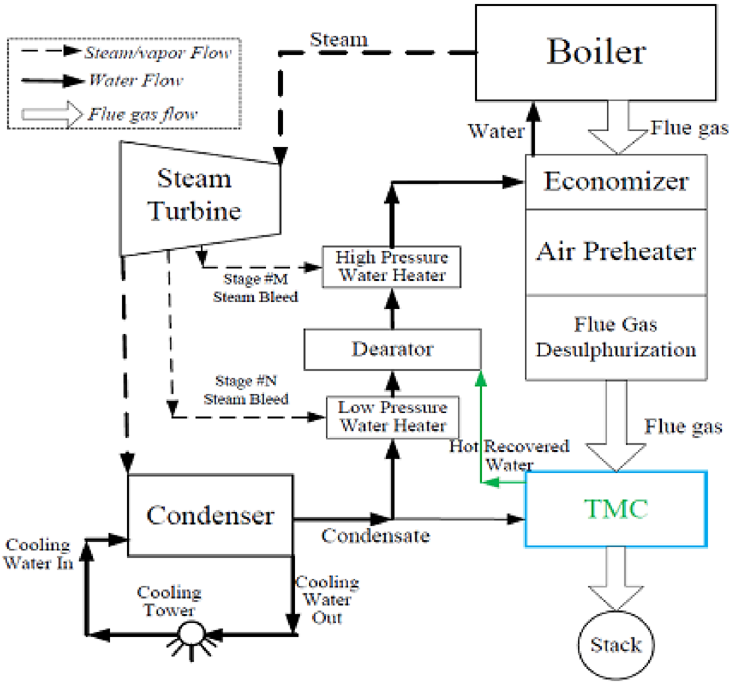

Figure 8-6. Single-Stage TMC Integration Diagram

The TMC system consists of multiple modules, and each individual module has a dimension of 4'L x 1.7'W x 1'H. According to the operating parameters of the flue gas, the primary design constraint of the TMC system is the requirement of having a single stage with 1,500 500-tube TMC modules arranged in five planes to form a 5-pass cross flow heat exchanger arrangement. Figure 8-7 shows the arrangement for each set of modular planes. Each plane contains 300 TMC modules which are arranged in the train as five rows to form a cross flow heat exchanger. Steam condensate will be supplied from the top row, and pass through the 2nd, 3rd, 4th and 5th rows (no module on the same row are connected in series).

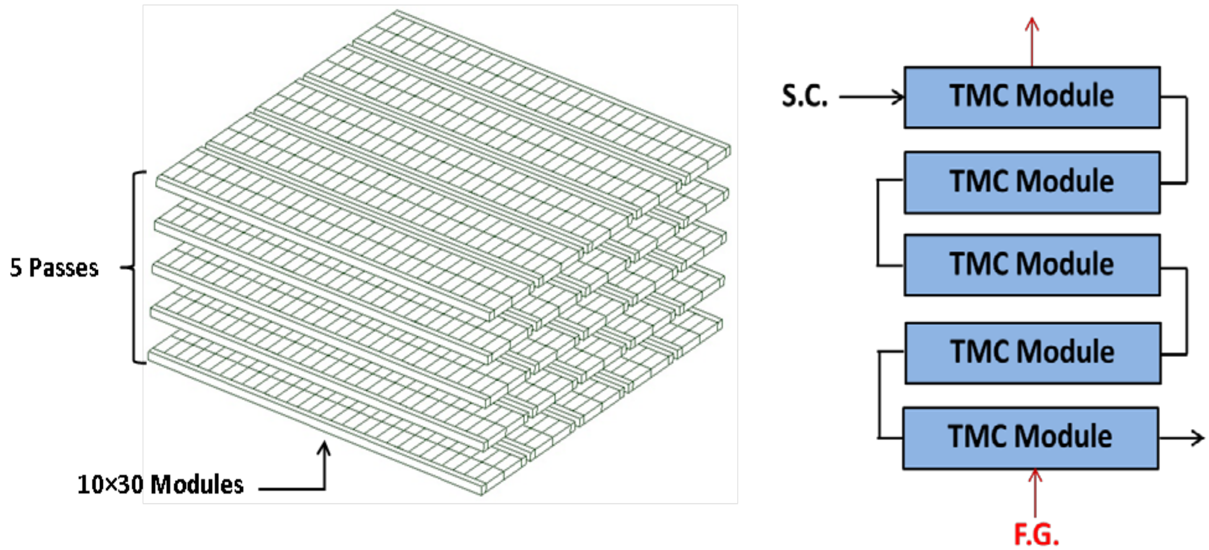

Figure 8-7. Arrangement of TMC modules in a TMC unit for a 550 MW Power Plant

8.5 Economic Analysis and Payback Estimation

Based on the above TMC layout design and its integration into a 550 MW coal power plant with the parameters from NETL report Case 9 [6], the payback was analyzed and estimated as listed in Table 8-5. The plant has Net Generation of 550 MW and the capacity factor is 85%. The net plant efficiency (HHV basis) is 36.8% and the net plant heat rate is 9,277 Btu/kWh. The fuel is Illinois No. 6 coal and higher heating value is 11,666 Btu/lb. The TMC working condition was based on design of S4 in Table 8-4. Savings of water and heat recovery were estimated from Case E1. Savings of heat recovery was assumed to be fully reused which is possible with a waste heat system applied, for example, Generalized Regeneration Technologies [7]. AECOM did the capital cost estimation of a two train design for the TMC system. In Table 8-5, the capital cost was estimated in a similar way, but only for a one-train design which necessarily decreased the cost of TMC island steel, vessels and ductwork. The piping cost is also lower if using low pressure pipes and decreasing the piping distance. In Case E1 with the demineralized water, the typical power plant price is estimated at $5.25 per 1,000 gallons, with a payback is 5.7 years. Some power plants are located in drought-prone areas and therefore could have a higher water price. Also as analyzed in Section IV, the typical cost of a mist eliminator and GGH also can be saved. Case E2 is for a plant with $10/1,000-gallon water price and the savings from not needing the mist eliminator was estimated at $1,000,000. The payback in this case is 3.5 years. In Case E2, when the additional estimated savings of $1,000,000 from not needing the GGH system was included in the analysis, the payback decreases to 2.4 years. For future development, if the TMC can recover 80% of the total moisture in the flue gas with less heat recovery as in Case E4, the payback can be as short as 1.2 years. Furthermore, reducing the moisture in the flue gas helps to reduce stack opacity which in turn could bring extra savings on other emissions controls.

Table 8-5. TMC System Payback Estimation for a 550 MW PC Power Plant

	E1	E2	E3	E4	Units
Net Generation	550	550	550	550	MW
Capacity Factor	85%	85%	85%	85%	
Net Plant Efficiency	36.8	36.8	36.8	36.8	%
Heat Rate	9277	9277	9277	9277	Btu/kWh
Flue Gas Water Content	15.17	15.17	15.17	15.17	Mole %
Net Water Recovered	92,756	92,756	92,756	371,024	lb/hr
Net Water Recovered	82,763,472	82,763,472	82,763,472	331,053,889	gal/year
Water Price	5.25	10	25	25	$/gal-1000
Saving of Water Recovery	$ 434,508	$ 827,635	$ 2,069,087	$ 8,276,347	$/year
Gross Heat Added to Steam Condensate	29.64	29.64	29.64	14.82	MW
HHV	11,666	11,666	11,666	11,666	Btu/lb
Heat Rate	9,277	9,277	9,277	9,277	Btu/kWh
Heat Saved	274,970,280	274,970,280	274,970,280	137,485,140	Btu/hr
Coal Saved per Hour	23,570	23,570	23,570	11,785	lb/hr
Coal Saved	175,503,918	175,503,918	175,503,918	8,775,1959	lb/year
Coal Price	$ 32	$ 32	$ 32	$ 32	$/short ton
Saving of Heat Recovery	2,808,063	$ 2,808,063	$ 2,808,063	$ 1,404,031	$/year
Total Saving of Water and Heat Recovery	$ 3,242,571	$ 3,635,697	$ 4,877,149	$ 9,680,379	$/year
Cost Savings on Mist Eliminator		$ 1,000,000	$ 1,000,000	$ 1,000,000	
Saving on GGH			$ 1,000,000	$ 1,000,000	
Cost of TMC per Module	$ 1,320	$ 1,320	$ 1,320	$ 1,320	$/module
Cost of TMC Modules	$ 1,536,000	$ 1,536,000	$ 1,536,000	$ 1,536,000	
TMC Island Steel & Vessels	$ 3,995,400	$ 3,995,400	$ 3,995,400	$ 3,995,400	
Piping	$ 10,003,704	$ 5,001,852	$ 5,001,852	$ 5,001,852	
Ductwork	$ 654,680	$ 654,680	$ 654,680	$ 654,680	
EI&C	$ 1,481,378	$ 1,481,378	$ 1,481,378	$ 1,481,378	
Equipment	$ 913,561	$ 913,561	$ 913,561	$ 913,561	
TMC System Capital Cost	$18,584,723	$ 13,582,871	$ 13,582,871	$ 13,582,871	
Payback	5.73	3.46	2.37	1.20	year

8.6 Summary

This section summarized the project efforts on the integration of the TMC system in a coal-fired power plant, the cost-benefit analysis and the design of TMC arrangement with detailed module layout. Based on the operating data of typical coal-fired power plants, the performance of a coal-fired power plant with a basic configuration and the addition of integrated TMC technology was analyzed and assessed by calculating changes in both the water recovery rate and the heat rate. The calculation results showed that the water recovery efficiency is related to both the TMC inlet water flow rate and the moisture content in the TMC inlet flue gas. The higher the TMC inlet cooling water flow rate and the higher the moisture content in the flue gas, the larger amount of water and heat that can be recovered by the TMC system. Results indicate that the potential benefit of installing a TMC system in coal-fired power plants is not only to recover the water but also to recover heat and increase the efficiency of the power plant. The unit heat rate can potentially increase by 5 to 8% for a 535 MW cyclone power plant or a 197 MW T-fired power plant if all of the recovered water and heat can be successfully reused. Such results indicate a significant contribution to CO_2 reduction and great potential in helping coal-fired power plants to meet ever more stringent emission regulations. Moreover, integrating the TMC system downstream from the FGD can be more efficient in terms of recovering water and improving heat rate in coal-fired power plants. As a result, more than 40% of the total moisture in the flue gas can be recovered and the unit heat rate can be improved simultaneously. The less the heat loss is in a wet FGD, the higher the heat rate can be improved by the TMC system.

Strategies for integrating the TMC system in coal-fired power plants were introduced along with some economic analysis including capital cost, O&M cost and annual cost for retrofit units and new units with a FGD system. Other effects introduced by the FGD and TMC systems including pressure drop and auxiliary power were also analyzed. Furthermore, potential approaches with several benefits for integrating TMC in a coal-fired power plant with wet FGD technology were summarized. First, the TMC can work as a mist eliminator for the FGD system to collect moisture after the FGD system with no extra load to the ID fan. This procedure would not only improve the mist eliminating efficiency but also recycle the recovered water. Second, if a TMC system was integrated, a Gas to Gas Heat exchanger (GGH) may no longer be necessary to reheat the exhaust for reducing visible stack plume. Therefore, the capital cost and O&M cost of the avoided GGH would be saved. Moreover, by improving coal-fired boiler efficiency, the coal consumption and CO2 emissions can be decreased by the TMC system. In addition, the TMC system can significantly decrease net water consumption of a coal-fired power plant. Recovered water from TMC can be used as boiler make-up water, cooling tower make-up water, FGD make-up water or PRI/SNCR dilute water.

Detailed layout design and incorporation of TMC modules were conducted. The one-train design of TMC placed on the top of the FGD was selected which not only requires less TMC modules, but also requires less ductwork than the two-train design therefore costs can be reduced. A single stage TMC with 1,500 TMC modules was arranged in five planes to form a 5-pass cross flow heat exchanger. Each plane contains 10× 30 TMC modules which are arranged in the train as five rows to form a cross flow heat exchanger. Each module was dimensioned in 4’L × 1.7’W × 1’H and has 500 tubes. The payback for a typical PC 550 MW power plant for installing a TMC system varies from 1.2 to 5.7 years.

Reference:

1. Paul S. Nolan. Flue Gas Desulfurization Technologies for Coal-Fired Power Plants, Coal-Tech 2000 International Conference. Nov. 2000.
2. Wet Flue Gas Desulfurization Technology Evaluation. Sargent & Lundy LLC. Jan. 2003.
3. Albert L. Moretti. State-of-the-Art Upgrades to Existing Wet FGD Systems to Improve SO_2 Removal, Reduce Operating Costs and Improve Reliability. Babcock & Wilcox Power Generation Group, Inc. Power-Gen Europe. June 3-5, 2014.
4. Air Pollution Control Technology Fact Sheet. EPA-452/F-03-034.
5. G.T. Bielawski, M.J. Schmeida, and N.T. White, Air Quality Control System Choices for U.S. Utility Power Plants. Babcock & Wilcox Power Generation Group, Inc. Power-Gen International. November 12-14, 2013.
6. NETL Report (DOE/NETL-2010/1397). Cost and Performance Baseline for Fossil Energy Plants Volume 1: Bituminous Coal and Natural Gas to Electricity. 2013.
7. Coal-Fired Top Plants: Shanghai Waigaoqiao No. 3. Power Magazine. Vol 159 No.10, October 2015